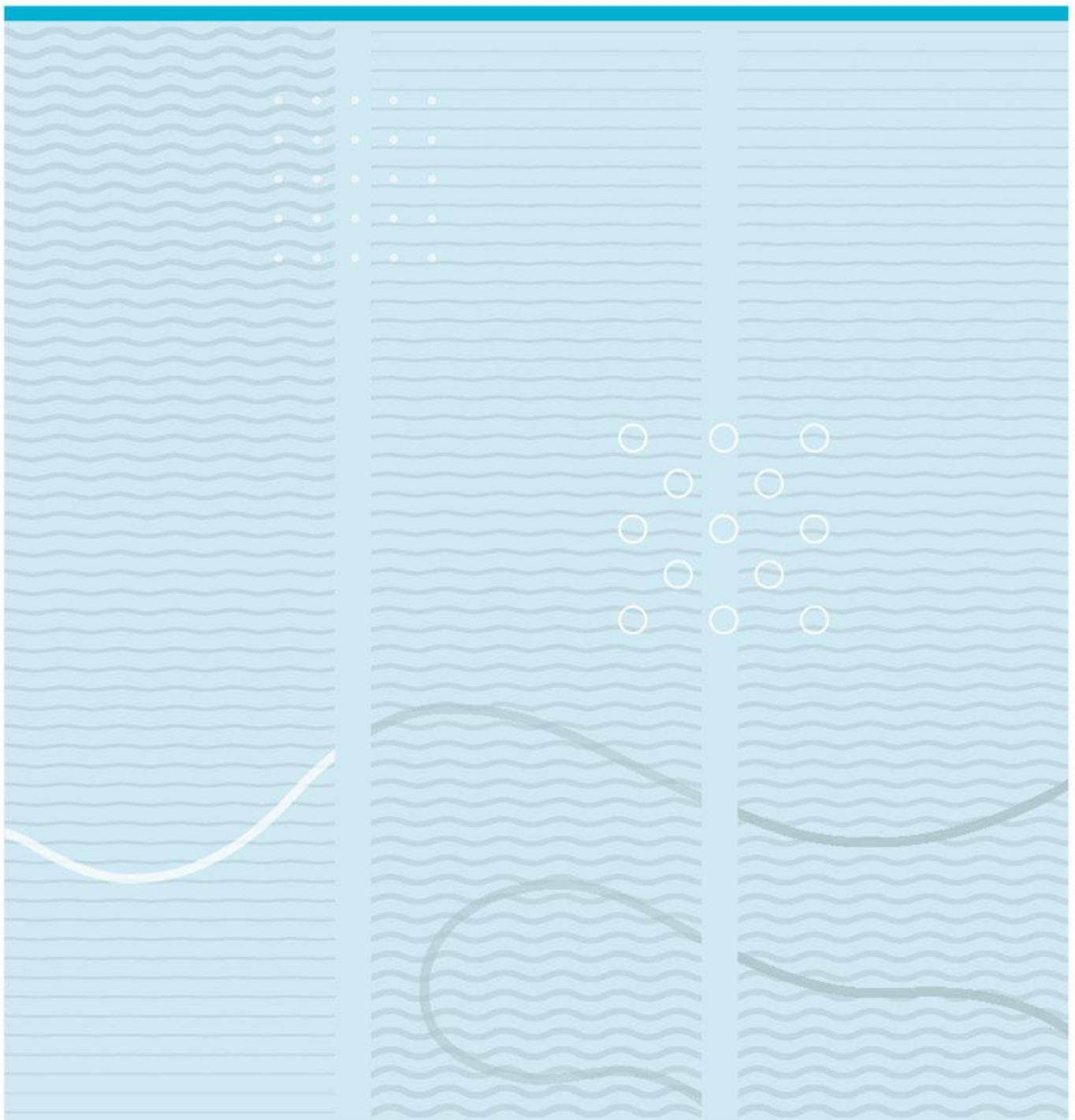


Ingelin Kristine Hagensen Karlsen

3D Subsurface Modeling based on Ground Penetrating Radar Survey of Glaciomarine Deposits – Hagadrag Aquifer, Norway

A sedimentological, hydrogeological and geophysical study



University of South-Eastern Norway
Faculty of Technology, Natural Science and Maritime Science
Department of Natural Sciences and Environmental Health
PO Box 235
NO-3603 Kongsberg, Norway

<http://www.usn.no>

© 2019 Ingelin Kristine Hagensen Karlsen

This thesis is worth 60 study points

Summary

Despite abundant surface water in Norway, groundwater can be a better resource for drinking water due to the good natural protection and filtration properties of the groundwater aquifer. In Norway, 70 % of the groundwater is found in unconsolidated aquifers, hence it is fundamental to understand the sedimentary characteristics of these aquifers if one want to utilize the groundwater as a drinking water supply. The connection between groundwater and sedimentology can be referred to as *aquifer sedimentology*.

Bø municipality uses groundwater as their main water supply, serving drinking water to approximately 4900 inhabitants. The water wells are placed in Hagadrag aquifer, in Bø Valley-fill deposits from the Quaternary time period. The Quaternary history for Bø Valley has been said to contain a glacier front terminating in a former fjord, and stagnating in a narrow part of the valley. Because of this, the area of interest is anticipated to contain large successions of glaciomarine deposits, of which this paper has analyzed.

This thesis comprises a survey executed to generate a 3D subsurface model for better understanding of the sedimentary characteristics of Hagadrag aquifer. The main method used is a Ground Penetrating Radar, collecting radargrams of the subsurface from the floor of Verpe gravel pit. The radargrams were interpreted with radar stratigraphic analysis, highlighting radar sequences/packages and their radar facies, and suggesting a depositional history with corresponding depositional environments for the analyzed sedimentary successions (lithofacies). A *geodatabase* was put together to aid interpretation of what grain sizes the identified subsurface packages may consist of. The *geodatabase* includes data from several previous drilling surveys done in and around the study area, and yields important geological information for this thesis.

A 3D model of the subsurface sedimentary packages and their bounding surfaces has been generated in *Voxler* and *ArcScene*. A bedrock grounding-line zone for a preexisting glacier was identified, together with several deposits derived from this grounding-line zone as glacial outwash material; stratified tills, gravity flow deposits, subaquatic grounding-line fan, scour pool infill deposits, and an ice-contact ridge (moraine ridge) on top of the bedrock threshold. The 3D subsurface model from this survey can be further used as a model for hydrogeological prospecting and groundwater modeling.

Key words: *Groundwater, Hagadrag aquifer, GPR, 3D modeling, Geodatabase, Glaciomarine deposits, Aquifer sedimentology, Facies, Lithofacies, Holocene valley-fill, Grounding-line fan.*

Contents

1	Introduction	8
1.1	Groundwater.....	8
1.1.1	Quaternary Deposits and Groundwater in Norway.....	9
1.2	Aquifer Sedimentology and GPR.....	10
1.2.1	Radar Stratigraphic Analysis	11
1.3	Background for this Thesis	12
1.3.1	Aim of Study.....	12
2	Study Area Characterization	13
2.1	Bedrock Geology	14
2.2	Quaternary Geology	15
2.2.1	Glaciomarine Sedimentation.....	17
3	Methods and Materials	19
3.1	<i>Geodatabase</i>	20
3.2	GPR.....	22
3.2.1	Theory.....	22
3.2.2	Implementation in Field.....	23
3.3	GPR Data Processing	31
3.3.1	Theory.....	31
3.3.2	Implementation	31
3.4	Interpretation of Radargrams - Radar Stratigraphic Analysis	34
3.5	3D Modeling	37
3.5.1	Voxler	37
3.5.2	ArcScene.....	40
4	Results	42
4.1	50 MHz Profiles	42
4.1.1	Interpretation of Radargrams – 50 MHz Profiles.....	43
4.1.2	Radar Facies inside Radar Packages – 50 MHz Profiles	50
4.1.3	3D Subsurface Model – 50 MHz Profiles.....	52
4.2	Grid 2 – 100 MHz	54
4.2.1	Interpretation of Radargrams – Grid 2.....	55

4.2.2	3D Radar Surfaces – Grid 2.....	58
4.2.3	Radar Facies inside Radar Packages – Grid 2.....	63
5	Discussion.....	65
5.1	Glaciomarine Sedimentation at Grounding Line.....	65
5.2	Interpretation of Lithofacies and Depositional Environments.....	66
5.2.1	Depositional Origin for Identified Radar Packages.....	67
5.3	Depositional Development for the Identified Subsurface Deposits.....	80
5.3.1	Conceptual Models for Glaciomarine Sedimentation.....	83
5.3.2	Comparison to Maps of Superficial Deposits.....	85
5.4	Hydrogeological Properties for the Identified Subsurface Deposits.....	86
6	Conclusion.....	87
7	Bibliography.....	88
8	Appendix.....	93

Foreword

The call I made to Harald Klempe before even applying for this Master's degree was the best decision I have made. Harald Klempe told me that it was absolutely possible to do a Master's Thesis with an aim towards sedimentology together with environmental science, with him as supervisor. And here we are, this is the result. Despite many hours of both fieldwork and learning at least two different data software by myself, I could not have done this without my supervisor, Harald Klempe. Thank you for countless hours of discussion about the study area and its geology, for being a very committed supervisor and for providing all the field equipment to me.

It has s been a real pleasure conducting my degree at the University of South-Eastern Norway Campus Bø, together with so many wonderful people. There is one peer standing out; Ingrid Gromstad. Thank you for being you, without whom I would not have such a good time conducting this thesis. Thank you for endless support, relevant academic discussions, fieldwork company, and for learning me how to use the Topcon HiperSR GPS.

I would like to thank Isak for all the support and patience on a daily basis, and for lending me his noise-cancelling headset to be able to stand the other students eating their lunch in the office. Most of all, I am so lucky to have such a supporting family, which is the reason why I am where I am today. Hence, a big thanks to my mother, my brother, and especially to my father whom traveled from Harstad to Bø to keep me company and make me quality food to keep me from starving. I love all of you!

Finally, thanks to everyone who have proofread my thesis, and to all my friends showing their support.

I have figured out the methods and procedures for making a 3D subsurface model from GPR data by myself along the way, including a lot of missteps and frustration. Hence, this thesis is a result of hard work, infinite curiosity for natural science and stubbornness.



Ingelin Kristine Hagensen Karlsen

Bø in Telemark, 14.05.2019

1 Introduction

1.1 Groundwater

Groundwater is a natural component of the water cycle, and is a widely used water resource around the world (Margat & van der Gun, 2013, p. 2). This utilization depends on the availability of other freshwater resources in the area, the amount of hydrogeological mapping carried out, and if groundwater is present in the relevant area or not. Some claim that groundwater magazines are being drained faster than they recharge, and that groundwater can be either renewable or non-renewable (Dimick, 2014; Kjensli, 2010; Sumner, 2015).

The United Nations World Water Development (Connor, 2015) classifies groundwater as a substantial water supply, which provides drinking water for at least 50 % of the global population. The report also estimates that 20 % of the world's groundwater aquifers are over-exploited and that the available freshwater in general is affected by pollution. As the world's population continues to grow, the demand for clean drinking water increases. In 2015, the United Nation member states adopted *The 2030 Agenda for Sustainable development* with 17 *Sustainable Development Goals* aiming to "... transform our world and to improve people's lives and prosperity on a healthy planet" (SDGS, 2015). Figure 1-1 illustrates goal number 6, which focuses on clean, accessible water for all. This sheds light on the importance of providing knowledge about freshwater resources in the world, for example by groundwater mapping to ensure sustainable exploitation.



Figure 1-1 – UN Sustainable Development Goal number 6; "Clean Water and Sanitation". [Illustration from the United Nation SDG website (SDGS, 2015), presented in accordance with guidelines for use of the SDG illustrations (see bibliography).]

In comparison to the rest of the world, Norway has an abundance of available, clean surface freshwater, thus rendering groundwater as a less practical source for drinking water. According to Carstens (2015), only 15 % of Norway's drinking water is derived from groundwater. Nevertheless, our groundwater is strictly regulated by *the Water*

Resources Act (Vannressursloven – vrl, 2001) governed by *the Ministry of Petroleum and Energy*. Despite abundant surface water, groundwater can be a better resource for drinking water due to the good natural protection and filtration properties of the groundwater aquifer. An aquifer is defined as a formation that contains sufficient saturated permeable material to yield significant quantities of water to wells or springs (Weight, 2008). How good the aquifer is protected from external sources of pollution, depends on the geological conditions around the groundwater well and in the catchment area for the aquifer (Gaut, 2017). Key geological, or hydrogeological, properties decide the yield for groundwater, aquifer storage capacity, groundwater flow, and degree of filtration for the aquifer. These hydrogeological properties are porosity and permeability (Asprion & Aigner, 1999; Bersezio et al., 1999), and depend on the composition of grain sizes and their spatial distribution in the subsurface. Information on the field of sedimentology in the subsurface is therefore essential to gain knowledge about groundwater as a resource.

1.1.1 Quaternary Deposits and Groundwater in Norway

Quaternary is the latest time period of earth's history, spanning over the last 2.6 million years, and Quaternary geology concerns the geological processes and formations from this period (Sigmond et al., 2013). The time period is in general characterized by a cool and variable climate, and in Norway the numerous glaciations have been shaping the surface geology producing U-shaped valleys, fjords and Alpine landscape close to the coast (Olsen et al., 2013, p. 5). These fjords and valleys made excellent catchment basins with huge accommodation space for erosional material transported by glaciers and its meltwater streams during the Holocene time period (Olsen et al., 2013, p. 6). Holocene is the most recent time period between the end of the last ice age (11700 years BP) and up until today, and together with Pleistocene they constitute the Quaternary time period (Sigmond et al., 2013). As the ice cap covering Scandinavia during the last ice age retreated, meltwater from the retreating ice sheet redistributed rock masses and sediments in all the available accommodation space, both as valley fills and large deposits on the continental shelf. Today, these valley fills are exquisite resources for sand/gravel, unconsolidated groundwater aquifers and agriculture (Olsen et al., 2013, p. 5).

In Norway, 70 % of the groundwater is found in unconsolidated aquifers as opposed to fractured bedrock aquifers (Carstens, 2015), and it is fundamental to understand the

sedimentary characteristics of these aquifer if one want to utilize the groundwater from them. Glacial deposits are examples of such unconsolidated aquifers, hence the purpose of this thesis is to map a part of an aquifer situated in subsurface sedimentary units from a proximal glaciomarine environment.

1.2 Aquifer Sedimentology and GPR

Several researchers have emphasized the connection between groundwater and sedimentology (aquifer sedimentology) (e.g. Anderson, 1989; Bayer et al., 2011; Bersezio et al., 1999; Huggenberger & Aigner, 1999; Klempe, 1988, 2015; Mele et al., 2012; Weissmann et al., 2015; Åberg et al., 2017). Huggenberger and Aigner (1999) says that “... *the focus of aquifer-sedimentology is primary to derive the structural relationship of the subsurface at different scales*”. By this quote, Huggenberger and Aigner (1999) mean to say that the study of aquifer sedimentology aims to examine the different deposits in the subsurface, their characteristics and how they are connected to each other in terms of groundwater flow. This is also referred to as the study of heterogeneity of an aquifer. Heterogeneous, by definition, means *differentiated* or *diverse* (Sigmond et al., 2013, p. 148), and when used in the context of sedimentology it means that the deposit consists of several different materials. Highly heterogeneous sedimentology causes constant change of hydraulic properties (porosity and permeability), thus a complex flow pattern of groundwater in unconsolidated aquifers (Herweijer, 1997).

A way to carry out a sedimentological study of an aquifer is the use of Ground Penetrating Radar (GPR) to look into the subsurface. As groundwater aquifers are concealed and sensitive resources, a good way to examine them would be to look into them without any physical interventions in the subsurface. The GPR imaging does exactly this by providing the possibility to look into the subsurface without any impact on the natural conditions therein. However, data collection and processing for three-dimensional (3D) GPR method can be tedious and difficult to implement.

Annan (2003), a pioneer within the use of GPR and the CEO of *Sensors & Software Inc.*, stated that the use of GPR in terms of sedimentological stratigraphy provides valuable insight for geologists studying groundwater flow and contaminant transport. This geophysical method applies electromagnetic (EM) waves and their reflections from the subsurface sediments to produce a two-dimensional cross section image of the

subsurface, a *radargram*. These radargrams, containing information of the sedimentary structures beneath the ground surface, are used to do a more detailed sedimentary interpretation. As mentioned earlier, the aim for analyzing aquifer sedimentology is to map out the heterogeneity of the sediments within the aquifer. Subsurface sedimentary heterogeneities and their three-dimensional formation identified from interpretation of radargrams will provide important hydrogeological information for the analyzed area.

1.2.1 Radar Stratigraphic Analysis

Heterogeneity mapping is a part of an analysis called *Radar Stratigraphic Analysis*, which is an interpretation of radargrams aiming to say something about the kind of depositions in the subsurface and their probable coherent depositional environment (Jol, 2009, pp. 283-284). This analysis of radargrams is based on what Boggs (2011, p. 372) describes as a *Seismic Stratigraphic Analysis*, which is a stepwise procedure to interpret subsurface reflection profiles. The first step is to subdivide the radargram into sedimentary sequences, differing from each other in terms of their sedimentary characteristics. These characteristics are referred to as sedimentary *facies*. The term “*facies*” was first introduced in a geological setting by Nicolas Steno in 1669, but modernized by Moore in 1949 to a more relatable meaning of the term used today; “*A sedimentary unit restricted in areal extent, but can be found at different levels within the same stratigraphic unit.*” (Boggs, 2011). It is important to differentiate between *sequence* and *facies*, where a sequence is constituted by one or more facies. The distribution of sedimentary facies in the subsurface controls the heterogeneity and therefore also the hydrogeological properties of a sedimentary aquifer (Bersezio et al., 1999). After identification and description of the facies in the subsurface, the last step of the radar stratigraphic analysis is to do a *lithofacies* interpretation. Lithofacies is one step further from facies interpretation by suggesting depositional event or environment for the sedimentary sequences (Bayer et al., 2011).

So, let us say there is an accident with a tank truck on the road across a groundwater aquifer near a drinking water supply. If you want to be able to know if the contaminants from the accident will reach a groundwater well used for drinking water, or how long it takes before the pollutants reaches a lake/river; knowledge about sedimentary facies in the subsurface is the key.

1.3 Background for this Thesis

Bø municipality in Norway uses groundwater as main water supply, feeding approximately 4900 inhabitants with drinking water (Bø-Kommune, 2014). The water derives from three groundwater wells placed in an unconsolidated aquifer at Hagadrag, close to Verpe gravel pit. Hagadrag unconsolidated aquifer is situated in valley fill deposits from the Quaternary time period, and it is desirable to gain knowledge about the subsurface in this area to best handle the groundwater resource for example in case of pollutants entering the aquifer or if a new water well is to be established. In addition, a study of an aquifer situated in deposits from the last ice age may contribute to knowledge about unconsolidated aquifers in the same type of deposits elsewhere in Norway, of which is quite abundant.

Verpe gravel pit has been chosen as the study area for the GPR survey for several reasons:

- It is situated above a part of the drinking water supply aquifer (Hagadrag)
- The plain surface of the gravel pit makes data collection with GPR convenient.
- The excavation of the upper masses in the gravel pit gives the survey an opportunity to look deeper into the subsurface, and also into Hagadrag aquifer.

1.3.1 Aim of Study

The aim for this study is to do a subsurface investigation to help understand the composition, development and properties of Hagadrag as an unconsolidated aquifer in Bø municipality in Telemark county, Norway.

By using the geophysical method GPR I will generate cross section profiles beneath Verpe gravel pit for further radar stratigraphic interpretation. The interpretations will serve as foundation for a 3D model, using 3D modeling software for visualization.

The study will give a better understanding of the Holocene geological history and depositional environments in the area around Hagadrag. This can be helpful in further investigations of the hydrogeology and the hydraulic properties for the defined area within Hagadrag aquifer. Subsurface sedimentary characteristics are very useful input parameters for groundwater modeling, as supported by Huggenberger and Aigner (1999), who stated that the analysis of sedimentary units and their heterogeneities in the subsurface will improve prediction and modeling of transport paths for groundwater and possible contaminants that may enter the aquifer.

2 Study Area Characterization

The GPR survey took place in Verpe gravel pit within Bø municipality in South-Eastern Norway. The gravel pit is marked with a red dot in Figure 2-1, situated 1.2km downstream Bø River from the outlet of Lake Seljord, and approximately 13km North-West from Bø city center. Bø River is running from Lake Seljord through Bø valley, a former fjord-valley shaped by glaciers and covered by surficial deposits from depositional processes due to glacial activity in the Quaternary time period (Bergstrøm, 1999; Jansen, 1983). The area also hosts the main transport route between Bø and Seljord (Rv. 36), two gravel pits, two rivers draining from the mountains in the north (Hønsåa and Bjønndøla, Figure 2-1) to Lake Seljord, and the drinking water aquifer for Bø municipality.

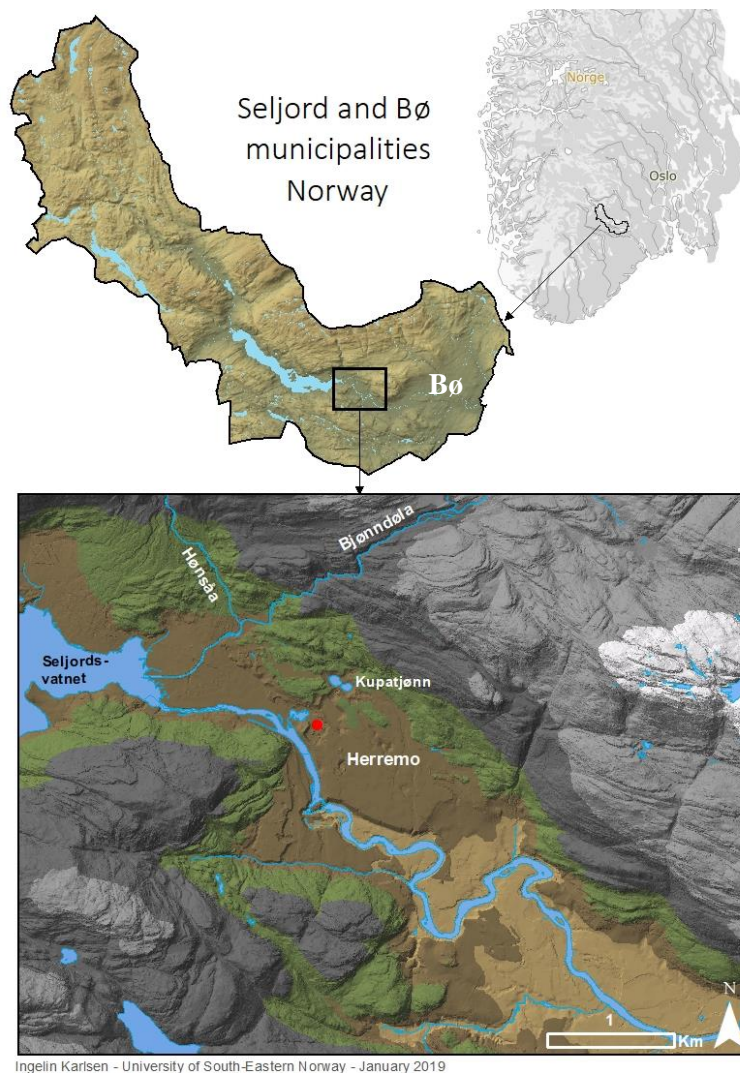


Figure 2-1 – Digital Terrain Model (TIN) produced from FKB data with contour lines (1m) in ArcMap. Red spot indicates position of the gravel pit, which is location for the GPR survey. Different colors indicate change in elevation (meters above sea level – m a.s.l.): Beige = 98-110m a.s.l. Brown = 110-135m a.s.l. Green = 135-200m a.s.l. Dark grey = 200-400m a.s.l. Light grey = 400-699m a.s.l. White = >699m a.s.l.

Today, the drinking water supply from Hagadrag consists of three groundwater wells with intermittent pumping, located circa 150m apart. Hagadrag aquifer is build up of glacial meltwater deposits, further elaborated in chapter 2.2 – *Quaternary geology*. Such deposits serve as terrific groundwater aquifers because they consist of sand and gravel with high hydraulic conductivity, and often appear in large quantities (Green et al., 1995).

2.1 Bedrock Geology

The central parts of Telemark is classified with Proterozoic igneous and *supracrustal* rocks, originating from a time period between 1700 million years ago (Ma) and 900 Ma, and metamorphosed during the Sveconorwegian orogeny event between 1130-1100 Ma (Solli & Nordgulen, 2013). *Supracrustal* means that the rocks were initially formed on the earth surface, either by sedimentary- or volcanic processes (Sigmond et al., 2013). These supracrustal rocks in central Telemark are referred to as the *Telemark-Supracrustals* (Dahlgren, 1993), forming a belt of meta-basalt, rhyolite, quartzite, and meta-gabbro going from the central parts of Telemark and North-Eastwards (Figure 2-2). North of this belt is a large mountain range of deformed quartzite called the Lifjell group (Lamminen, 2011), represented by the yellow color in Figure 2-2. The study area of Hagadrag, marked with a red dot in the map, is surrounded by granitic gneiss with a sharp contact to the thin belt of quartzite in the North (Lamminen, 2011). Jansen (1983) did an analysis on the dominating rock types constituting the glaciofluvial sand/gravel deposits in Verpe gravel pit. The results show a very high content of quartzite (75-80 %), probably transported by glacial meltwater streams from the large quartzite mountain area of Lifjell group, and some granitic gneiss (10-15 %) from the bedrock area underlying the gravel pit.

Glaciers are known to follow fracture zones in the bedrock, eroding them to get deeper and maybe even produce large U-shaped valleys, as Bø Valley. According to Jansen (1986), the dominating direction for fracture zones in Telemark is SW-NE and NW-SE, which coincides with the NW-SE direction of Bø Valley.

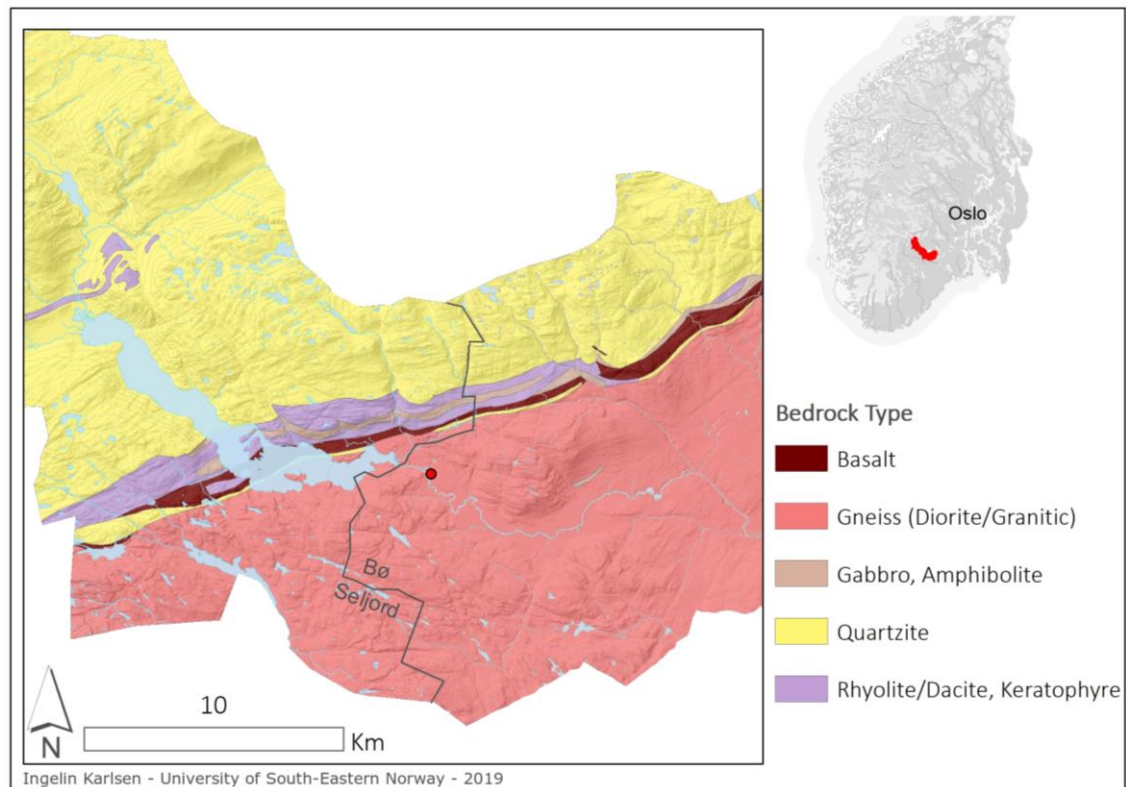


Figure 2-2 – Bedrock distribution in Bø and Seljord municipalities. The map was generated with ArcMap using N250 bedrock data put together by NGU in 2016 and downloaded from <https://kartkatalog.geonorge.no/search>. Red dot on the left map is the study area (Verpe gravel pit), and the red area on the map of Southern Norway (right) is Seljord and Bø municipalities.

2.2 Quaternary Geology

Telemark is in general dominated by deep, U-formed valleys due to glacial erosion, e.g. Bø Valley. The sediment supply to the valley basins has been especially large in the valley-areas earlier covered by ocean, i.e. under marine limit (ML) (Jansen, 1986). These ocean-influenced valleys was a part of fjord-systems connected to the coast of Telemark, including Bø Valley with a marine limit of 134 meters above sea level (m a.s.l) (Jansen, 1986). Due to isostatic uplift after the last ice age, the massive deposits of deglaciation material were raised above sea level. This makes the deposits easy to examine today. The isostatic uplift also sank the base level for erosion, hence the rivers running through the valleys cut down into the Quaternary sediments.

Most of the surficial deposits in South-Eastern Norway were formed during Late Weichselian and Holocene (Bergstrøm, 1999), where Weichselian is referred to as the last ice-age in Northern Europe between 117 000 years BP and 11 500 years BP (Sigmond et al., 2013). As one can see in Figure 2-3, the surficial deposits surrounding the study

area (red dot) consist of glaciofluvial outwash deposits meeting massive marine/fjord deposits with fluvial deposits on the top and in between. The sediments are situated in a valley with steep hillsides of exposed bedrock (pink), with an occasional thin layer of till (green) indicating former glacial activity in the valley. As marine deposits make good farmlands, there is a lot of agriculture situated South-East of the study area.

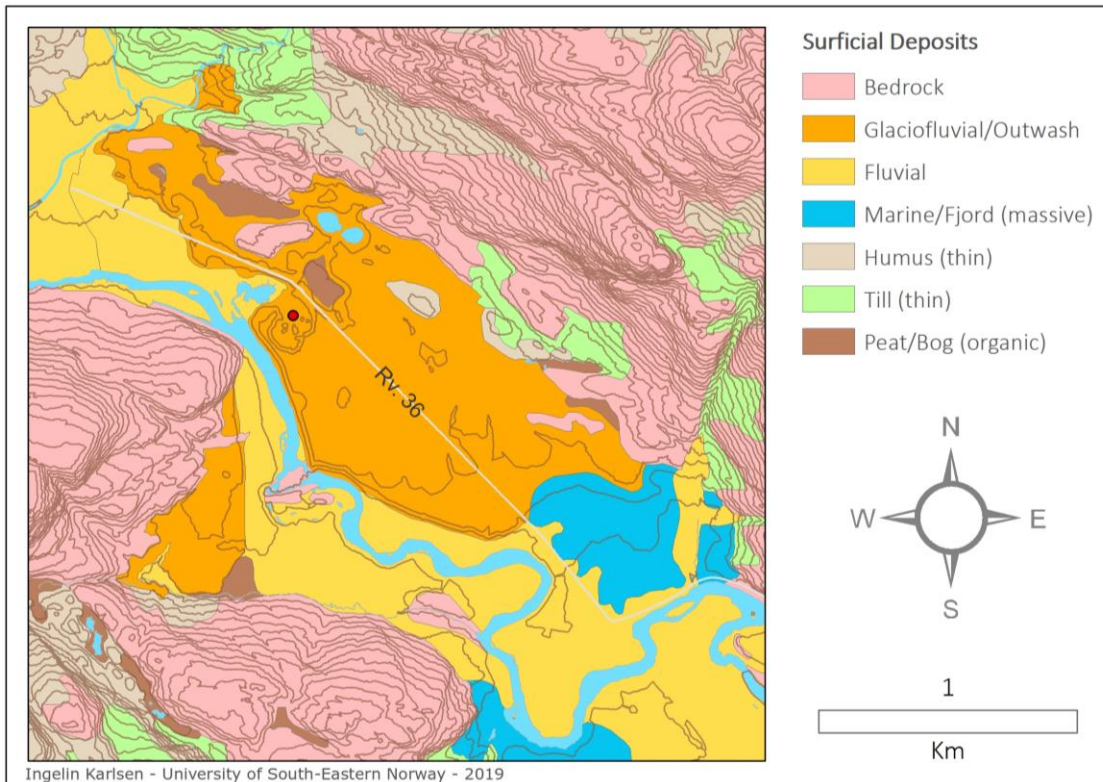


Figure 2-3 – Surficial deposits in Bø valley around the study area, which is marked by a red dot. The main road between Bø and Seljord (Rv. 36) lies on top of the valley sediment infill, and Bø River runs through the valley. The contour lines have 10m equidistance. Dataset with subdivision of surficial deposits retrieved from <http://geo.ngu.no/kart/losmasse/>. Map generated with ArcMap.

Jansen (1980) proposed a formation history for the surficial deposits at Herremo, comprising all of the orange area in Figure 2-3. The formation history is illustrated in Figure 2-4, and suggests four stages: A) ice front stagnation in narrow part of Bø Valley, meeting ocean with marine deposits (blue), B) stillstand and ice front melting, with buildup of glaciofluvial material (orange), C) complete deglaciation of Bø Valley, Bø River eroding into glaciofluvial delta and deposition of fluvial sediments, and D) the situation today with fluvial deposits, glaciofluvial delta, fluvial fans, and marine deposits. As the figure is based on surficial Quaternary geological mapping, the depositional processes were probably more complicated, thus a more detailed survey of the subsurface sedimentology is needed.

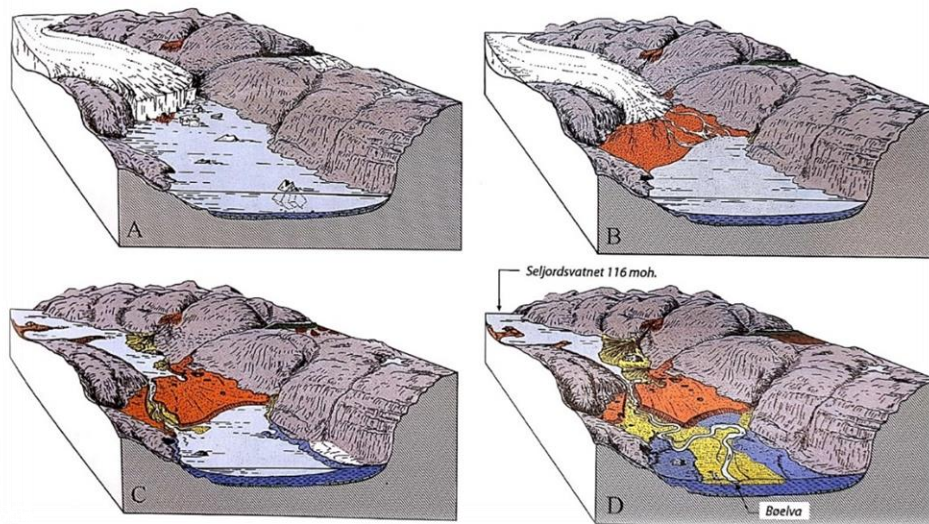


Figure 2-4 – A four-step formation history of deposits in Bø Valley. See text for description of the different steps in the illustration. [Obtained from Ramberg et al. (2013), modified from Jansen (1980), published in collaboration with Telemark regional college (today University of South-Eastern Norway).]

2.2.1 Glaciomarine Sedimentation

Assuming Bø Valley has been a glacial fjord with the ocean meeting the glacier front approximately at Verpe gravel pit, it is important to establish some fundamental frames around what kind of sedimentary processes that may have taken place here. Referring to Bennett and Glasser (2010 - Ch. 10.2), glaciomarine sedimentation can be closely compared to sedimentation in glacial lakes, but tend to be larger and present over a wider area. Bennett and Glasser (2010) include eleven key processes for glaciomarine sedimentation, presented in this thesis with permission from *Wiley Books*, the publisher of “*Glacial Geology – Ice sheets and Landforms*” (see bibliography):

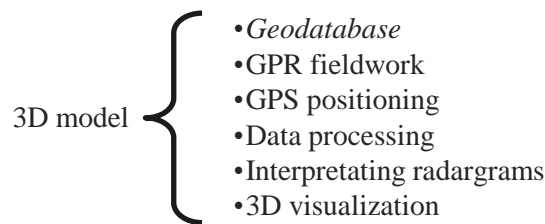
1. Direct deposition from glacier front (ice margin).
2. “Rain-out” from icebergs and seasonal sea-ice. The sediments produced by “rain-out” can for example be drop stones or dump structures and large diamictic deposits.
3. Deposition from meltwater flows (freshwater) into the sea (saline water). The deposition is rapid, and a fan of sand and gravel usually marks the proglacial point of meltwater outlet.
4. Settling from suspended sediment introduced into the sea.
5. Subaqueous resedimentation by gravity flows. May result in diamicts.

6. Subaerial rock fall and mass flow directly from valley sides into the fjords.
7. Re-mobilisation by iceberg scour, where large icebergs may ground in shallow water and scoop out deposited sediments into suspension.
8. Current reworking in sediments by waves and tides close to the shore, especially in fjords.
9. Shoreline sedimentation may modify already existing materials.
10. Biological sedimentation, where skeletal remains of micro-organisms may be found in the sedimentary records. Includes bioturbation.
11. Coriolis force, especially affecting the sedimentation in fjords. In the Northern hemisphere, sedimentation seem to deflect towards right-hand side of the fjord.

These sedimentary processes will be used as a reference during discussion of results from this survey.

3 Methods and Materials

Several methods were used in order to create a 3D model of the subsurface in the analyzed area. A short summary of the steps is presented in the flowchart below:



Fieldwork planning is essential to conduct efficient surveys with the GPR in field. This planning included a field inspection in May 2018, a review of previous work conducted in the area and discussion with supervisor, Harald Klempe, to determine where and how to best carry out the GPR survey.

A database was established in *Excel*, containing geological information in drilling points from previous surveys in the area of interest. This *geodatabase* was created in collaboration with peer Ingrid Gromstad, and used as important geological background information (“*ground truth*”). The benefits of creating such a database is appraised in “*Identification of Quaternary subsurface glacial deposits using 3D databases and GIS*” by Klempe (2004).

Duration of the **GPR fieldwork** was eleven days between 5th of September and 29th of October, and took place in Verpe gravel pit. **GPS positioning** for all the data collected in field were transferred to the *Geographical Information System (GIS) ArcMap*, delivered by ESRI, to generate maps and store their geographical information for later work. Coordinates is found in the appendix. All radargrams were reviewed and **processed** in *EKKO_Project v5* from Sensors&Software (2009-2018) to optimize quality of the EM-signals before interpretation of each radargram.

Interpretation of radargrams in terms of subsurface sedimentary stratigraphy can also be referred to as *radar stratigraphic analysis*. Interpretation was done with *EKKO_Project V5*. The final steps before finishing a **3D subsurface model** was to interpolate radar surfaces from the interpretations, and visualize these surfaces together with extruded radar packages in 3D software. Below (Figure 3-1) is a list of the computer software used in this thesis, and their field of application:

Excel 2016 from Microsoft	<ul style="list-style-type: none"> • Used for compilation of <i>geodatabase</i>
ArcMap 10.6.1 from ESRI	<ul style="list-style-type: none"> • Generation of maps, and for <i>Surface Aspect</i> analysis
EKKO_Project V5 from Sensors&Software	<ul style="list-style-type: none"> • Used to view, process and interpret radargrams
ArcScene 10.6.1 from ESRI	<ul style="list-style-type: none"> • Interpolation of radar surfaces and 3D modeling
Voxler 4 from Golden Software	<ul style="list-style-type: none"> • 3D modeling

Figure 3-1 - All software programs used for this thesis, together with the corresponding companies that provide the software.

3.1 Geodatabase

As stated by Zuk (2011, p. 131), preliminary knowledge about the subsurface is beneficial when deciding the most effective survey mode for a sedimentological study. In addition, a good understanding of local Quaternary geology is crucial for aiding the interpretation of the GPR data. The use of data from previous scientific work from the same area is the best information you can get about “*ground-truth*” without digging a trench or drill a well yourself.

The surficial deposits located at Hagadrag attracts interest in both the field of hydrogeology and sand- and gravel resources because of its great volume and sedimentary composition. Hence, the area around Verpe gravel pit has been well examined (e.g. Aarnes, 2015; Halvorsen & Strømme, 1989; Jansen, 1983; Klempe, 1979, 2009, 2010; Kraft, 2011; Lavik, 2017; Østmo, 1974). These examinations mostly concern sedimentological- and hydrogeological mapping by probe- and test drillings for water wells, which include analysis of change in grain sizes and hydraulic properties.

The purpose of the *geodatabase* is to gather borehole data from all these previous surveys, making them more convenient to use as guidance for geological decisions made during the scientific work. The data were categorized with filtering options for each category in *Excel*. The *Excel* database include categories for the following properties for each drilling point: well name, coordinates, top elevation, maximum depth, type of drilling, from elevation (Fm a.s.l), to elevation (Tm a.s.l), average grain size, thickness for each depth

interval, MD50 (mm), packing, hydraulic conductivity K (m/s), transmissivity T (m^2/s), and discharge Q (m^3/s). Not all values are recorded for all drillings, but the most important information for this thesis is the distribution of grain sizes in the drilling logs.

For a more readily comparison between data in the *geodatabase* and the results from this survey, maps including grain sizes in each drilling were generated. An example from one of these maps is presented in Figure 3-2, and the rest of the *geodatabase* maps are attached as appendix 7 and 8.

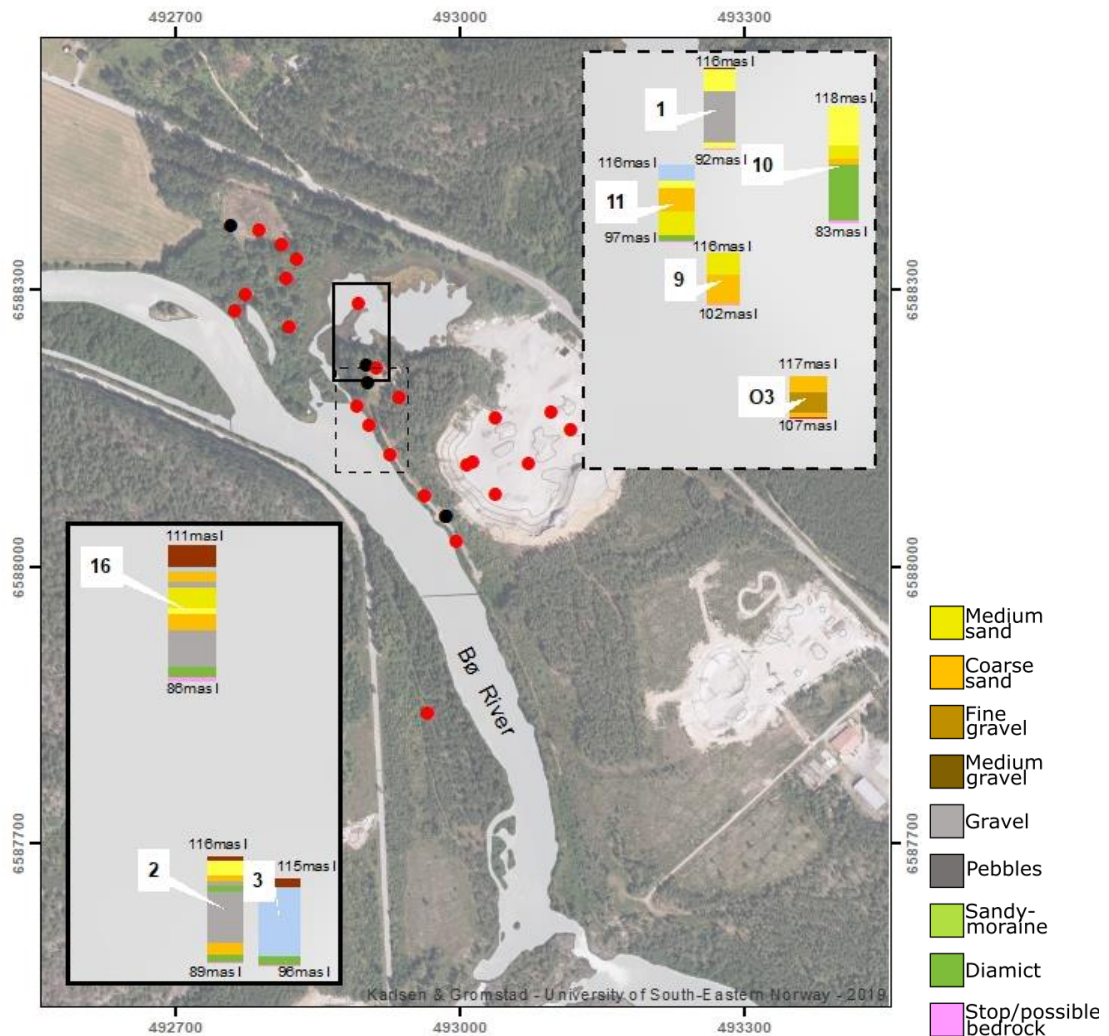


Figure 3-2 - All drilling points included in the *geodatabase*, with grain size distribution presented for some drilling points close to the gravel pit. The map is made with ArcMap. The grain size-columns include top and bottom elevation for the different drillings. All *geodatabase*-maps are presented in appendix 7 and 8.

3.2 GPR

Neal (2004, p. 321) suggests that the success rate of radar stratigraphic interpretation depends on the interpreters understanding of several factors; scientific principles of the GPR technique, the GPR system setup parameters during data collection, topographic variations in field, vertical and horizontal resolution, depth of penetration, the causes for *noise* or other “non-geological-structures” on the radargram, and the function- and effect of each processing step used to enhance data.

One of the most important advantages by using the geophysical method of GPR for monitoring the subsurface, is its ability to bring forward information about the subsurface with little or no impact on the natural conditions therein (Takahashi et al., 2012).

3.2.1 Theory

The foundation for the GPR method lies within electromagnetic (EM)–properties of the subsurface (Jol, 2009). Electromagnetic waves are propagated from a transmitter and through the subsurface, where any changes in dielectric properties with depth will initiate a reflection of the electromagnetic wave at the transition between the medias with different dielectric properties. These properties are called *dielectric permittivity* (ϵ), and are strongly dependent on the water content of a material, as water has a much higher conductivity of electricity than air (Robinson et al., 2013, p. 2). The amount of water content is highly associated with the porosity of the sediments.

A receiver at the ground surface registers the reflected electromagnetic wave signals, and the result is a GPR profile (radargram) with reflected signals. The reflected signals are based on the amplitude of the received signals as a function of time and position (Takahashi et al., 2012). The strength of the reflection depends on the reflection coefficient (R), which is proportional to the magnitude of change in relative dielectric permittivity (ϵ_r) between the adjacent upper and lower medium the electromagnetic wave travels through (Eq.1) (Neal, 2004).

$$R = \frac{\sqrt{\epsilon_{r2}} - \sqrt{\epsilon_{r1}}}{\sqrt{\epsilon_{r2}} + \sqrt{\epsilon_{r1}}} \quad (Eq. 1)$$

The setup for the GPR system is illustrated in Figure 3-3, and show the connection between transmitter, receiver and the control/display unit. The control/display unit for the *pulseEKKO pro* GPR system controls the settings and functions of the GPR.

GPR System

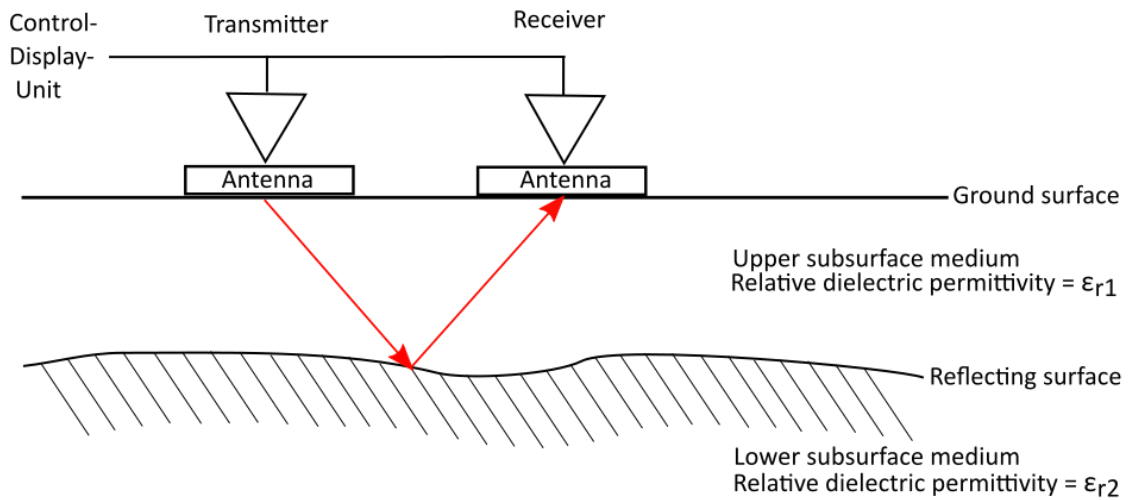


Figure 3-3 - Flow diagram illustrating the GPR system setup and performance in field. The GPR unit consists of a control display (DVL) and a transmitter and receiver connected to antennas. The transmitter produces a signal travelling through the upper subsurface medium, and is reflected at the boundary between upper- and lower subsurface medium. The receiving antenna perceives the reflected signal and registers its properties.

3.2.2 Implementation in Field

The GPR instrument *PulseEKKO Pro* delivered by *Sensors & Software Inc.* was used for the survey, together with 50- and 100 MHz antennas and pulseEKKO 100 transmitter. In total, a length of approximately 5.5km of GPR profiles were manually ran.

As the project aims to display data as a 3D volume, most of the data were collected from a densely spaced grid with radar lines in both x- and y-direction, illustrated in Figure 3-4. The spacing between radarlines is determined by what type of features targeted in the subsurface, e.g. archeological surveys often use 0.5-1m spacing while geological surveys often use 1-2m spacing.

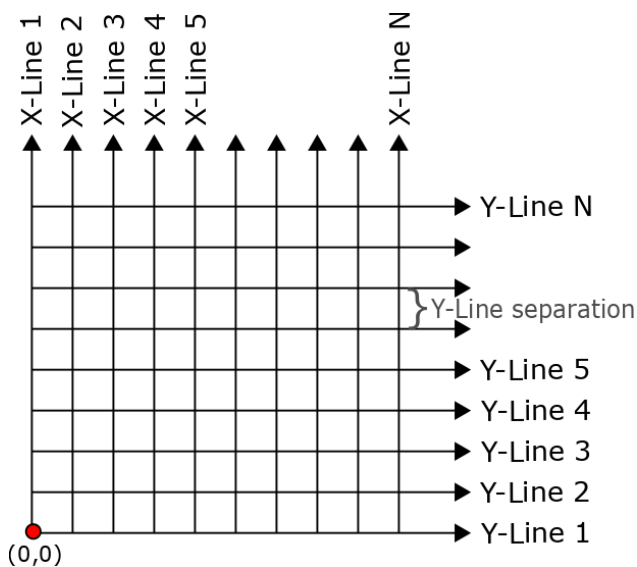


Figure 3-4 - The construction for an *xy-grid-survey* in field, with start position for the first lines in both *X* and *Y* direction at point $(0,0)$. The separation distance between the lines is constant and predefined.

When conducting a GPR survey, the position for each line is vital to relocate targets that may be of interest, and a *Topcon Hiper SR* GNSS-system was used to mark grid corners and start/end position for the 50 MHz lines (Figure 3-5). All data and products in this paper, both assembled in field and created with ArcMap, are signed the *European Terrestrial Reference System 1989 (ETRS89)* with *Universal Transverse Mercator (UTM)* set to be zone 32.

100 MHz antennas were used for all three grids, and 50 MHz antennas were used for supplementary lines to get a deeper penetration across the gravel pit. Figure 3-5 and Figure 3-6 show *SmartCarts* used for 100 MHz and 50 MHz antennas respectively. The cart for the 50 MHz antennas is constructed by Professor Harald Klempe to get approximately 1.8m spacing between the antennas, and later modified by me for better stability.



Figure 3-5 - Ingrid Gromstad assisting with the Topcon Hiper-SR GNSS system. To the left is the SmartCart for the 100 MHz antennas with transmitter, receiver and DVL connected.



Figure 3-6 - The SmartCart for the 50 MHz antennas with 1.8m spacing. The gravel pit in which the survey took place is in the background.

Survey Positioning and System Setup Parameters

To cover most of the gravel pit and assure best possible representation of the subsurface conditions, data collection was done for three grids (100 MHz) and three deeper penetrating profiles (50 MHz) spread out in the gravel pit (Figure 3-7). Grid 1 and 2 is positioned with the longest axis parallel with the direction of Bø Valley (NW-SE), representing assumed flow direction of glacial meltwater. The decision on placement was made together with my project supervisor, and the objective was to be able to see forest

beds from a possible delta situated in the subsurface. The GPR collection in both x- and y-direction started in the North-Western corner for all grids, and the arrows on the red lines show direction for GPR data collection for the 50 MHz profiles. The most interesting radargrams came from Grid 2, hence Grid 2 and the three lines with 50 MHz profiles are presented and analyzed. Detailed maps for the two excluded grids, 1 and 3, are included in appendix 1 and 2.

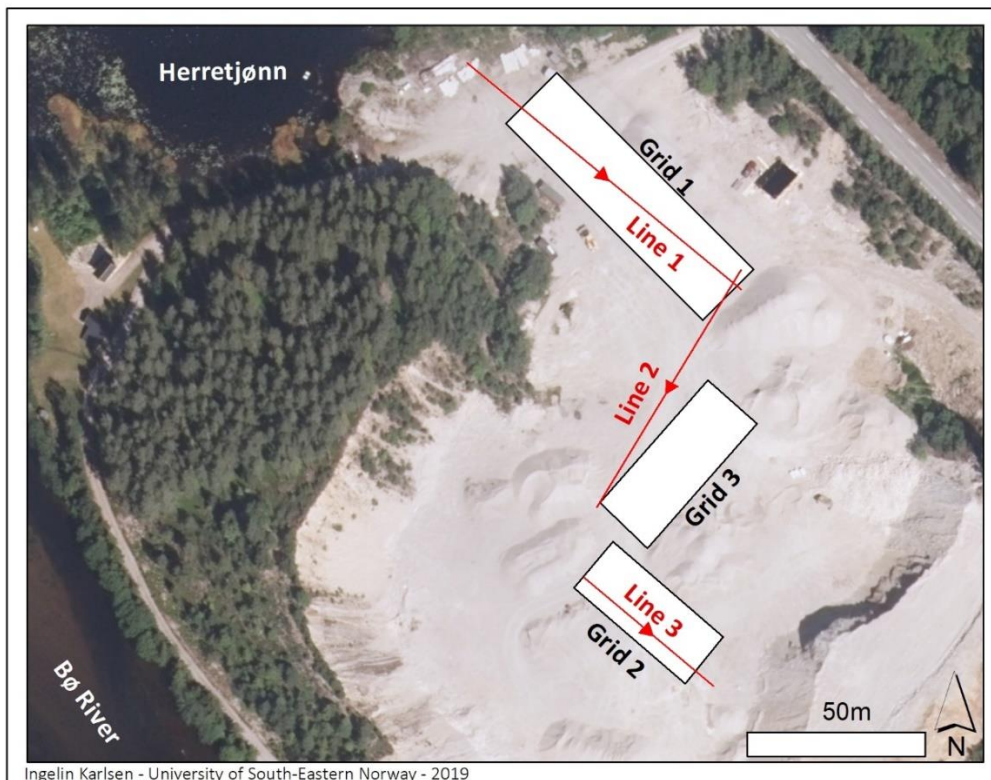


Figure 3-7 - Overview map of Verpe gravel pit with position for all three grids and 50 MHz lines (red). Map generated with ArcMap.

Grid 2 – 100 MHz

Figure 3-8 show the grid formation of Grid 2, with 1m spacing between x- and y-lines. All together, the grid holds 58 GPR lines. The 100 MHz antennas were used for Grid 2, penetrating approximately 20m down in the subsurface with a predefined velocity for the electromagnetic waves set to 0.06m/ns. The 100 MHz antenna frequency was selected for the grids as it gives more details about the subsurface structures than the 50 MHz antennas. A higher frequency was not considered as it would have less penetration depth.

The system setup parameters for the GPR are presented in appendix 4, together with the corner coordinates for the grid. A calibrated *odometer* was used to get accurate length of each GPR profile. The assumed subsurface EM-velocity of 0.06m/ns in Grid 2 was determined according to surrounding drilling logs, showing mostly sand and gravel. Table 3-1 presents a velocity of 0.06m/ns in saturated sand and gravel, assuming the subsurface is mostly saturated with water as a part of Hagadrag aquifer. System stacking was set to 8 for Grid 2, in order to do efficient collection of data in field. System stacking is a way to improve *signal-to-noise* ratio by collecting more than one trace at a time and stack them to make an average signal from them (Sensors & Software Inc, 2012, p. 74). Noise is a product of interference with the GPR signals. Sources for noise can for example be the GPR itself, surrounding objects on the surface reflecting the EM-signals sent out from the GPR, and surrounding objects on the surface transmitting radio waves. One might assume that stacking should be increased indefinitely as it makes the signal of the radargrams much clearer. However, increased stacking may slow down the survey production as one has to reduce the walking pace with a higher number of stacks. Normal stacking is between 4 and 64. In addition, the amount of sources for noise at the gravel pit was assumed to be small, thus less need for a high stacking number.

Table 3-1 - Electromagnetic properties for a selection of common geological materials at 80-120 MHz. The table show relative dielectric permittivity, electromagnetic-wave velocity, conductivity, and attenuation for both unsaturated and saturated materials. [Table from “Ground-penetrating radar and its use in sedimentology: principles, problems and progress” by Neal (2004), presented with permission from publisher Elsevier. Permission license number: 4577780060928].

Medium	Relative dielectric permittivity (ϵ_r)	Electromagnetic-wave velocity (m ns^{-1})	Conductivity (mS m^{-1})	Attenuation (dB m^{-1})
Air	1	0.3	0	0
Fresh water	80	0.03	0.5	0.1
Seawater	80	0.01	30,000	1000
Unsaturated sand	2.55–7.5	0.1–0.2	0.01	0.01–0.14
Saturated sand	20–31.6	0.05–0.08	0.1–1	0.03–0.5
Unsaturated sand and gravel	3.5–6.5	0.09–0.13	0.007–0.06	0.01–0.1
Saturated sand and gravel	15.5–17.5	0.06	0.7–9	0.03–0.5
Unsaturated silt	2.5–5	0.09–0.12	1–100	1–300 ^a
Saturated silt	22–30	0.05–0.07	100	1–300 ^a
Unsaturated clay	2.5–5	0.09–0.12	2–20	0.28–300 ^a
Saturated clay	15–40	0.05–0.07	20–1000	0.28–300 ^a
Unsaturated till	7.4–21.1	0.1–0.12*	2.5–10	^b
Saturated till	24–34	0.1–0.12*	2–5	^b
Freshwater peat	57–80	0.03–0.06	<40	0.3
Bedrock	4–6	0.12–0.13	10^{-5} –40	7×10^{-6} –24

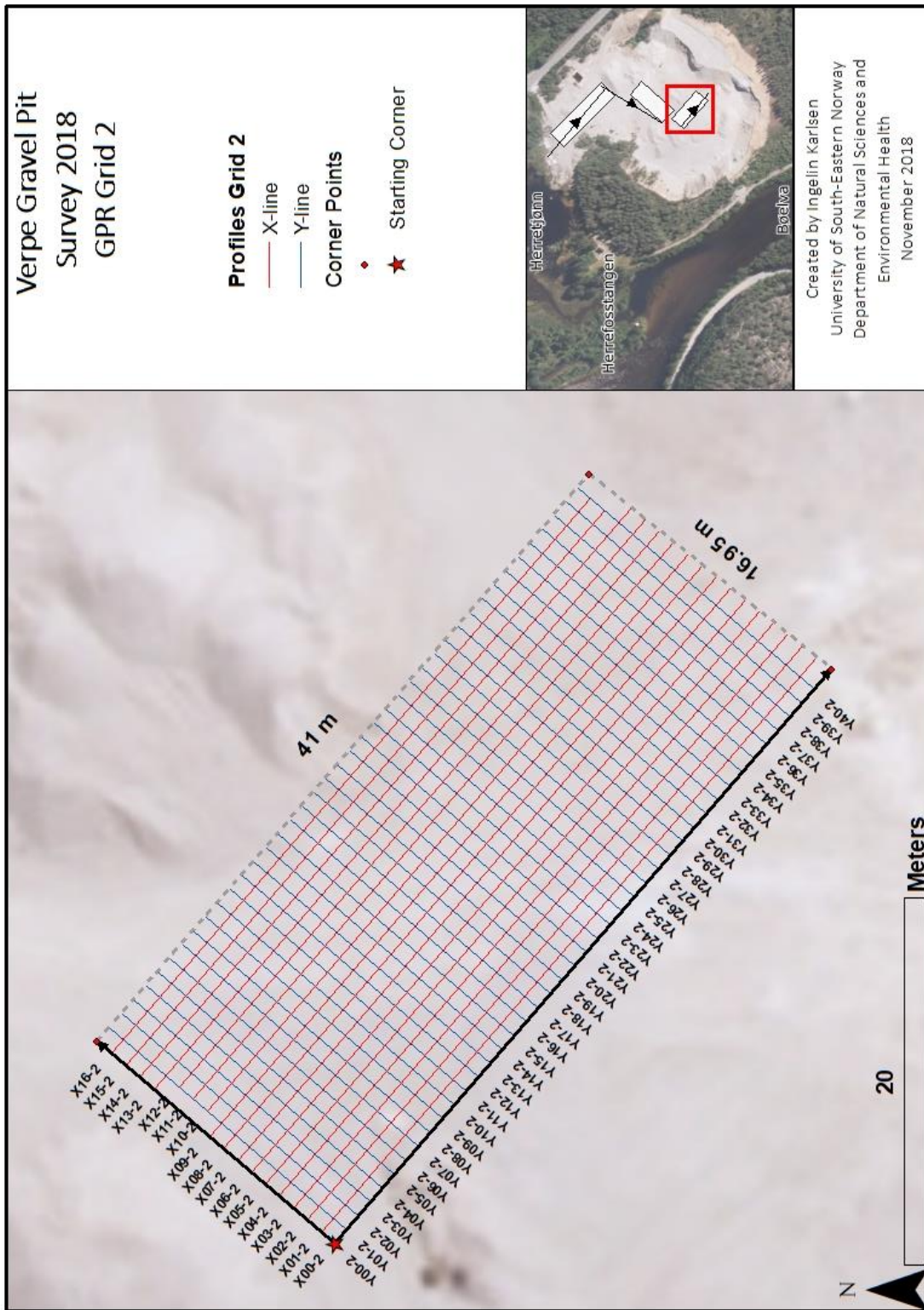


Figure 3-8 - Grid formation of Grid 2. The star marks the starting corner, red lines represent x-lines and blue lines represent y-lines. The smaller map show the position of Grid 2 in the gravel pit. Thematic map made with ArcMap.

50 MHz Profiles

Figure 3-9 shows the positions for the collected radargrams with 50 MHz antennas. Two to three radargrams were collected for each of the three 50 MHz lines, and the most optimal radargram for each line was used for interpretation. All the system setup parameters and the end-coordinates of each line are presented in appendix 6.

The goal for using the 50 MHz antenna was to reach the bedrock in order to determine the thickness of the surficial deposits. The decision on what assumed subsurface velocity to choose for the EM-waves was more complicated for the 50 MHz antennas than the 100 MHz antennas. This is because the radargrams from the 50 MHz antennas will penetrate deeper, and the length of the profiles are longer, thus a more complex composition of deposits could be expected. In general, when the composition of the subsurface is uncertain, an assumed velocity of 0.1m/ns should be set (Sensors & Software Inc, 2012, p. 73). Accordingly, a velocity of 0.1m/ns was used while collecting the 50 MHz profiles, and was later adjusted during *data processing* before interpretation.

As there were only three profiles to be collected, a stacking number of 16 was used for most of the 50 MHz lines. The radargram collection was done with *Free run* instead of *Odometer*, and lengths of the profiles were measured by hand in field and adjusted during *data processing* afterwards.



Figure 3-9 – The 50 MHz lines gathered in Verpe gravel pit. The arrows on the lines indicate the direction of data collection. The smaller map show the position of the profiles relative to the grids. Well 4 is marked with a yellow point. Thematic map made with ArcMap.

3.3 GPR Data Processing

3.3.1 Theory

The goal when processing GPR data is to increase the signal-to-noise ratio to enhance the interpretability of the data. Processing of raw data from the GPR is a delicate and decisive step, based on techniques within seismic reflection processing (Neal, 2004, p. 295). It is important to have knowledge about what the different processing tools may do to the radargrams before applying them, considering features you want to enhance or phase out to make interpretation of desired features easier. Cassidy (2009) states that it is easy to over-process GPR data, and *“the key to good data interpretation is good data collection in the first place”*. He also inspired this thesis in terms of the amount of processing needed with the saying:

“If it cannot be seen in the raw data – is it really there?”

The “journey” of processing depends on what you are aiming to interpret from the radargrams. If the interpreter is looking for utilities like pipes or buried barrels, one would want to enhance the hyperbolas from point targets, and reduce background signals from the media surrounding the target. On the other hand, when doing a sedimentological investigation of sequence stratigraphy, everything in the subsurface is the target. Hyperbolas can for example indicate boulders, and can be difficult to distinguish from anthropogenic utilities. The majority of GPR data collected in sedimentary environments require minimal processing before interpretation (Bristow & Jol, 2003). When processing radargrams, it is always a risk of losing signals from important features or produce signals that was not there in the first place. Considering this, processing tools with the purpose of removing or boosting signals with specific attributes were more or less avoided in this thesis.

3.3.2 Implementation

The program *EKKO_Project V5* from Sensors & Software was used to view and process the radargrams collected. The raw data gathered in field for this thesis is too good to risk tampering too much with, thus a decision was made to strictly use processing techniques that amplified already existing signals. Table 3-2 gives an overview and description of every processing/editing tool applied to raw GPR data in this survey. Filters can work

both in the time- (vertical) and spatial domain (horizontal). The changes of velocity vertically in the subsurface is anticipated to have large variations (heterogeneous) in this study area, due to the complexity of the sequence stratigraphy that can occur in deposits from a former glaciomarine environment. The use of filters in the time domain can therefore ruin the data, rather than improve it, and was excluded. Migration is an example of such filters. In addition, the ground level at the gravel pit is generally flat, except for some sand, silt and gravel heaps, and no application of topographic correction for the ground surface on the radargrams was needed.

Table 3-2 – All processing tools used during data processing, with coherent purpose and parameters for each tool.

GPR data editing and processing		
Processing tool	Purpose	Parameters used
Reposition trace	Adjust length of vertical position in radargram if the vertical position is not correct from data collection in field.	Radargrams were corrected to the length measured with measuring tape in field, with start position remaining the same.
Velocity calibration with hyperbola curve fitting	Alter the depth (m) axis (vertical) in terms of travel time of the wave (ns). The editing does not modify the signals.	The equation and principle is further discussed in the text. In short: the velocity of the desired sequence is measured, and used as input in Eq. 2 to calculate depth in meters. For the 50 MHz profiles, an average velocity of 0.08m/ns was applied. For the 100 MHz Grid 2, an average velocity of 0.06m/ns was used.
Dewow	Removal of unwanted low frequency signals (“wow”) caused by the large transmit pulse from the GPR followed by a slowly decaying transient (Sensors&Software, 2018).	The only parameter to adjust is Window Width, measured in wave pulses. The default is 1.33 pulse widths, which was used for the radargrams in this thesis.
Gain (SEC2)	Gain makes the radar signals stronger. SEC is short for Spreading & Exponential Calibrated Compensation. It attempts to compensate for exponential attenuation of radar signal, and because it does not gain all signals with the same factor, it is considered the gain type closest to physical reality (Sensors&Software, 2018). Hence, the reflectors can still be compared for relative signal strength.	There are three parameters to decide for this processing tool: <ul style="list-style-type: none"> - Attenuation = the attenuation of radar waves in db/m. - Start Value = A constant value deciding at what DC the SEC2 gain raises from. - Maximum gain = determines the maximum gain applied to any data point. Prevents data from being “over gained”.

Depth Calibration

To be able to estimate depth to a target in the radargram, a more reliable depth for the radargrams were calibrated with velocity calibration in *EKKO_Project*. This was conducted with hyperbola curve fitting, a tool based on the occurrence of hyperbolas in radargrams (Figure 3-10). Hyperbolas are produced when the EM-waves from the transmitter hits a buried object like a rock, pipe or other utilities. As the radiation pattern from the GPR transmitter emits energy in a cone and not a straight line, objects that are smaller than the wavelength will make the radio waves bend around the object (Takahashi et al., 2012). This is illustrated in Figure 3-11. The constant change in position of the GPR relative to the buried object makes the distance to the object from each position variate. Taking these variations in to account, the velocity for the radio wave in the soil can be extracted. A depth calibration will not alter the signals in the radargram, only change the depth axis in meters through Eq. 2 from Annan (2003). The equation represents the relationship between the position of the GPR (x), the depth from the GPR to the object (d), the velocity for EM-waves in the material (v), and travel time (T). T_0 is the travel time when the GPR is directly above the buried object.

$$T = \frac{2\sqrt{(x^2 + d^2)}}{v} \quad \text{and} \quad T_0 = \frac{2d}{v} \quad (\text{Eq. 2})$$

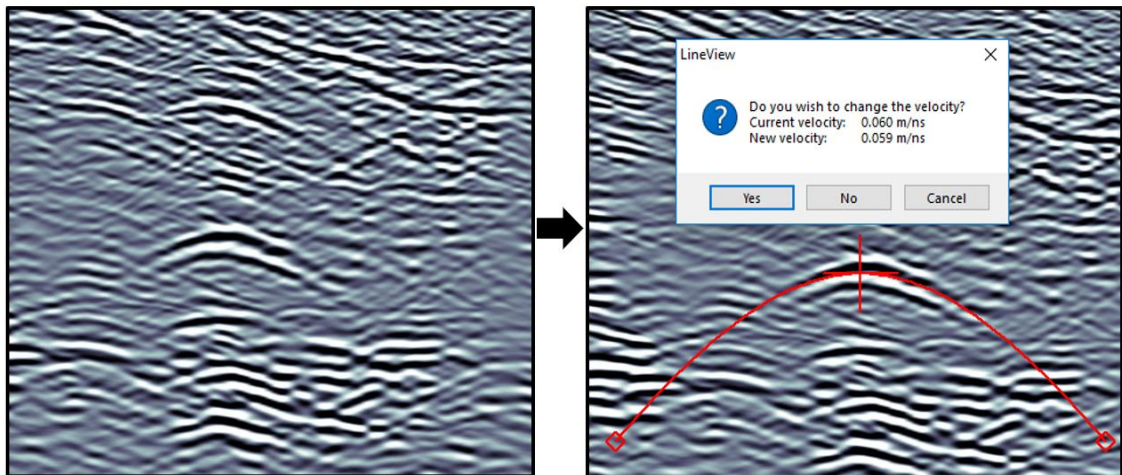


Figure 3-10 - Left: Example of hyperbola diffraction from a radargram in Grid 2. Right: The hyperbola curve fitting tool in *EKKO_Project* estimating the average velocity for the materials above the hyperbola.

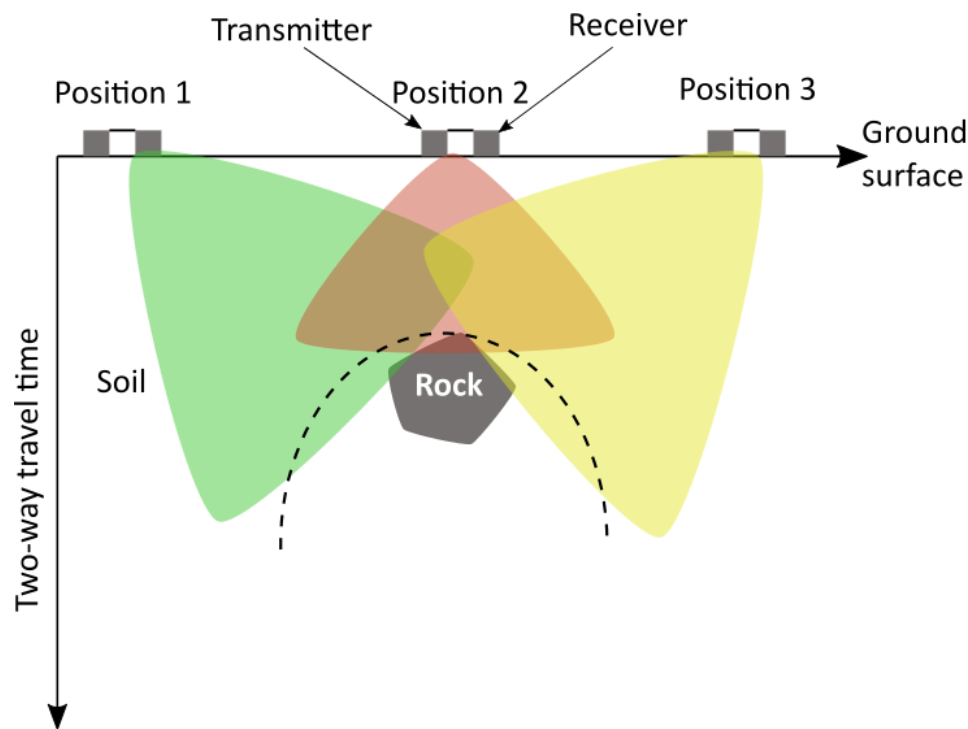


Figure 3-11 – Illustration of how hyperbolas occur when the GPR moves from position 1 to position 3 on the ground surface above, emitting radio waves. The green, red and yellow cone-shapes are the signal from the antenna in position 1, 2 and 3 respectively.

3.4 Interpretation of Radargrams - Radar Stratigraphic Analysis

After processing radargrams, interpretation of radargrams including identification of subsurface sedimentary features can start. This interpretational process can be referred to as radar stratigraphic analysis (Jol, 2009, pp. 283-284). The goal is to identify the subsurface sedimentary sequences and their probable depositional history. The term *sequence* is in this thesis used with the definition from both Boggs (2011, p. 365) and Sigmond et al. (2013, p. 342), which say that a sedimentary sequence is a stratigraphic unit that consists of one cycle of deposits with genetically related strata differing from the adjacent sequences. The sequences are bounded by upper and lower boundaries or unconformities.

Stratigraphic analysis can be used in the same way for interpretation of both seismic- and radar profiles, and according to Boggs (2011) includes the three following steps:

1. Radar sequence analysis
2. Radar facies analysis
3. Interpretation of lithofacies and depositional environments

The first step of radar sequence analysis involves the identification of unconformities bounding the sequences. In the format of three-dimensionality, these sequences are in this thesis equivalent to *radar packages* with bounding *radar surfaces* at top and bottom. A radar package can for example be a prograding delta sequence. Examples of different radar surfaces is found in part A of Figure 3-12, while examples of the external form of 3D radar packages are shown in part B.

The second step of the radar stratigraphic analysis is the identification of radar facies. Radar facies analysis involves examining radar reflection configurations within the radar packages. These configurations represent the gross stratification patterns in the radar packages (Boggs, 2011) (section C i, ii, iii, and iv of Figure 3-12). This step is strictly descriptive. Boggs (2011) also states that the objective of radar facies analysis is regional interpretation of depositional environments, corresponding sedimentary processes and geological history (*lithofacies*). These objectives are further considered in the third and last step of the radar stratigraphic analysis: interpretation of depositional environments.

Interpretation of lithofacies and depositional environments involves a comparison between the results from this survey, results from previous conducted studies in the same area (*geodatabase*) and already developed models for depositional environments in areas with similar surrounding geology. The goal for this step is to be able to suggest sedimentary processes for the identified sedimentary packages.

Interpretation of radargrams was done with *EKKO_Project V5* by manually highlighting the bounding surfaces between radar packages. The file-export option in the software presents the possibility to export files with *Comma Separated Values* (CSV) of interpretations, of which can be imported into 3D programs as point clouds. It is also possible to export 3D models as HDF-files from *SliceView*-mode for input in 3D software such as *Voxler*. Table 3-3 show a section in a CSV-file containing data from interpretation of a surface called “50 – S7 – Convex” from the 50 MHz profiles.

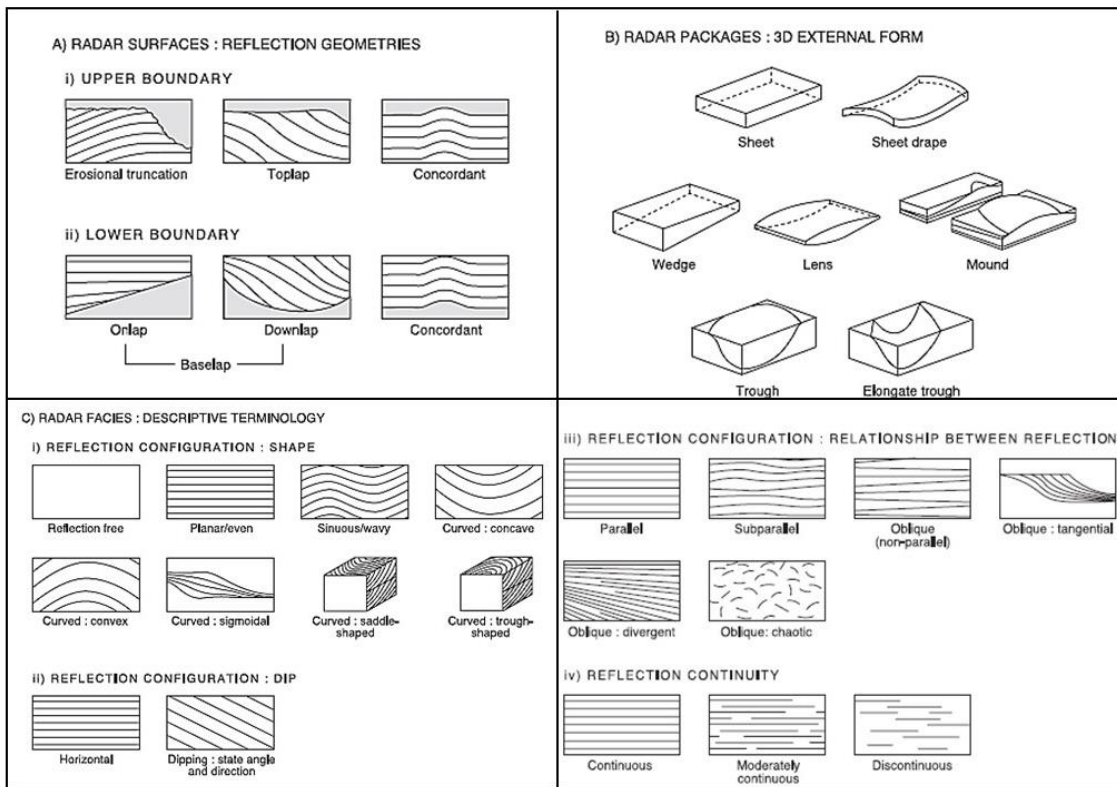


Figure 3-12 - Types of radar surfaces, -packages and -facies with names and descriptions. A) Radar surfaces (upper- or lower boundaries). B) Radar packages. C) Radar facies and associated reflection configurations. [Figure from “Ground-penetrating radar and its use in sedimentology: principles, problems and progress” by Neal (2004), presented with permission (4577780060928) from Elsevier].

Table 3-3 - Properties for an interpreted surface from the 50 MHz profiles, including vertical position, x- and y-position, depth to subsurface point, travel time to subsurface point, amplitude of signal, assumed velocity, and coordinates for each extracted point.

Tool	Interpretation	GPR Line	Position(m)	X(m)	Y(m)	Depth(-m)	Depth(m)	Time(ns)	Amplitude(m)	Velocity(m/ns)	GPS-Easting	GPS-Northing
Polyline	50 - (S7) - Convex	Line07	16	16	0	-12.513	12.513	307.63	-303.525	0.08	493067.369	6588109.594
Polyline	50 - (S7) - Convex	Line07	17	17	0	-12.577	12.577	309.23	-227.37	0.08	493068.136	6588108.952
Polyline	50 - (S7) - Convex	Line07	18	18	0	-12.682	12.682	311.84	-40.509	0.08	493068.903	6588108.31
Polyline	50 - (S7) - Convex	Line07	19	19	0	-12.794	12.794	314.64	78.323	0.08	493069.67	6588107.668
Polyline	50 - (S7) - Convex	Line07	20	20	0	-12.906	12.906	317.44	36.774	0.08	493070.437	6588107.027
Polyline	50 - (S7) - Convex	Line07	21	21	0	-13.018	13.018	320.23	37.779	0.08	493071.204	6588106.385
Polyline	50 - (S7) - Convex	Line07	22	22	0	-13.154	13.154	323.62	-63.239	0.08	493071.971	6588105.743
Polyline	50 - (S7) - Convex	Line07	23	23	0	-13.348	13.348	328.45	29.83	0.08	493072.738	6588105.101
Polyline	50 - (S7) - Convex	Line07	24	24	0	-13.544	13.544	333.35	-98.816	0.08	493073.505	6588104.46
Polyline	50 - (S7) - Convex	Line07	25	25	0	-13.743	13.743	338.3	68.425	0.08	493074.271	6588103.818
Polyline	50 - (S7) - Convex	Line07	26	26	0	-13.952	13.952	343.52	-347.286	0.08	493075.038	6588103.176
Polyline	50 - (S7) - Convex	Line07	27	27	0	-14.162	14.162	348.77	-129.525	0.08	493075.805	6588102.534
Polyline	50 - (S7) - Convex	Line07	28	28	0	-14.372	14.372	354.01	-192.047	0.08	493076.572	6588101.892

3.5 3D Modeling

3D results require data in x-, y- and z-direction. In this survey, x- and y-direction are the Easting- and Northing-coordinates, while z-direction is subsurface depth. *EKKO_Project V5* communicates well with third party 3D software, and both an HDF 3D model and CSV-point cloud can, as mentioned earlier, be exported for use in *Voxler* and *ArcScene*.

3.5.1 Voxler

Voxler is a powerful 3D visualization software delivered by *Golden Software*. On their website, they present the following examples for what 3D models the software can do:

- Borehole (well)
- Surfaces
- Point clouds
- LiDAR
- Contour
- Block
- Streamlines
- Vector

Figure 3-13 is a 3D digital terrain model (DTM) generated with *Voxler*, using LiDAR-data downloaded from “*høydedata*” (Kartverket, 2018). The terrain model is very detailed, and one can make out the abandoned river channels on top of the delta terrace on the right hand side. Below, in Figure 3-14, is an illustration of how easy one can do visualization of a *geodatabase* containing well log-information on grain sizes. The 3D map show the grain size distribution in the subsurface from drilling points around the gravel pit. The data input for the 3D wells was the *geodatabase* made with *Excel*, and Figure 3-15 show how the *Excel*-sheet was used for information on sampling data, trajectory of drillings and collars as input for the *WellRender* graphical output. The *collars* are the headings for the columns, where the required collars to do a *WellRender* are: Well ID, x-location, y-location, top z (elevation), and total measured depth (GoldenSoftware, 2018). These maps and 3D visualization of well logs in *Voxler* have been frequently used both during interpretation to get results and when discussing them.

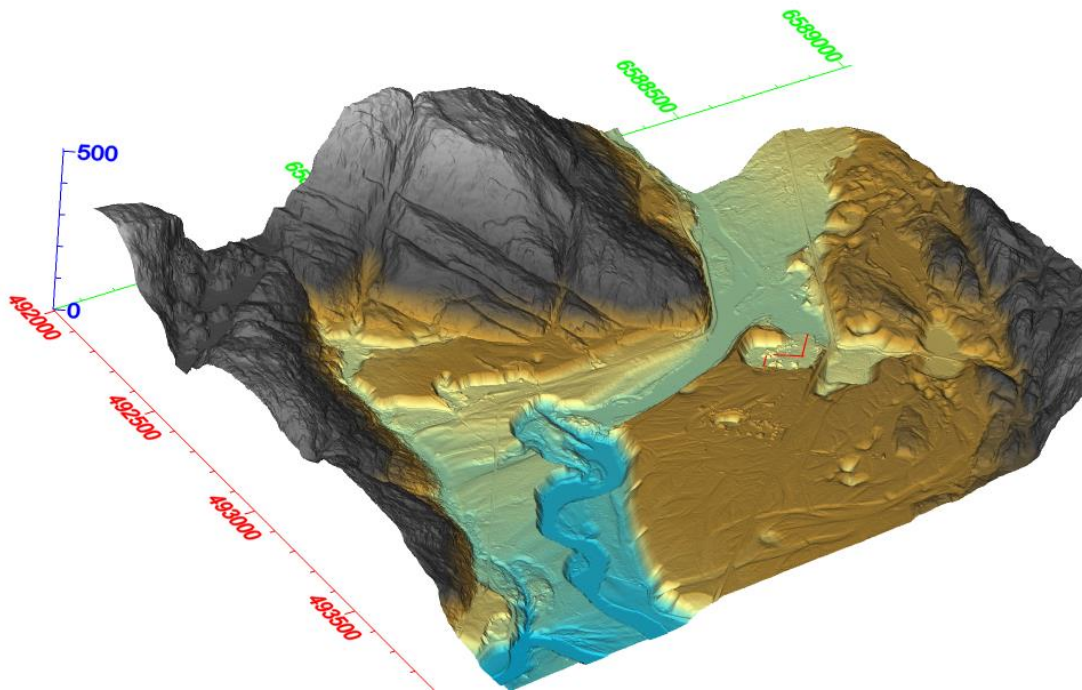


Figure 3-13 - Digital Terrain Model in Voxler, produced from topographic LiDAR data from www.hoydedata.no. The red and green axes are Easting and Northing (ETRS89 UTM zone 32). The blue axis is m a.s.l. The three red lines in the gravel pit are the 50 MHz profiles. Colors represent height intervals.

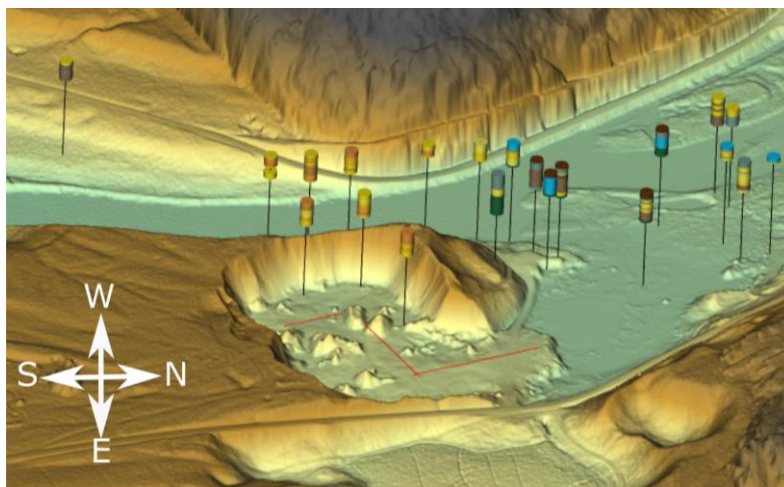


Figure 3-14 – Verpe gravel pit with surrounding wells. The map illustrates Voxler’s ability to visualize multi-component data for geologic models, here with well logs from the geodatabase presented with different colors for different grain sizes. The Excel-geodatabase was the input to generate the wells.

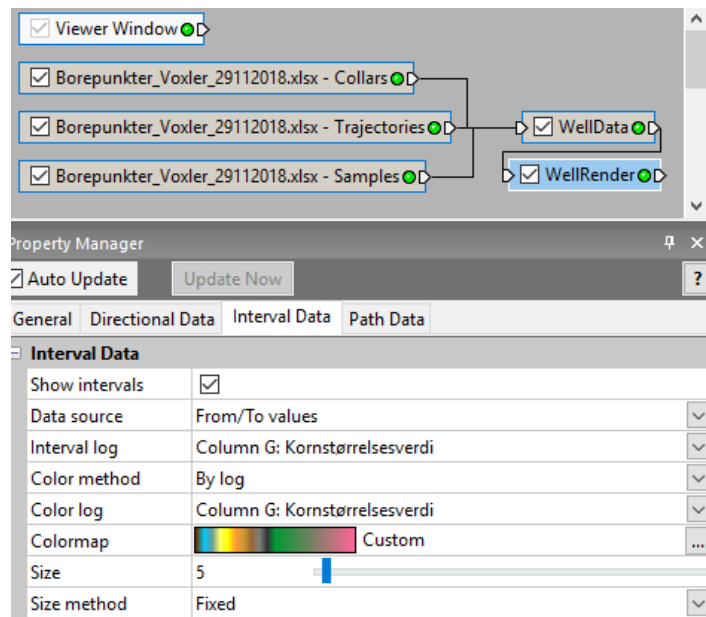


Figure 3-15 - A section from the model builder in Voxler, with settings for visualization of grain sizes from the geodatabase with WellRender as graphics output.

Voxler was also used to combine the interpreted radar surfaces and a 3D volume from Grid 2 including GPR signals exported as HDF from *EKKO_Project* (Figure 3-16). This presents a unique opportunity to visualize the interpreted bounding surfaces above and below the radar packages together with their signal characteristics. To interpolate a surface from the CSV-file holding interpretations (Table 3-3), the calculation tool called “*Gridder*” was used. The parameters for the gridder-tool was set to *isotropic inverse distance interpolation*, as shown in Figure 3-16, with power and smoothness depending on the irregularities and trends of the surfaces. The interpolation method in *Voxler* is not necessarily mathematically the best option to get the most realistic surface, but rendered an aesthetic visualization together with the radar signals. The volume in Figure 3-16 is generated by putting together all the GPR signals from Grid 2 and visualize them in *Voxler* by coloring amplitude values for the reflections in the subsurface (blue, white and red). These colors emphasize the sedimentary structures in the subsurface, whereas stronger signals indicate larger change in relative dielectric permittivity from one geological material to another. The strength of the signals also indicates attenuation of electromagnetic waves.

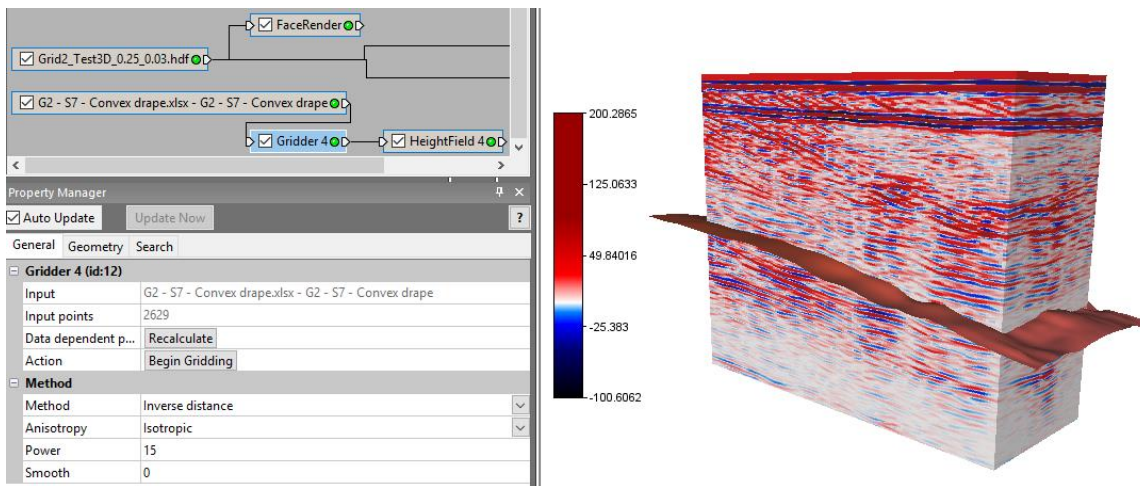


Figure 3-16 - A 3D volume colored by change of amplitude in GPR signal-reflections in the subsurface, together with one of the interpolated surfaces in Grid 2. The legend show amplitude values, and on the left side of the figure is an example of how the Network Manager and Property Manager in Voxler looks like.

3.5.2 ArcScene

ArcScene was utilized to increase the mathematical precision when interpolating surfaces for analysis and construction of sedimentary packages for Grid 2. Point clouds for each interpreted surface were imported to *ArcScene*, and interpolated with either *Inverse Distance Weighting (IDW)* or *Kriging*, depending on the dispersion and trends in the data points. For surfaces with a clear trend to the data points, for example constantly inclining in one direction, an interpolation method of *Universal Kriging (UK)* with a *Semivariogram model* of “*Linear with Linear-drift*” was implemented. The UK interpolation method is an extension of *Ordinary Kriging* by incorporating the local trend within the decided neighborhood search radius as a smoothly varying function of the coordinates (Li & Heap, 2008).

For the surfaces with more irregularities to be evoked, e.g. the top surface of a sedimentary package containing large boulders, *Ordinary Kriging*, with *spherical semivariogram model*, or *IDW* was used for interpolation. *IDW* uses a linear combination of values in sampled points to decide the values in the voids between the points. Here, the closest data point values are higher weighted in the distance function for interpolation, assuming they are more similar to the unsampled area than the data points further away (Li & Heap, 2008).

The results from these interpolations are *raster data*, with one height value within each cell (cell size resolution 0.16). Interpolated rasters were converted to a *Triangular*

Irregular Network (TIN) model with the possibility of 3D visualization. Figure 3-17 show the points from the CSV-file together with the corresponding interpolated TIN-surface from Grid 2. The last step to get a 3D model for subsurface sedimentary packages was to generate radar packages with the tool “*Extract Package*” between desired radar surfaces in *ArcScene*.

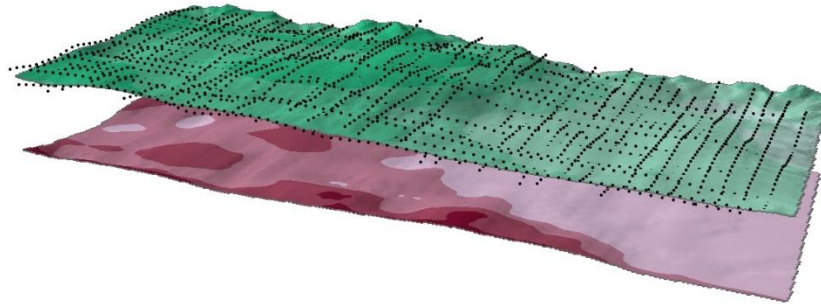


Figure 3-17 - Point cloud from exported CSV-file together with the corresponding interpolated surface (TIN-model) for surface G2 - S5 - bs in Grid 2. Interpolation done with *ArcScene*.

The interpolation and creation of TIN-models from point clouds was only necessary to get 3D results for Grid 2. The 50 MHz data were collected in 2D lines, hence the 3D visualization in the subsurface is limited. Here, the underground points along the interpreted radar surfaces were converted to polylines with the *Data Management*-tool “*Points to Line*” in *ArcScene*, and “*Extrusion*” in *Layer Properties* was implemented for each line. The result is a cross section with radar packages in the subsurface along the 50 MHz profiles.

4 Results

The results include interpretation of radargrams and corresponding 3D models of subsurface features for the three 50 MHz profiles and Grid 2. The presentation of results from each of these two GPR surveys (50 MHz and Grid 2) are divided into sub-results:

- Interpretation of radargrams in two dimensions
- Radar surfaces and radar packages with corresponding dominating radar facies
- 3D subsurface models generated from interpretation of radar surfaces and - packages

The results chapter is strictly descriptive, and analysis of lithofacies in terms of depositional environment is reviewed in the discussion (Ch. 5). All the presented results are part of the radar stratigraphic analysis introduced in the methods (Ch. 3.4). They should give a foundation for discussing types of subsurface deposits, and probable depositional processes and –environment for the identified sedimentary packages.

4.1 50 MHz Profiles

Locations for the three deep penetrating 50 MHz profiles in the gravel pit are presented in Figure 4-1. Line 1 reaches from the edge of Herretjønn and 101m in South-East direction, Line 2 starts at the end of Line 1 and ends 79m in South-West direction, and Line 3 starts 20m from the end point of Line 2 and reaches 49m in South-East direction. Well 4, one of the three drinking water supply wells for Bø municipality, is situated 100m from Line 3.

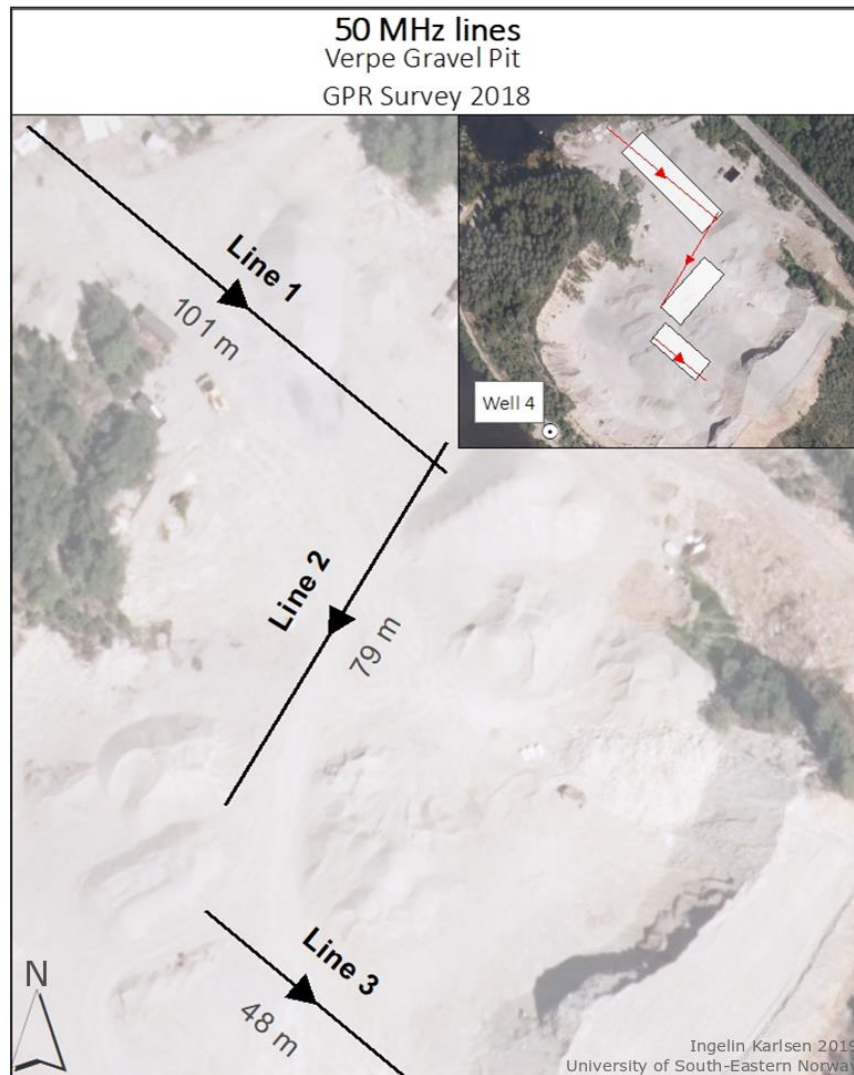


Figure 4-1 - Verpe gravel pit with locations for 50 MHz profiles. Well 4 is presented in the upper right map. Line 1 is 101m long going NW-SE. Line 2 is 79m long going NE-SW. Line 3 is 48m long heading NW-SE.

4.1.1 Interpretation of Radargrams – 50 MHz Profiles

Interpretation was performed separately on the three 50 MHz profiles, and radar surfaces were identified individually and given unique names for Line 1, 2 and 3. The radar surfaces are not correlated between the profiles. However, the radar packages interpreted for all the 50 MHz profiles are linked, with correlating names and colors for equivalent packages. This correlation of radar packages across the 50 MHz profiles are based on comparison of depth to the package, radar facies signatures in the package, and the nature of the upper and lower bounding surface. The result is an identification of nine unique radar packages, named P1-P9 (Figure 4-8).

LINE 1:

The first radar signal to notice in Line 1 is the horizontal, continuous and strong reflector at approximately 2.5-3m depth. The signal is slightly pressed down and disrupted at the left side of the radargram (Figure 4-2), which may be caused by the composition of the green package (50-P9) with chaotic signals (Figure 4-3).

The chaotic signals in the uppermost green package in Figure 4-3 gradually turns into more continuous, dipping, parallel radar signals towards right hand side. These dipping signals are captured with the yellow color (50-P2). Below the yellow radar package is an area with more stratified and nearly horizontal layered radar signals. This area has weaker signals, and is confined to the right hand side of the radargram between 20m and 48m depth. These stratified radar signals are subdivided into three packages; 50-P5 and 50-P6 (grey color in Figure 4-3), and 50-P7 (light green color).

All reflectors seem to be terminating towards, and draping over, a relatively reflection free area with some crossing radar signals at the bottom of the radargram. This area is represented by the pink package 50-P8 in Figure 4-3, dominating most of the left hand side of the radargram in Line 1.

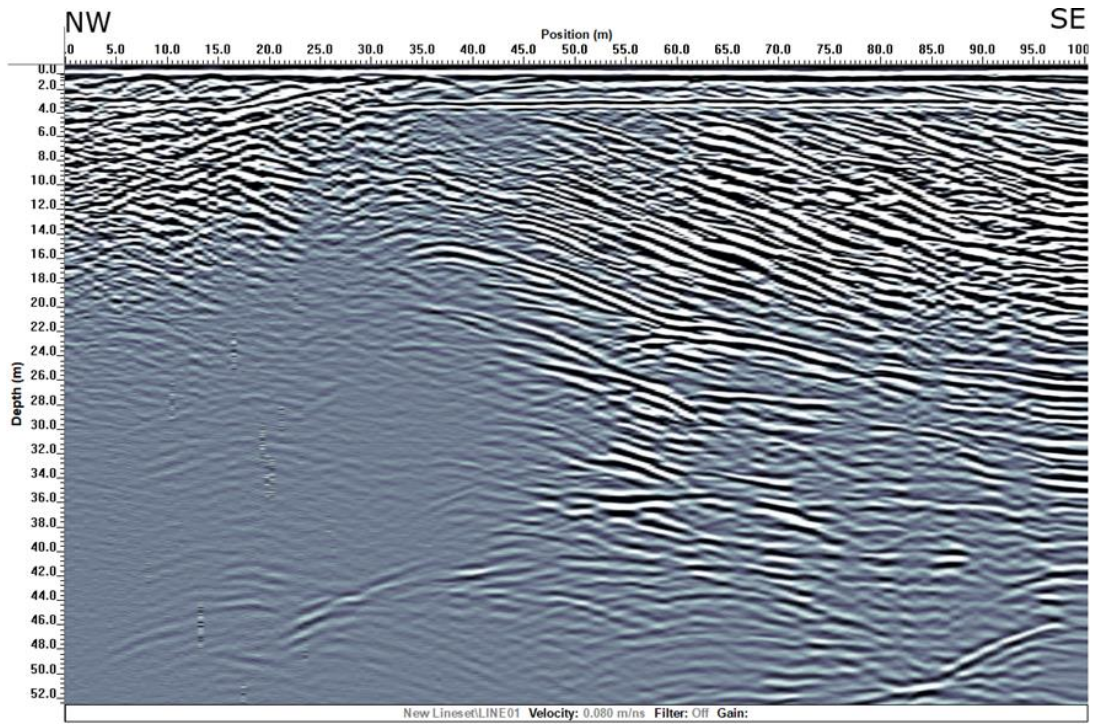


Figure 4-2 - Radargram from Line 1 of the 50 MHz profiles, without interpretations. The velocity for depth conversion is 0.08m/ns, no filters, with dewow and SEC2 gain (1, 1, 80) applied. The profile is penetrating 52m down and is 101m long.

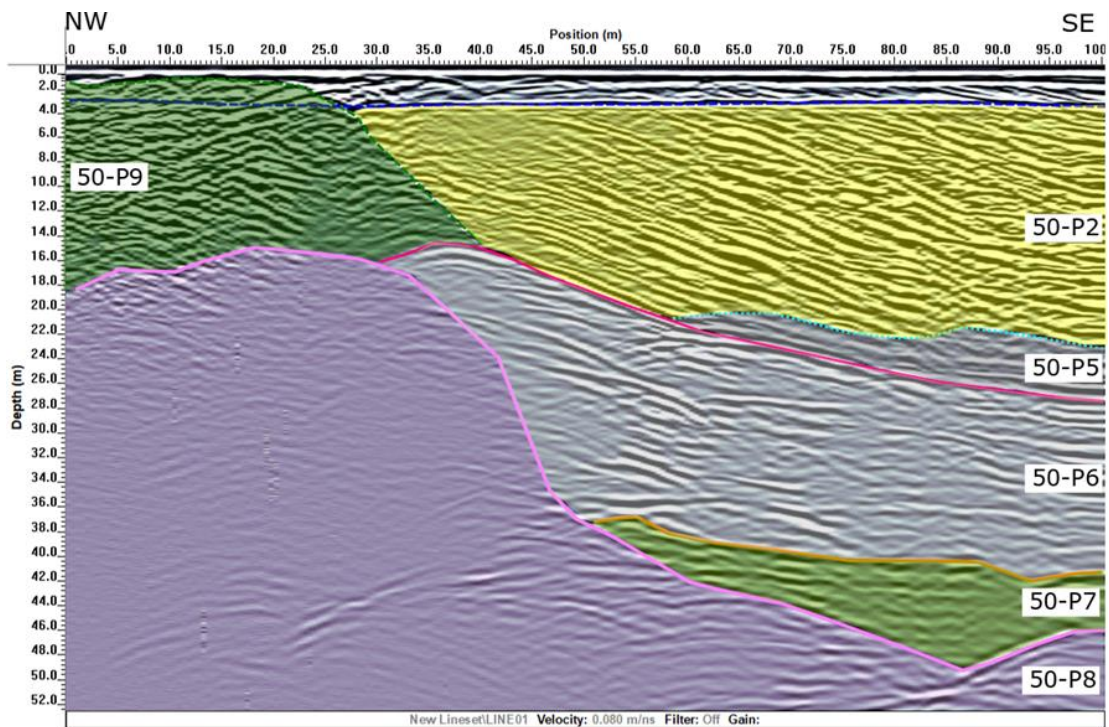


Figure 4-3 – Same radargram as Figure 4-2, with colored interpreted radar packages added to it. From top to bottom: Dark green = 50-P9, yellow = 50-P2, two grey packages=50-P5-P6, light green-50-P7, pink-50-P8. The colored lines represent bounding surfaces (radar surfaces) for top and bottom of the radar packages.

LINE 2:

Compared to Line 1, Line 2 also contains the strong, continuous, horizontal reflector across the entire radargram at approximately 3m depth (Figure 4-4). This reflector is marked as the same radar surface for all three 50 MHz profiles (blue stippled).

Line 2 is situated perpendicular to Line 1 and 3, hence perpendicular to assumed glacial meltwater flow direction. Because of this, the radar facies characteristics in the packages in Line 2 are expected to differ from the other two 50 MHz lines, even though the radar packages identified are of same origin.

The upper part of the radargram has strong, semi-continuous and, to some degree, horizontal layered radar signals between 4-22m depth. This package is accentuated with the yellow color (Figure 4-5), and named 50-P2. The radar package is corresponding to the yellow package in Line 1 (Figure 4-3).

Another primary set of radar signals is found in the lower part of the radargram between 21-38m. This area is dominated by weaker radar signals, but include continuous, stratified and horizontal reflectors. A comparison with Line 1 and Line 3 aided the subdivision of the lower part of Line 2 into three packages, whereas two of them are grey (50-P5 and 50-P6) and the lowermost package is light green (50-P7) in Figure 4-5. These are equivalent to the packages with the same names in Line 1 and Line 3.

The reason the pink colored package of 50-P8 is not present in this radargram may be due to the short depth extension of only 38m in the profile.

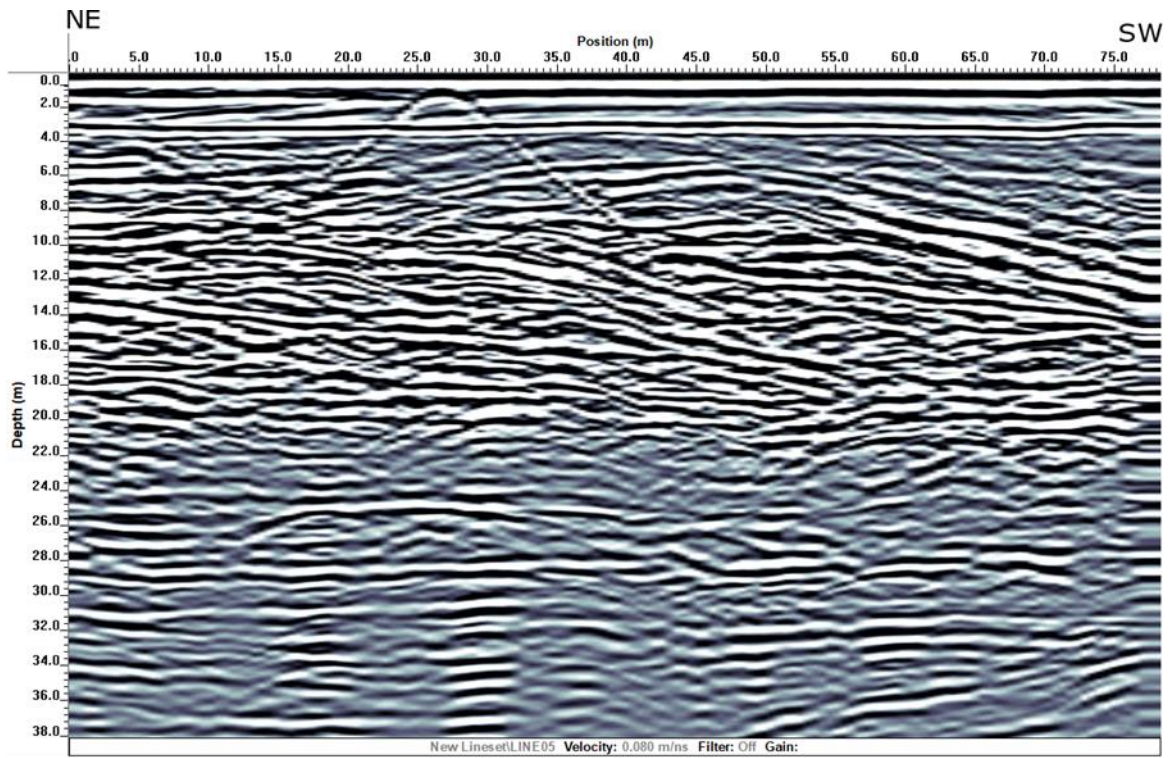


Figure 4-4 - Radargram from Line 2 of the 50 MHz profiles, without interpretations. The velocity for depth conversion is 0.08m/ns, no filters, with dewow and SEC2 gain (1, 1, 80) applied. The profile is penetrating 38m down and is 79m long.

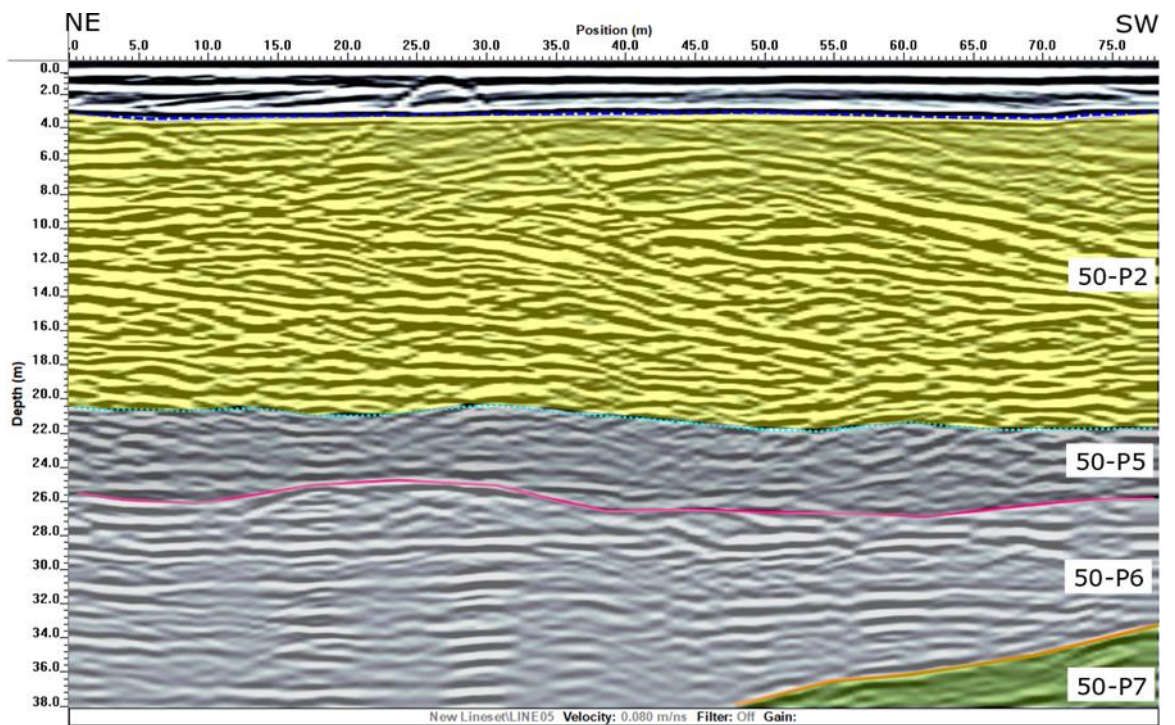


Figure 4-5 - Same radargram as Figure 4-4, with colored interpreted radar packages added to it. From top to bottom: Yellow = 50-P2, two grey packages = 50-P5 and 50-P6, light green=50-P7. The colored lines indicate radar surfaces bounding the packages.

LINE 3:

The uppermost continuous and horizontal radar signal at 3m is marked with a stippled blue line, similar to Line 1 and 2. Line 3 (Figure 4-6 and Figure 4-7) crosses the location of Grid 2, and the same five uppermost packages can be found in both surveys. The results for Grid 2 is presented in the next subchapter, but the coloring of the packages differs. This is because random colors with no association to geology were used for the interpretation and manufacturing of results for Grid 2. The only package with similar color is radar package 50-P2 (yellow) with a domination of dipping radar signals.

The first radar package catching the eye is the dark grey package of 50-P1 between 3-8m on the right hand side in Figure 4-7. This sequence with wavy/chaotic radar signals stands out from the adjacent radar package (50-P2), and it seems like package 50-P1 is cutting down into 50-P2. Package 50-P2 between 3-14m depth is colored yellow (Figure 4-7). The radar package show the same characteristics for Grid 2, Line1 and Line 3, which includes strong radar signals of parallel, clinoform reflectors dipping in South-East direction.

The clinoforms of 50-P2 are draping over the underlying sequences. These sequences include four grey colored packages with similarities regarding the radar signals, but changing signal strength, separated by reflection terminations in each subunit. The four grey packages are named 50-P3, 50-P4, 50-P5, and 50-P6 (Figure 4-7), reaching from 12m to 34m depth.

Below the succession of grey radar packages, a thin lens of radar package 50-P7 (light green) appears. The package has weak signals with a maximum thickness of 8m, and is overlaying a radar package of weaker signals; the pink 50-P8 radar package. The 50-P8 package is situated at the bottom of Line 3 (Figure 4-7), and extends from 36m to 46m depth.

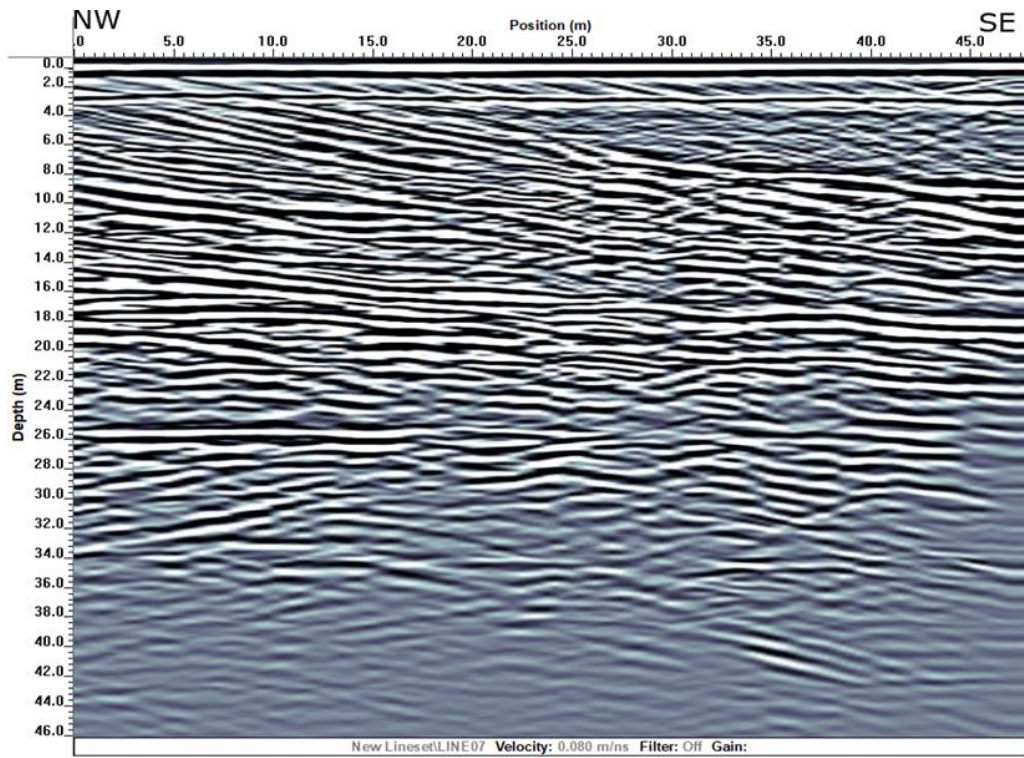


Figure 4-6 - Radargram from Line 3 of the 50 MHz profiles, without interpretations. The velocity for depth conversion is 0.08m/ns, no filters, with dewow and SEC2 (0.7, 1, 80) gain applied. The profile extends to a depth of 46m and is 48m long.

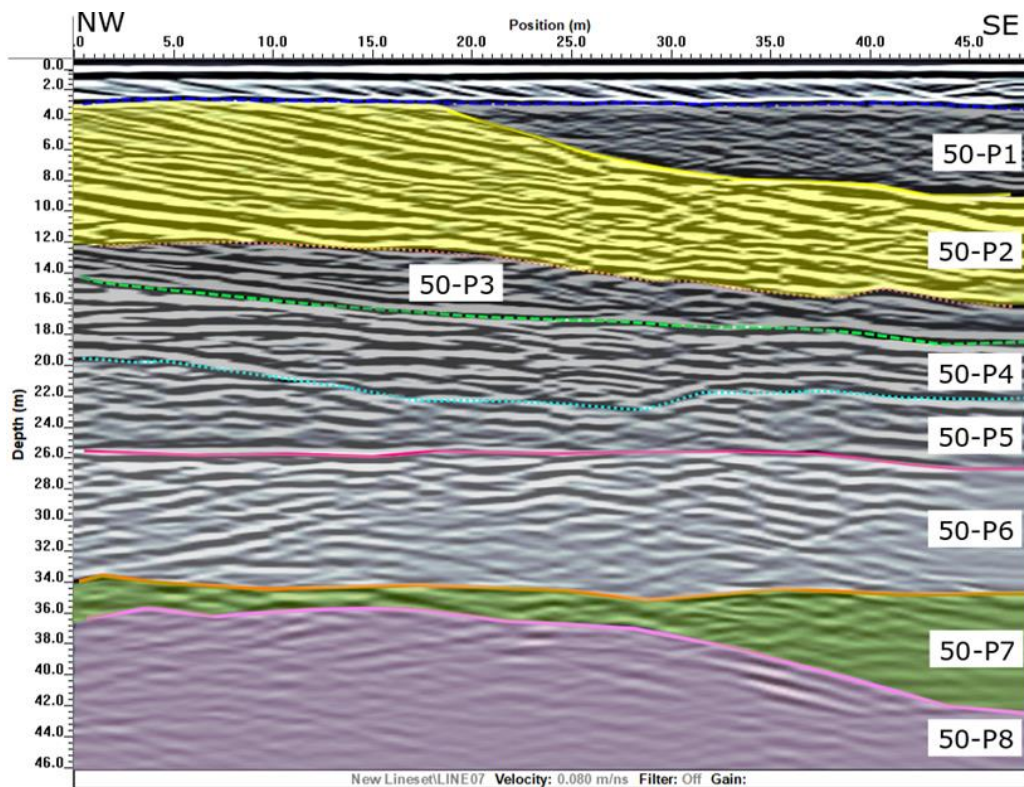


Figure 4-7 - Same radargram as Figure 4-6, with colored interpreted radar packages added to it. From top to bottom: Dark grey = 50-P1, Yellow = 50-P2, four grey packages = 50-P3, 50-P4, 50-P5 and 50-P6, light green = 50-P7, Pink = 50-P8. The colored lines indicate radar surfaces bounding the packages.

4.1.2 Radar Facies inside Radar Packages – 50 MHz Profiles

In this subchapter, the dominating radar facies for each radar package in the 50 MHz profiles are presented (Table 4-1). Description of each radar facies is guided by Neal (2004) (see Ch. 3.4 in methods). Radar facies identification is step number two towards interpreting what type of subsurface deposits the identified packages are, and their depositional origin.

The small sections of radar facies presented in Table 4-1 are obtained from different 50 MHz lines. The radargram location, from which the small section is extracted, is specified in the table with coordinates referring to position and depth on stated 50 MHz line. To get a perspective of the positions for the different radar packages in the subsurface, Figure 4-8 illustrates the interpreted cross sections and their correct geographical positioning relative to each other under the surface of the gravel pit.

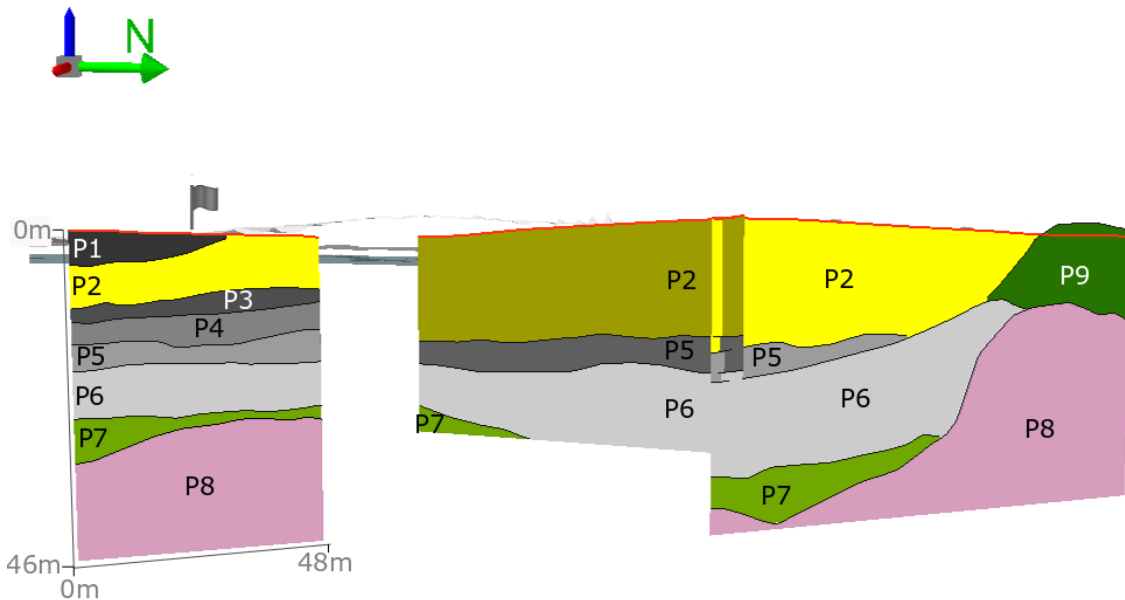








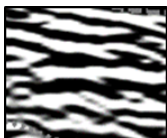


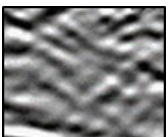

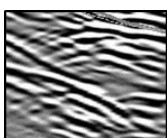
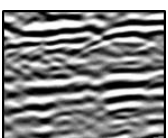

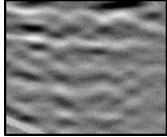

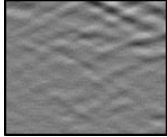




Figure 4-8 - Line 1 (right), Line2 (middle) and Line 3 (left) of the interpreted 50 MHz profiles seen from the subsurface of the gravel pit. The interpreted radar packages are colored and marked with package numbering. The flag to the left indicates position for water well 4 on the surface by Bø River. ArcScene was used to generate this 3D model.

Table 4-1 - (Left to right): Package name and color from the 50 MHz lines, together with dominating radar facies for each package and description of the radar facies. Coordinates under description represent what line the illustration of radar facies is obtained from, and what position (m) and depth (m) it has in the radargram.

Package name	Dominating radar facies	Description (coordinates)
50-P1 Dark grey 		Wavy, chaotic. Weak reflections (Line 3 - 42,6)
50-P2 Yellow 	 	Left: Continuous conform, high-angle, parallel, strong reflectors (Line 1 – 50,15) Right: Hyperbolic, chaotic, strong signals. (Line 3 - 30,11)
50-P3 Grey 		Hyperbolic and chaotic in-between continuous, semi-horizontal, conforming reflectors (Line 3 - 20,15)
50-P4 Grey 		Undulating and discontinuous strong reflections dipping in different directions, with some areas of chaotic signals (Line 3 - 15,20)
50-P5 Grey 	 	Left: Low-angled, conforming reflectors in-between chaotic signals (Line 1 - 95,25) Right: Chaotic and weak signals (Line 2 - 40,24)
50-P6 Grey 	 	Left: Strong, undulating reflectors mounding on top of each other (Line 1 - 60,26) Right: Strong, continuous, parallel/subparallel, horizontal signals, with surrounding weaker and chaotic signals (Line 2 - 55,32)
50-P7 Light green 		Very weak signals with a glimpse of horizontal, parallel signals (Line 1 - 85,45)
50-P8 Pink 		Signal free/weak crossing signals (Line 1 - 50,48)
50-P9 Dark green 		Highly chaotic/wavy, discontinuous, strong signals (Line 1 – 10,8)

4.1.3 3D Subsurface Model – 50 MHz Profiles

The result for the generated 3D model from 50 MHz profiles is presented in Figure 4-9, together with location of well 4 (white flag), and locations for surrounding drilling points included in the *geodatabase*. The 3D illustration in Figure 4-9 shows that there are several drillings in the gravel pit, of which can provide sedimentary information about the subsurface. This information is utilized in the discussion (Ch. 5).

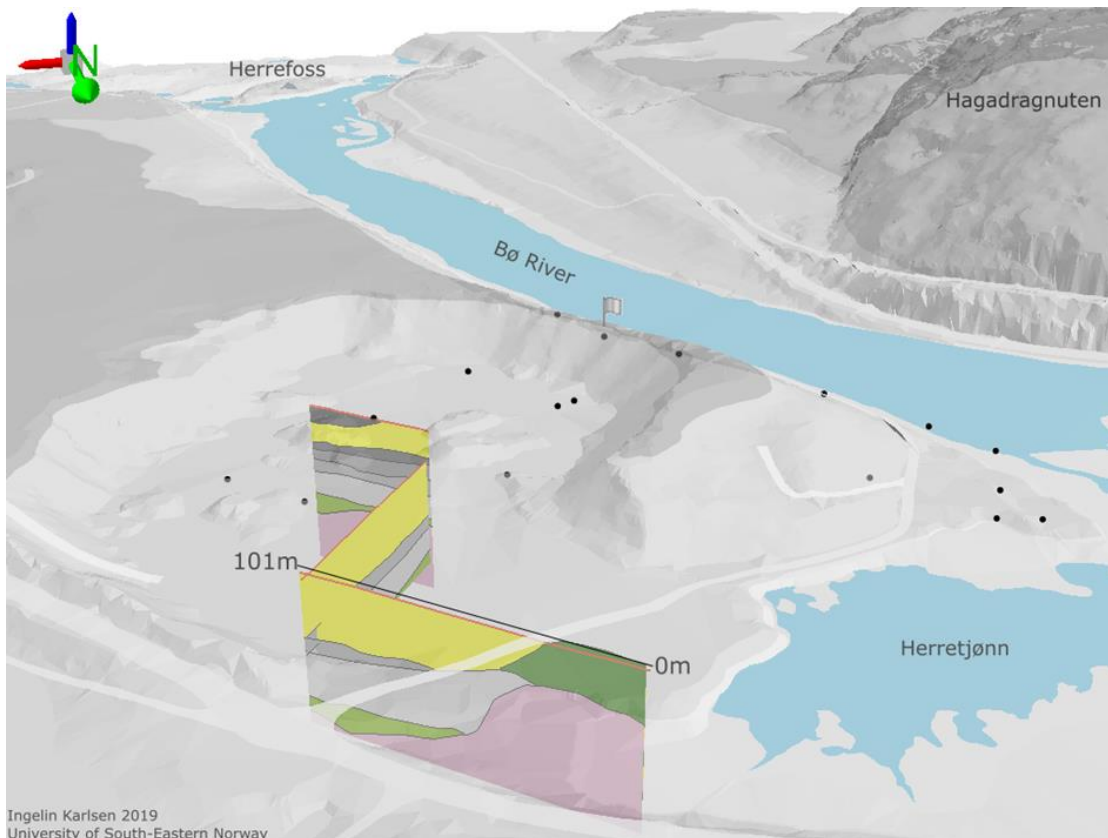


Figure 4-9 - 3D model of radar packages in the 50 MHz profiles, presented with correct geographical positioning under the surface of Verpe gravel pit. The white flag by Bø River is well 4, and all the black points are locations of surrounding probe- and test drillings from the geodatabase. The roads are draped over the Digital Terrain model (grey), and the three 50 MHz profiles reach from 118 m a.s.l and down in the subsurface. The illustration is generated with ArcScene.

Another relevant thing to review is location of Grid 2 relative to the 50 MHz profiles in Verpe gravel pit. This is demonstrated in Figure 4-10, showing that Line 3 of the 50 MHz profiles are positioned across Grid 2. This causes the results for Line 3 and Grid 2 to be similar, and can be compared when identifying radar packages. However, there will be differences between the results for these two surveys. First of all, Line 3 reaches a depth of approximately 46m, while the radargrams in Grid 2 only extends to a depth of 20.5m. Another difference is that the 100 MHz radargrams from Grid 2 provide more details than

the 50 MHz radargrams. Finally, Grid 2 presents the possibility to generate a 3D volume of the radar signals together with interpreted radar surfaces as the GPR lines are collected in a grid-formation (x-, y- and z- directions). This is not the case for the 50 MHz lines, as they only present two-dimensional cross sections in the subsurface.

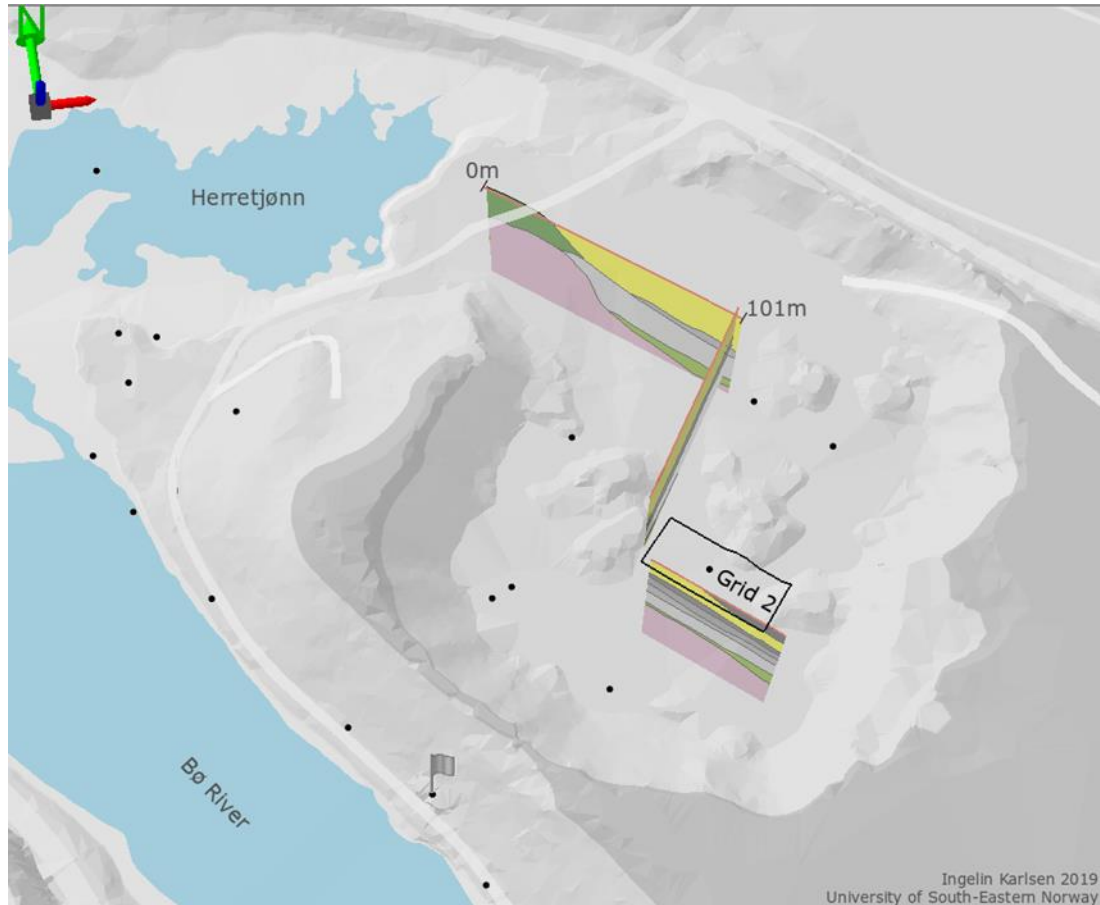


Figure 4-10 - Same scenery as Figure 4-9 with the study area seen from above, including the location of Grid 2 relative to the 50 MHz Line 1 (upper), Line 2 (middle) and Line 3 (lower). The flag indicates the position of water well 4, and the black points are locations for surrounding drillings included in the geodatabase. Illustration generated with ArcScene.

4.2 Grid 2 – 100 MHz

Grid number 2 is the innermost grid in Verpe gravel pit (Figure 4-11), 100m from Bø River and the water supply well number 4 for Bø municipality. The thick red line in the grid in Figure 4-11 indicates the sample radargram (XLine8) used to demonstrate interpretational steps in the next subchapter (Ch. 4.2.1).

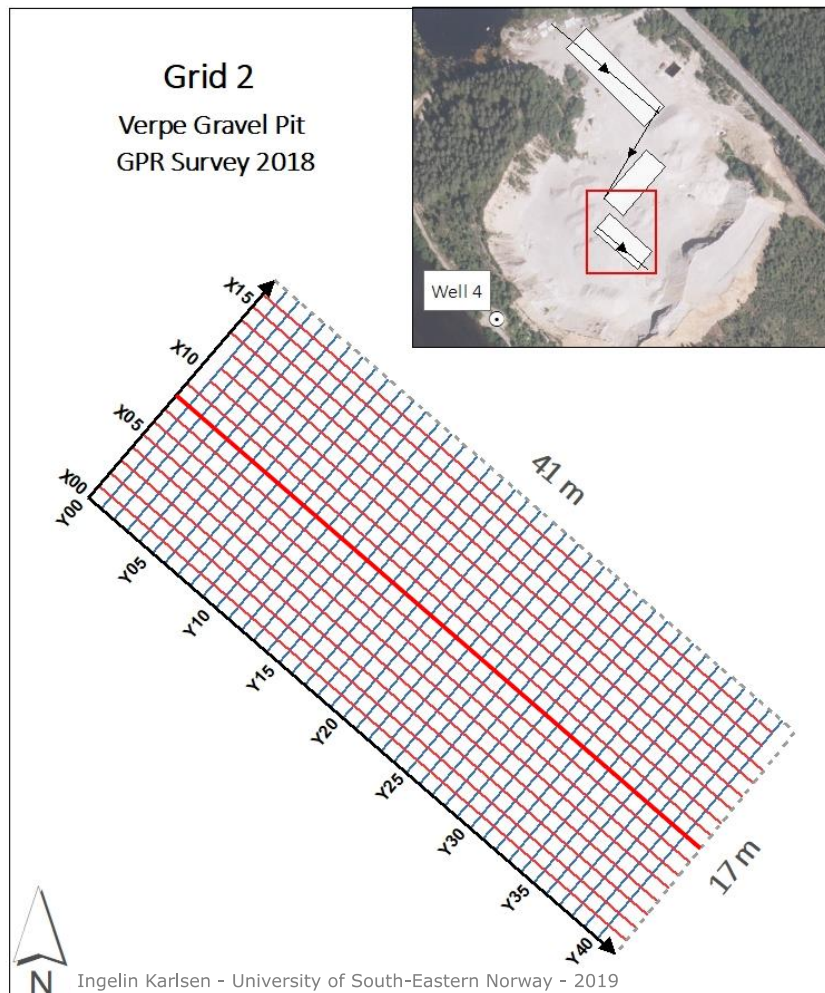


Figure 4-11 - Grid 2 with positioning of all lines (x,y), length of grid sides and overview map indicating position of Grid 2 in the gravel pit relative to water well number 4. The thick red line indicates the radargram (Xline8) used as specimen to visualize the interpretational process in the next subchapter.

4.2.1 Interpretation of Radargrams – Grid 2

XLine8 is chosen to represent the whole grid in this chapter because it is located in the center of the grid, and contains all the radar packages interpreted. See Figure 4-11 for the position of XLine8.

The radar signals in Figure 4-12 are easy to follow, and especially easy to notice is the continuous, horizontal radar signal at approximately 2.5m depth similar to the uppermost surface interpreted for all the 50 MHz profiles. The reflection is a negative phase peak (black-white-black), which indicates an increase in dielectric permittivity from above to below the continuous reflector (Baker et al., 2007). This reflector is indicated as the uppermost blue stippled radar surface (G2 – S1 – gwt) in Figure 4-13, and represents the uppermost bounding surface of the blue radar package (G2 – P1) in Figure 4-14.

On the right half of the radar profile in Figure 4-12, a trough-shaped package of wavy and undefinable radar signals stands out from the surrounding signals in the radargram. The package reaches from approximately 2.6m to 6m depth, and the bottom of the package has been interpreted as a truncational surface (G2 – S2 – ts) marked yellow in Figure 4-13. The scour-formed package has been given the light blue color (G2 – P1) in Figure 4-14.

From G2 – S1 – gwt and down to between 11-13m, a radar package of dipping parallel and tangential reflectors can be identified. The package starts with dipping, continuous reflectors on the left hand side of the radargram (NW), and ends up with more chaotic and hyperbolic signal configurations on the right hand side (SE) between 6-13m depth. The lower bounding surface for this package is marked as the green line (G2 – S4 – bs) in Figure 4-13, and the entire package is colored yellow (G2 – P2) in Figure 4-14 with the yellow and blue radar surfaces as top bounding surfaces.

A set of signals not so different from the signals in G2 – P2 are present below the green surface of G2 – S4 – bs. The signals are strong, generally discontinuous and alternately dipping in different directions. The package extends from the green line (G2 – S4 – bs) as top bounding surface, to a undulating bounding surface at the bottom marked as the dashed turquoise line between 14-16m (G2 – S5 – bs in Figure 4-13). The package (G2 – P4) between the green and turquoise radar surfaces has been added the green color in Figure 4-14.

A sequence of much weaker signals, with chaotic reflections, hyperbolic diffractions and some horizontal layering, appear at the lower half of the radargram, between 15-20m. This is the pink package (G2 – P5) in Figure 4-14. The upper bounding surface for this package is the dashed turquoise surface (G2 – S5 – bs) in Figure 4-13. The lower boundary is located at approximately 20m depth, and is marked with a pink line (G2 – S6 – bl).

The last feature interpreted is the mounding, convex surface at the bottom of the yellow (G2 - P2) radar package (Figure 4-14). The dipping reflectors inside P2 show a tendency of draping over this mounding package, and the red dashed convex line (G2 – S7 – Convex) in Figure 4-13 indicates the top bounding surface for this package, with the green line (G2 – S4 – bs) indicating the bottom bounding surface. The package is colored red (G2 – P3) in Figure 4-14, and contains slightly dipping, discontinuous reflectors with some wavy and hyperbolic features in between. This mounding package (G2 – P3) is roughly 4m thick at its highest peak.

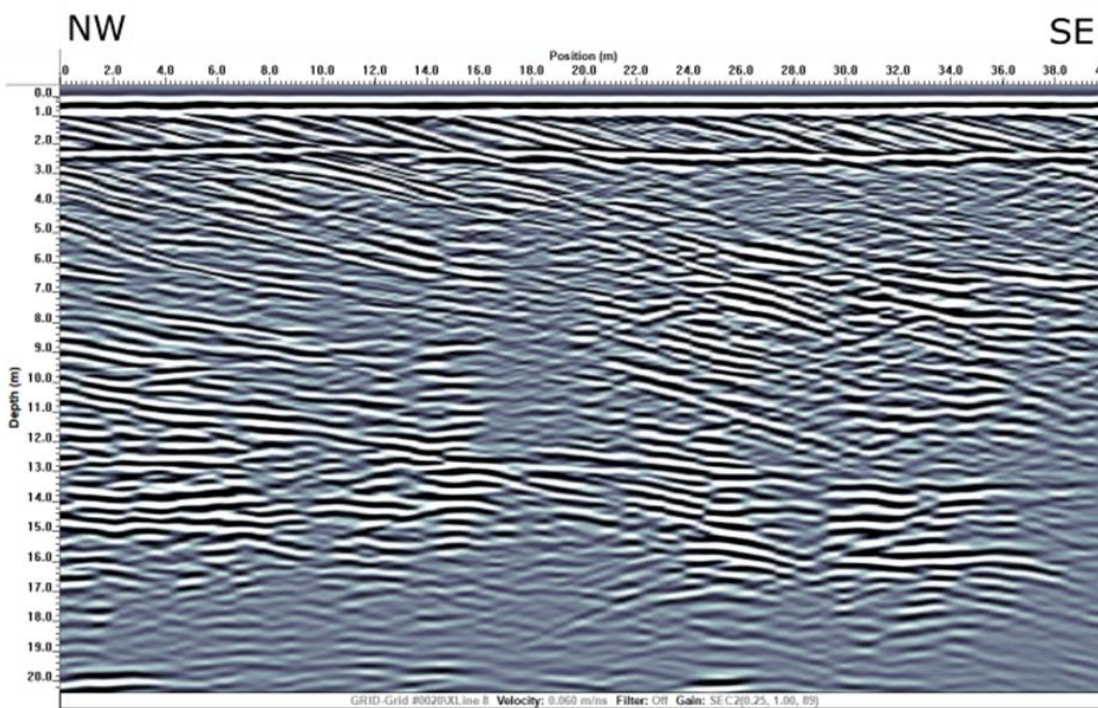


Figure 4-12 - Xline8 from Grid 2, without interpretations. The velocity for depth conversion is 0.06m/ns, no filters, with SEC2 (0.25, 1, 89) gain applied. The profile is penetrating 20m down, and is 40m long.

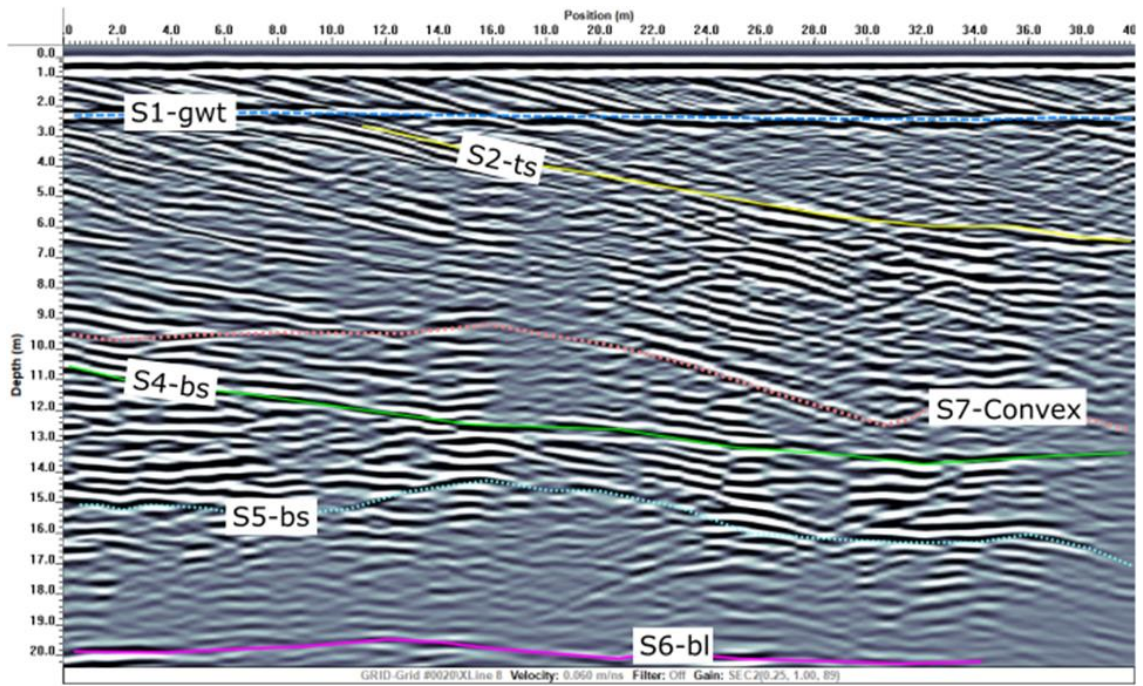


Figure 4-13 - Same radargram with same settings as Figure 4-12, with radar surface interpretations visualized. Blue = G2 - S1 - gtw, Yellow = G2 - S2 - ts, Red = G2 - S7 - Convex drape, Green = G2 - S4 - bs, Turquoise = G2 - S5 - bs, Pink = G2 - S6 - bl.

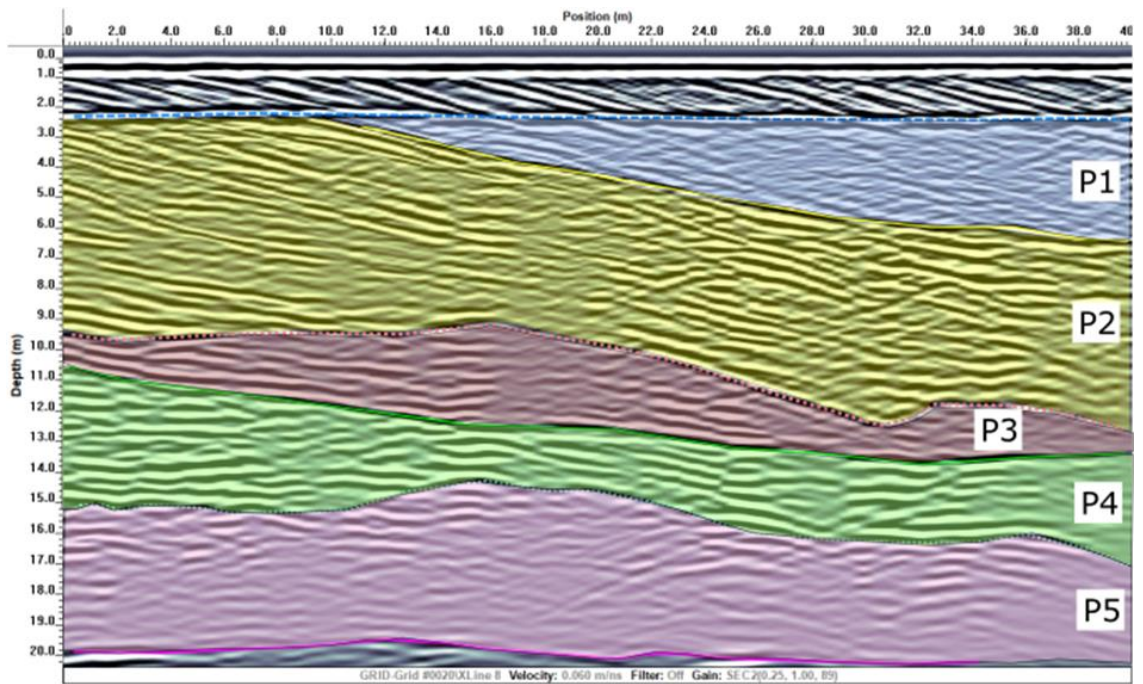


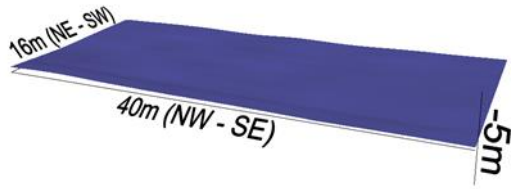
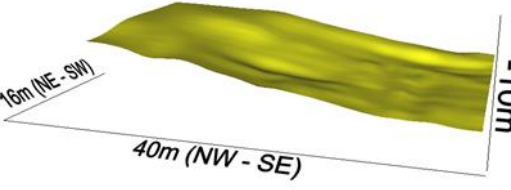
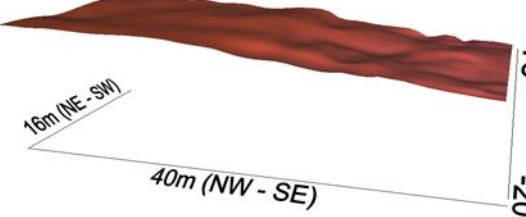
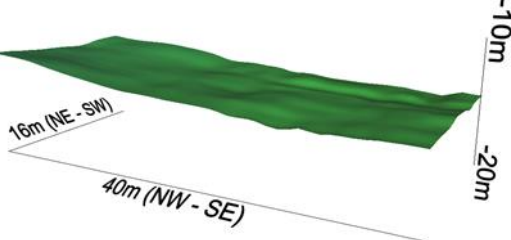
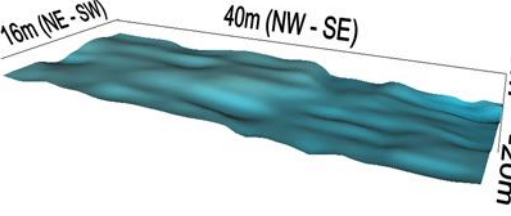
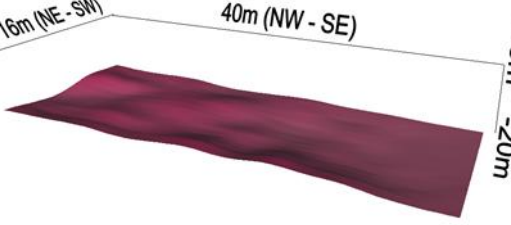
Figure 4-14 - Same radargram as Figure 4-12 and Figure 4-13, with added coloring on interpreted radar packages between the bounding radar surfaces. Blue = G2 - P1, Yellow = G2 - P2, Red = G2 - P3, Green = G2 - P4, Pink = G2 - P5.

4.2.2 3D Radar Surfaces – Grid 2

3D surfaces, representing top and bottom boundaries for radar packages, were generated for each interpreted radar surface in Grid 2. Table 4-2 presents the 3D shape for all interpolated radar surfaces found in Grid 2, with the short name for each surface, description of the short name and characteristics of the surfaces.

The different amplitude values (red, blue and white) in the 3D radar signal volume in Figure 4-15 give a good indication of dominating stratification patterns (radar facies) between the radar surfaces in Grid 2. The dominating internal radar facies for each radar package are presented later on. However, already in Figure 4-15, the differences in signal characteristics for each package between surfaces can be noticed. For example, the dipping radar signals in the yellow package P2 are easy to notice.

Table 4-2 - Short name, explanation for short name, 3D illustration from Voxler, and description of characteristics for each surface interpreted in Grid 2.

Surface name	Description	3D Illustration (Voxler)	Characteristics
G2 – S1 – gwt	Grid 2, Surface 1, Groundwater table		<ul style="list-style-type: none"> - Flat horizontal - Smooth - No inclination
G2 – S2 – ts	Grid 2, Surface 2, Truncational surface		<ul style="list-style-type: none"> - Slightly uneven - Through-shaped - Sloping S/SE - Flat at start/end
G2 – S7 – Convex	Grid 2, Surface 7, Convex draping		<ul style="list-style-type: none"> - Convex, mound. - Undulating and uneven surface. - Sloping from NW to SE.
G2 – S4 – bs	Grid 2, Surface 4, Bounding surface		<ul style="list-style-type: none"> - Relatively smooth - Slightly sloping from NW to SE
G2 – S5 – bs	Grid 2, Surface 5, Bounding surface		<ul style="list-style-type: none"> - Very uneven and undulating - Overall horizontal
G2 – S6 – bl	Grid 2, Surface 6, Base line		<ul style="list-style-type: none"> - Relatively smooth - Horizontal with some irregularities

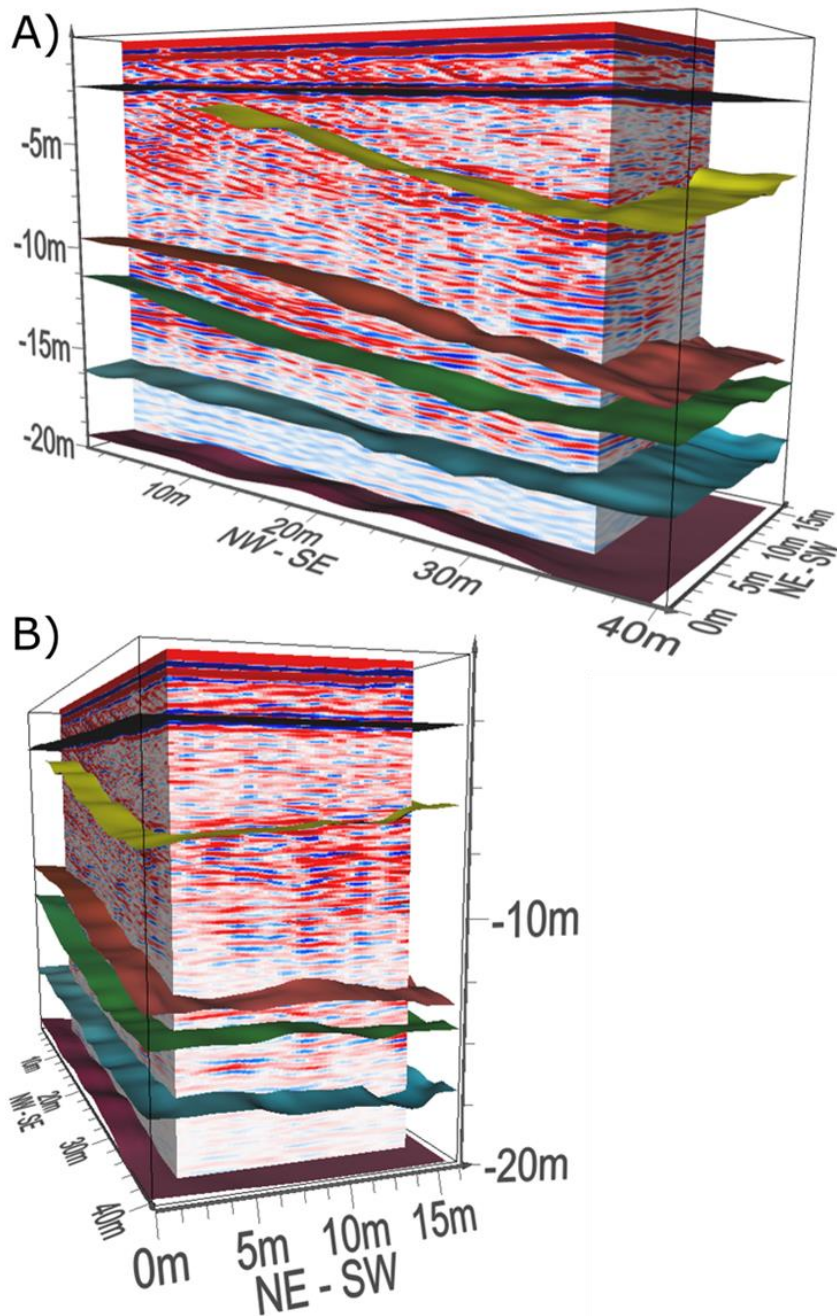


Figure 4-15 - Radar surfaces from Grid 2 together with a FaceRender 3D volume with amplitude values for GPR signals in blue, white and red. Blue = negative amplitude, red = positive amplitude and white = amplitude value of zero. A) Cross section along Xline-direction of grid 2. B) Cross section along Yline-direction.

Figure 4-16 presents the interpolated radar surfaces from *ArcScene* in relation to each other. The blue/turquoise color on surface G2 – S5 – bs is, unfortunately, not identical for the presentations in *Voxler* and *ArcScene* due to lighting difficulties when exporting the 3D model from *ArcScene*.

As the top purple surface is almost perfectly horizontal, the inclination of the surfaces beneath are easy to see. The yellow surface (G2 – S2 – ts) stands out from the other surfaces as it seem to be sloping in more than one main direction, and is described as a truncational surface bounding the bottom of radar package P1 (trough/scour-infill) presented in Table 4-3.

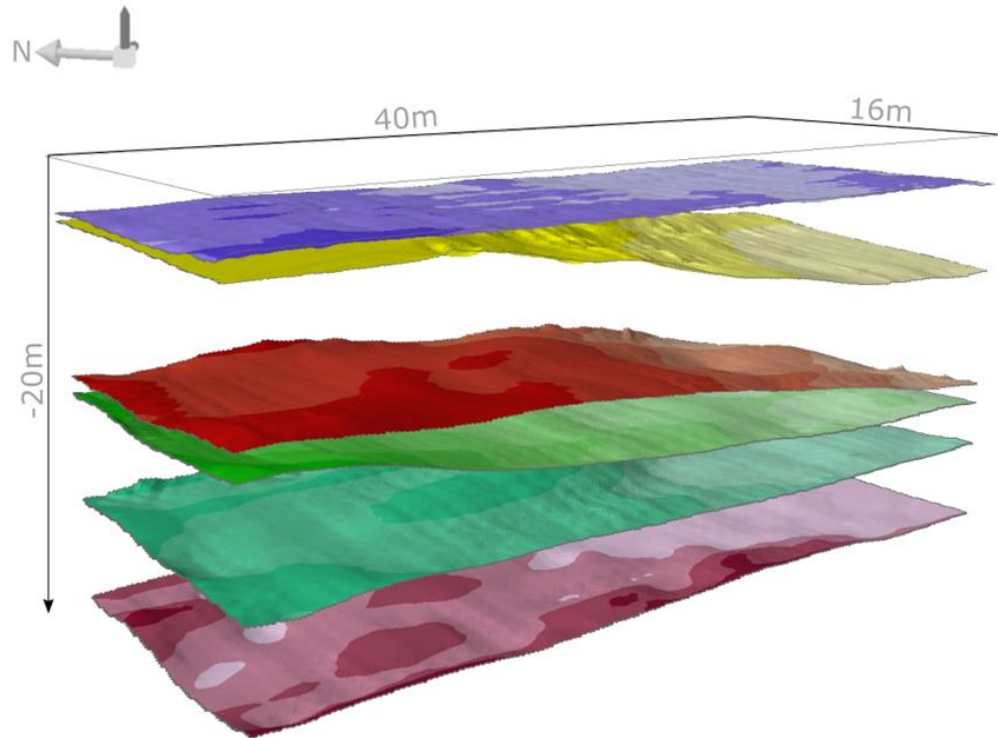


Figure 4-16 - 3D surfaces from Grid 2 interpolated and visualized with ArcScene. Purple = G2-S1-gwt. Yellow = G2-S2-ts. Red = G2-S7-convex drape. Green = G2-S4-bs. Turquoise = G2-S5-bs. Pink = G2-S6-bl.

To see if the yellow radar surface has a different sloping orientation than the other surfaces, the tool “*Surface Aspect*” in *ArcScene* was utilized. The tool was applied to the yellow (G2 – S2 – ts) and green (G2 – S4 – bs) surfaces in order to do a comparison. The result for the yellow surface (G2 – S2 – ts) is presented in Figure 4-17. The analysis reveals that the surface is mostly green and turquoise, which, according to the *AspectCode* in the figure, symbolizes a sloping orientation towards South and Southeast. This differs from the *Surface Aspect*-analysis of the green surface (G2 – S4 – bs), which indicates a domination of yellow and green on the surface, symbolizing sloping orientation towards East and South-East (Figure 4-18). The sloping orientation for the green surface can be assumed to represent the sloping orientation of the dipping radar facies between yellow (G2 – S2 – ts) and red (G2 – S7 – Convex) surfaces (radar package P2 in Figure 4-19).

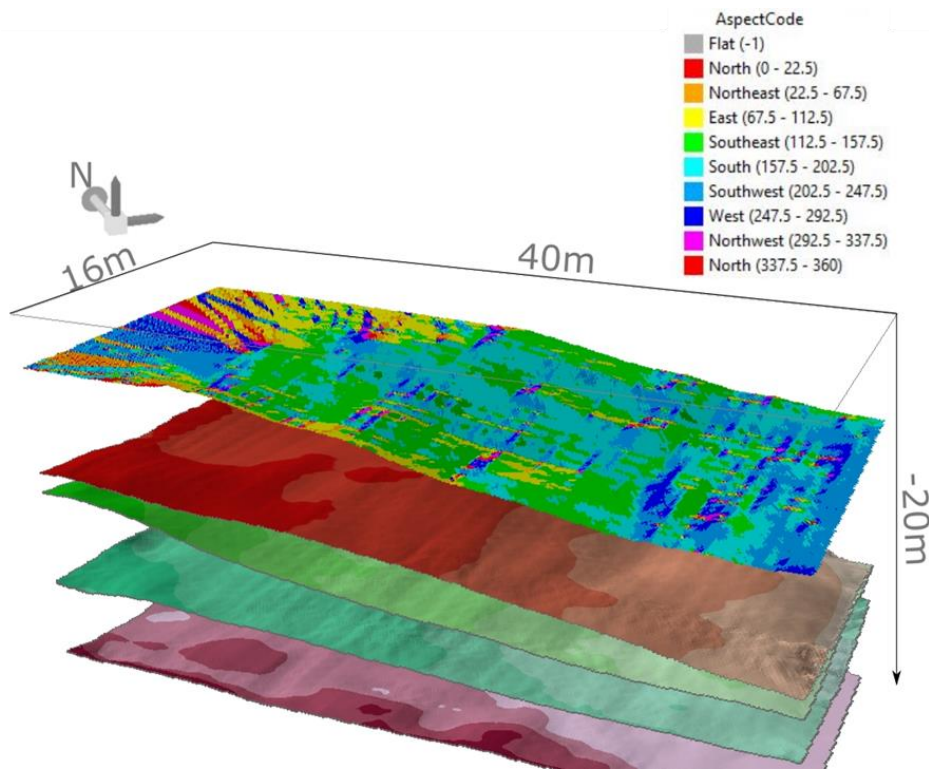


Figure 4-17 – Presentation of results from Surface Aspect analysis on G2 - S2 - ts, with colors representing the orientation of which the surface is inclining. Aspect codes with colors for different orientations are put in the upper right corner.

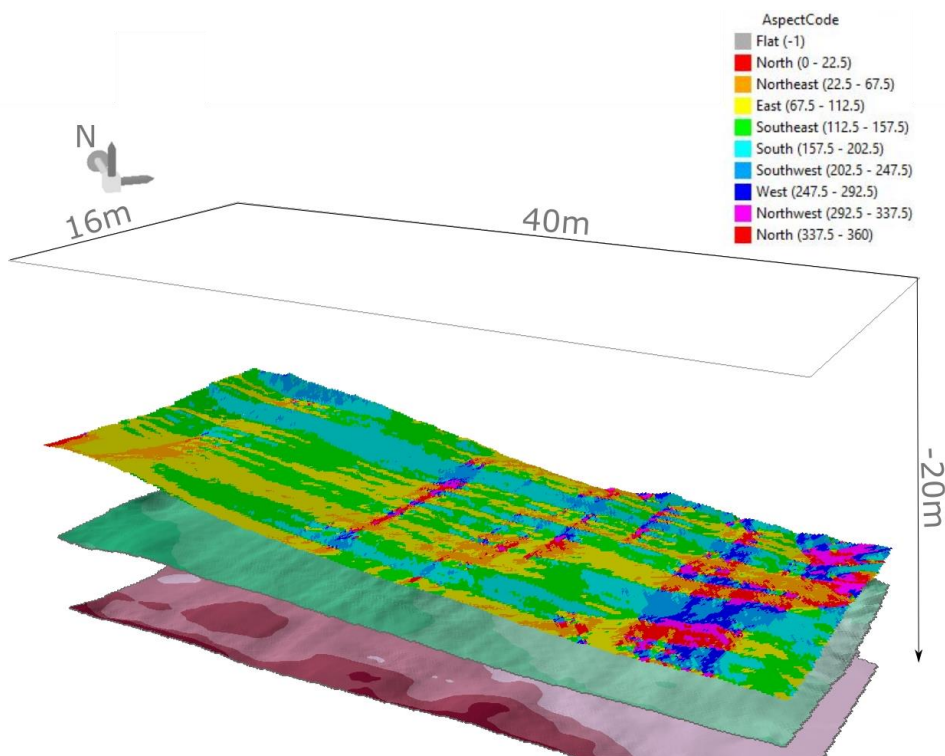


Figure 4-18 - Radar surfaces from G2 - S4 - bs and down, presenting results from Surface Aspect Analysis on G2 - S4 - bs with colors representing the orientation of which the surface is inclining. Aspect codes with colors for different orientations are in the upper right corner.

4.2.3 Radar Facies inside Radar Packages – Grid 2

After the identification and 3D interpolation of radar surfaces beneath Grid 2, the coherent radar packages were extracted between the surfaces. The resulting 3D model for all subsurface packages is presented in Figure 4-19 (seen from South). The packages are colored blue, yellow, red, green, and pink. The colors are randomly picked, except the yellow package of which is applied the same color as the corresponding radar package 50-P2 from the 50 MHz survey results.

The three-dimensional shape for all individual packages were isolated with *ArcScene*, and are presented in Table 4-3, with dominating radar facies for each package. The radar facies' sections are extracted from radargram *Xline10* (Appendix 9). Radar facies' presented in Table 4-3 are described with guidance from Neal (2004).

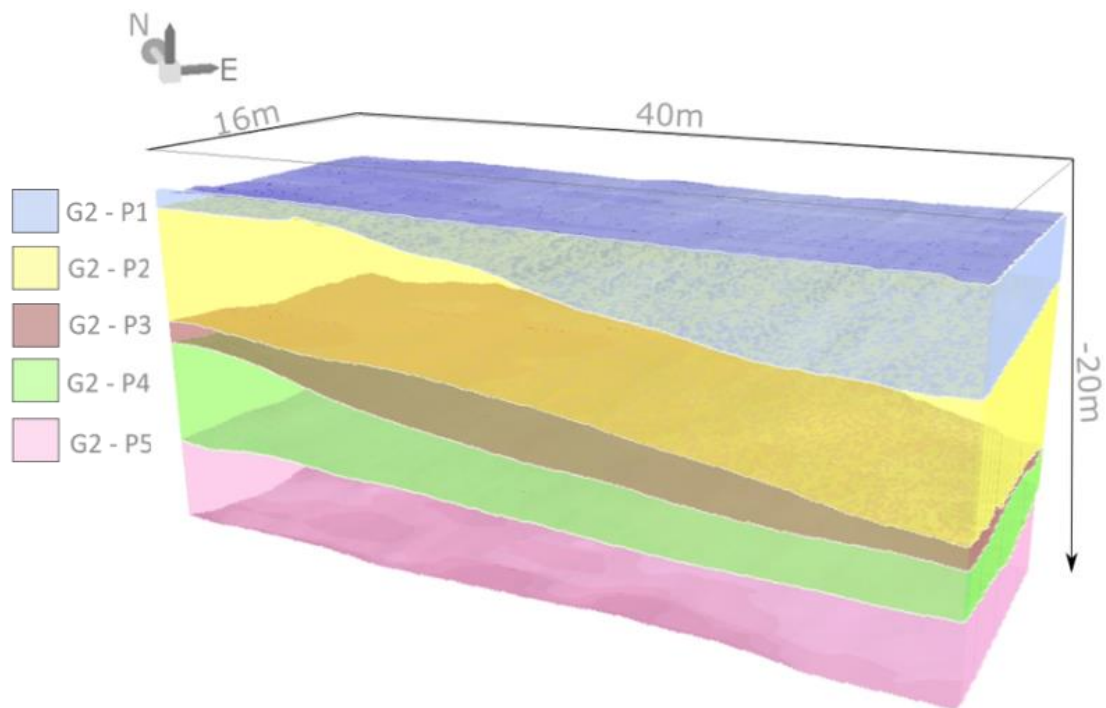
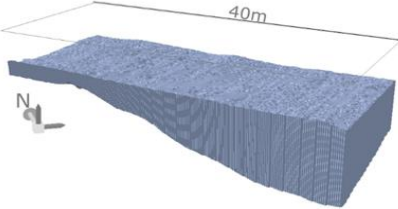
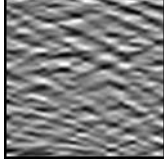
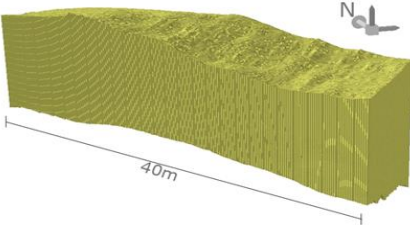
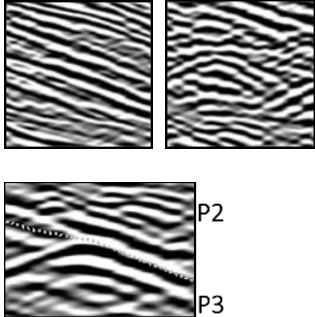
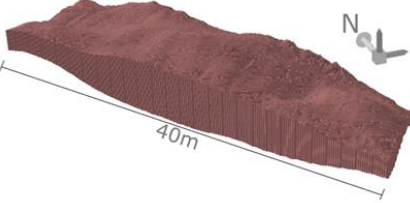
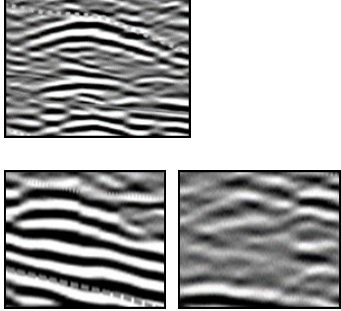
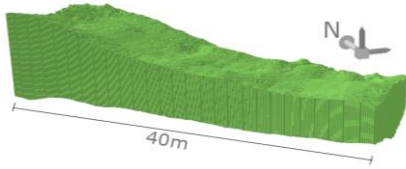
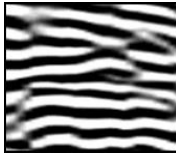
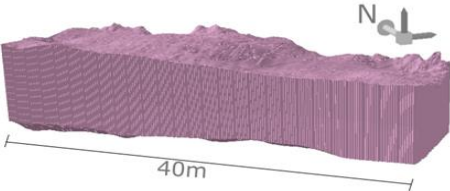
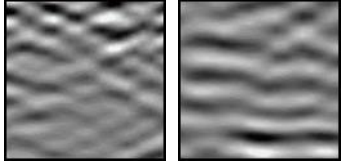


Figure 4-19 -3D model visualized with *ArcScene*, containing radar packages between radar surfaces from Grid 2, seen from south towards north. Blue = G2 - P1. Yellow = G2 - P2. Red = G2 - P3. Green = G2 - P4. Pink = G2 - P5.

Table 4-3 - 3D radar packages, dominating radar facies and description of the facies. 3D shapes are two times vertically exaggerated. Sections of radar facies is extracted from Xline10 in Appendix 9.

Package name and 3D shape Two times vertical exaggeration	Dominating radar facies (x-lines)	Description (Xline10: Position(m), Depth(m))
G2 – P1 (Trough/Scour-infill) 		Wavy, chaotic (36,3)
G2 – P2 (Wedge) 		Left: Continuous, dipping parallel (10,5) Right: Hyperbolic, chaotic (28,8) Continuous reflectors draping over P3 (30,10)
G2 – P3 (Lens) 		Hyperbolic at the end (down slope) (26,11) Left: Continuous, semi horizontal reflect(8,10) Right: Chaotic / reflection free (18,10)
G2 – P4 (Wedge) 		Alternating reflections dipping in different directions (8,14)
G2 – P5 (Sheet) 		Left: crossing signals and reflection free (30,17) Right: Weak, semi- continuous, horizontal parallel (10,16)

5 Discussion

A subsurface investigation, with the geophysical method GPR, has been carried out to give insight to Hagadrag unconsolidated aquifer. The GPR survey generated good quality radargrams serving as an excellent foundation for radar stratigraphic analysis. The radar stratigraphic analysis resulted in identification of nine unique radar packages (P1-P9) with description of different radar facies configurations for each of them. The identified radar packages have been modeled for 3D visualization, and georeferenced to give a good indication of what the subsurface beneath Verpe gravel pit in Hagadrag aquifer looks like. The last step of the radar stratigraphic analysis is to discuss lithofacies and depositional origin for each radar package, and finally suggest a depositional development for the identified subsurface deposits.

5.1 Glaciomarine Sedimentation at Grounding Line

As a premise for discussing the results, it is assumed that the study area during Late Weichselian was a part of a drowned glacial valley, or fjord, and that the sedimentary environment involved a glacier front terminating in the sea. This assumption can be supported by, most of all, Jansen (1983), by whom the illustration (Figure 2-4) of theorized development of sedimentation in Bø Valley during the last deglaciation was made (Ch.2.2). His theory and illustration is used as a premise for several relevant studies from the same area (e.g. Aarnes, 2015; Klempe, 2010; Langeland & Moe, 2003; Lavik, 2017).

At the point of contact between the sea and the ice margin, the meltwater outflow supplying sediments to the sea will lead to formation of subaquatic outwash fan or grounding-line fan (Powell, 1990). According to Lang et al. (2017), such subaqueous fans are deposited by meltwater jets discharging from meltwater tunnels at the grounding line of a glacier into a water body. If submarine fans in a proximal glaciomarine environment get to grow freely because of a stationary ice front, the fan can reach the sea surface and take form as an ice-contact delta (Bennett & Glasser, 2010, p. 319). This fits well with Jansen (1983)'s illustration of a stagnating ice front at a narrowing across Bø Valley. The narrowing is assumed to start by Hagadragnuten, adjacent to the study area for this thesis (Verpe gravel pit), and continue inwards to Lake Seljord. This threshold at Hagadragnuten can represent a grounding-line zone, of which have affected the formation of subsurface sedimentary successions in the area.

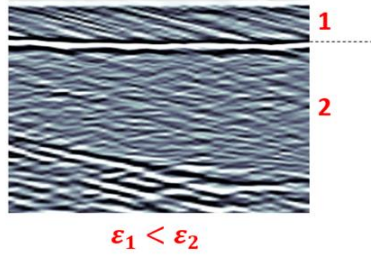
The eleven key processes comprising glaciomarine sedimentation according to Bennett and Glasser (2010), presented in Ch. 2.2, will be used as reference sedimentary processes when discussing lithofacies for the radar packages and their depositional development.

5.2 Interpretation of Lithofacies and Depositional Environments

Nearby drillings with sedimentary information from the *geodatabase* will be used as guidance to what grain sizes the different sequences may contain, thus a map including position of the drilling points is presented in Figure 5-4. It is important to have in mind that the velocity of EM-waves in the subsurface chosen for the 50 MHz radargrams (0.08m/ns) is only an average estimate, as the compositions of sediments in these radargrams are very complex and heterogeneous. The depth to targets may therefore vary with +/- 3-4m.

The first thing to notice is the uppermost strong, horizontal reflector that appears in all 60 radargrams, interpreted as the groundwater table. Figure 5-1 is put together from a radargram in Grid 2 to illustrate the principle behind polarity and strength of GPR signals, where the uppermost white-phased reflector is the assumed groundwater table. The strength and white phased properties of the reflector indicate that the EM-waves are traveling from a medium (1) with low dielectric permittivity, to a medium (2) with much higher dielectric permittivity. Larger difference in relative dielectric permittivity between the two adjacent mediums yields stronger radar signal reflections. From Table 3-1 (Ch. 3.2.2 p.27), the group of mediums with the lowest relative dielectric permittivity are unsaturated deposits, air and bedrock, and the group with the highest value of relative dielectric permittivity are saturated deposits, freshwater and seawater. Because we know from drillings in the area that the bedrock is much deeper, and because the reflector is strong, horizontal, continuous, and positioned approximately at the same depth in all examined radargrams, it is credible to say that this is the reflector for the groundwater table. This suggests that all the sediments below this line are saturated with groundwater, representing parts of Hagadrag groundwater aquifer.

Electric permittivity



From dry to wet soil = white phase reflection

Figure 5-1 - Section of radar signals taken from Xline01 in Grid 2. The illustration shows a white phase reflector appearing between a radar unit with low dielectric permittivity (1) and a radar unit with higher dielectric permittivity (2). This is based on the study of polarity of GPR signals (Annan, 2003).

5.2.1 Depositional Origin for Identified Radar Packages

The first unit deposited in a sedimentary sequence is the one at the bottom. Hence, interpretation of lithofacies in terms of sedimentary processes starts at the bottom with package P8, and proceeds upwards through P7, P6, P5, P4, P3, P2, P1, and P9. Figure 5-2 and Figure 5-3 was first presented in the results chapter, but are also presented here to make it easier to distinguish the different radar packages during the discussion. Figure 5-4 show the positions for surrounding drilling points in the *geodatabase*, which are used when discussing possible grain sizes from the different sedimentary packages. The ground surface in the gravel pit is elevated 118m a.s.l.

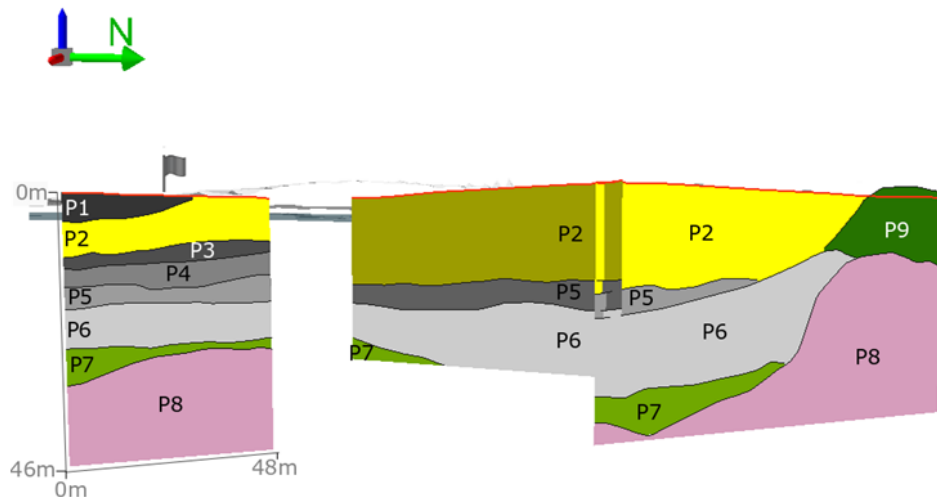


Figure 5-2 – Line 1 (right), Line 2 (middle) and Line 3 (left) from the interpreted 50 MHz profiles seen from the subsurface of the gravel pit. The interpreted radar packages are colored and marked with package numbering. The flag indicates the position of water well 4.

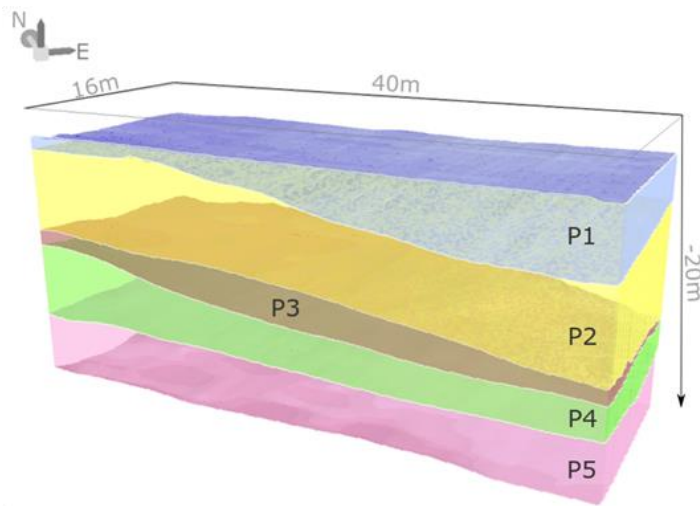


Figure 5-3 – Subsurface 3D model for Grid 2, with different colors and names for the individual radar packages. The colors are not correspondent with the colors used for radar packages in Figure 5-2, but the names for the packages are the same.

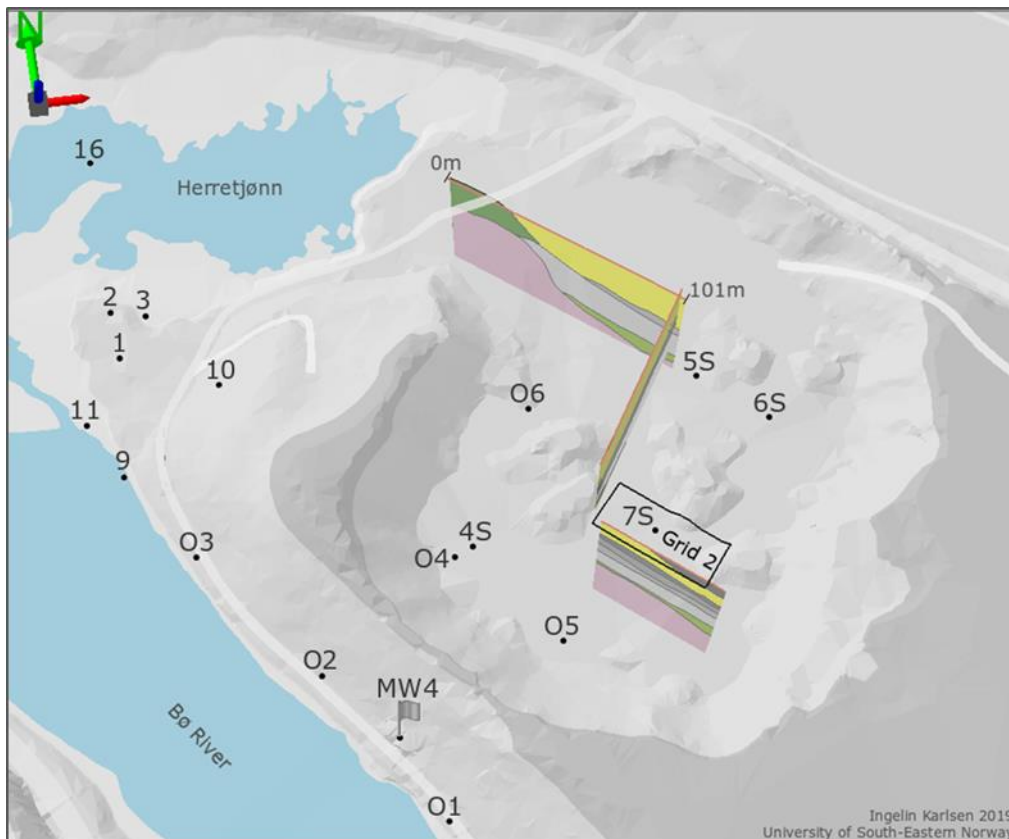


Figure 5-4 - 3D model from the interpreted 50 MHz profiles, together with surrounding drilling points from the geodatabase near the gravel pit. Line 1 is the uppermost, Line 2 is in the middle and Line 3 is the lowermost on the map. Water well 4 for Bø water works is marked «MW4». 3D visualization made with ArcScene.

P8 – BEDROCK

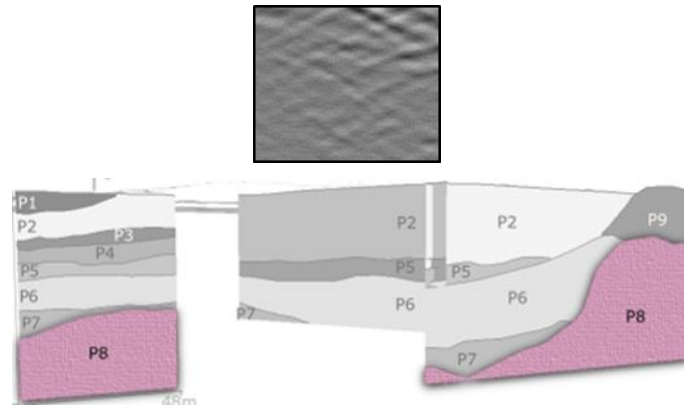


Figure 5-5 – Top: Section of dominating radar facies in radar package P8. Bottom: Highlighting of package P8 (pink) among the other identified radar packages from this survey.

Package P8 is only present in the deepest radargrams, Line 1 and Line 3 from the 50 MHz profiles, and bears the pink color in Figure 5-5. The package is overall reflection free, with weak, crossing reflectors in most of it, and the top horizon is quite undulating and situated between 15-50m depth (103-68m a.s.l). The sequence is interpreted as bedrock, which concurs with nearby drillings in the *geodatabase*. For example, probe drilling number 3 (Figure 5-4) is registered with possible bedrock at 19m depth. Test drilling in observation well O5 reaches down to at least 20m depth without hitting bedrock. This also applies for drilling O6, 5S, 4S, and O4, which has been drilled to between 20-23m depth without hitting bedrock. The packages above P8 seem to drape over the upper horizon of P8, which agrees with this being a bedrock, as the topography of bedrock in a valley controls the sediment-infill geometry (Eilertsen et al., 2006).

The steep bedrock cliff in Line 1 of the 50 MHz profiles (to the right in Figure 5-5), where the bedrock surface plunges from 94 to 81m a.s.l in 9m vertical distance, may be a part of the grounding-line threshold or valley sill adjacent to Hagadragnuten. The threshold would have controlled the sedimentary processes around it, and a glacial meltwater outlet is assumed to have been situated on top of it. Similar depositional sequences around bedrock thresholds have been described in several studies, which is used as comparison to the findings in this study (e.g. Eilertsen et al., 2006; Hansen et al., 2009; Lønne & Nemeč, 2011b; Lønne et al., 2001).

P7 – STRATIFIED TILL OR LODGEMENT TILL

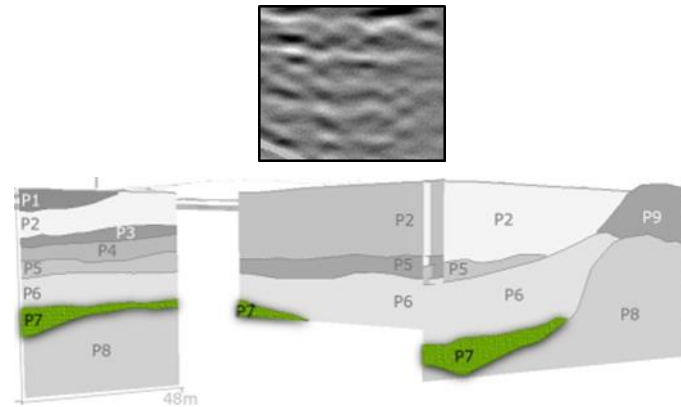


Figure 5-6 - Top: Section of dominating radar facies in radar package P7. Bottom: Highlighting of package P7 (green) among the other identified radar packages from this survey.

The sequence of weak and slightly layered depositional radar signal overlying the bedrock (green in Figure 5-6), is interpreted to be hard packed lodgement till or stratified tills from glacial outwash. The top surface of the package is between 34-42m, equivalent to 84-76m a.s.l, and its thickness varies between 1.5-9m. Comparison to the nearby drillings in the *geodatabase* show that drilling O6 encountered very hard packing at approximately 99m a.s.l. Drilling point 4S, situated close to Line 3 (Figure 5-4), hits a diamictic sequence at 95m a.s.l. The same applies for drilling 5S, close to Line 2, which hits a diamictic sequence at 99m a.s.l and down to 94m a.s.l (5m thick). According to Bennett and Glasser (2010, p. 324), it is hard to distinguish glaciomarine diamicts from glacial tills, especially in a radargram. One way to tell them apart is that waterlain diamicts are often stratified with graded bedding to some degree. The dominating radar signals for P7 show tendency of horizontal layering (top in Figure 5-6), which fits with Bennett and Glasser's (2010) description of glaciomarine diamicts. Glaciomarine diamicts belongs to key process number 1 of glaciomarine sedimentation; "*Direct deposition from glacier front of supraglacial and englacial debris at the ice margin*". Green et al. (1995) have also used the identification and term "stratified tills" to describe sedimentary packages among end moraine sediments from a glaciomarine environment.

The weak radar signals may be due to presence of fine sediments as silt/clay or glaciomarine muds in the glacial outwash. Such fine sediments belong to key process number 4 of glaciomarine sedimentation, which is "*Settling from suspended sediment introduced to the sea*". These finer sediments have a high attenuation of EM-signals (Table 3-1).

P6 AND P5 – GRAVITY FLOW OF ICE FRONT MATERIALS INTO STRATIFIED TILLS/DIAMICTS

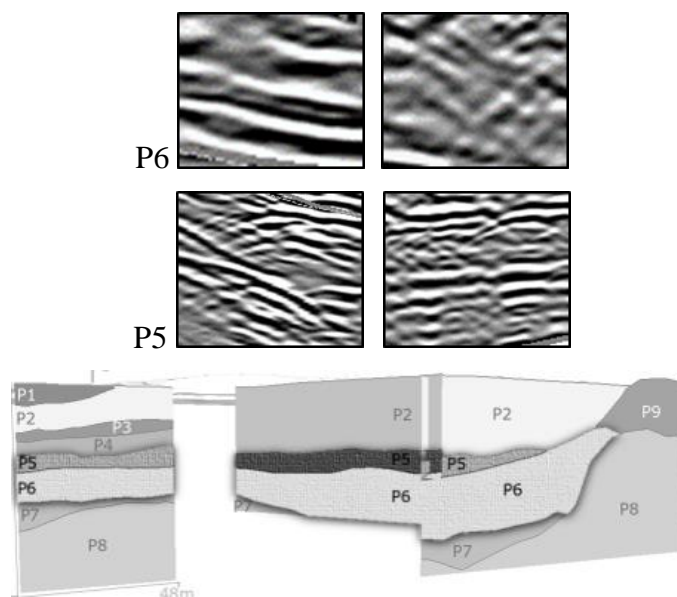


Figure 5-7 - Top: Sections of dominating radar facies' in radar package P6. Middle: Sections of dominating radar facies' in package P5. Bottom: Highlighting of package P6 (light grey) and P5 (darker grey) among the other identified radar packages from this survey.

The radar signal characteristics in package P5 and P6 are quite similar (top and middle of Figure 5-7), with P5 overlaying P6 as a smaller package with undulating upper sequence boundary.

Package P6 has strong reflectors with semi-horizontal layering, slightly sloping down towards South-East in the radargrams of Line 1 and Line 3. The package contains mounding radar signal characteristics terminating towards the bedrock cliff in Line 1 of the 50 MHz profiles, together with some weaker, chaotic and wavy signals in between the strong reflectors. The upper bounding surface for P6 plunges off the bedrock cliff in Line 1 at 15m depth (103m a.s.l), inclines down, and flattens out at approximately 26m depth (92m a.s.l) (bottom of Figure 5-7). Its thickness varies between 8-17m. The sequence is interpreted to be a mixture of number 1 and number 5 of the eleven key processes for glaciomarine sedimentation. Number 1 is mentioned above as direct deposits from glacier front, and number 5 is “*Subaqueous resedimentation by gravity flows, of which sediments may become unstable on steep slopes. This slumping or flow may result in a range of diamicts*” (Bennett & Glasser, 2010). P6 is thus a part of glacial dumping into the ocean, where the composition and nature of the sediments are controlled by the water discharge from the glacial meltwater outlet at the grounding line. The

horizontal layers are similar to the underlying unit, P7, but the signal amplitudes in P6 are much stronger. This may indicate less amount of fine-grained materials, which is plausible as P6 is closer to the assumed meltwater outlet at grounding line. Higher energy of water results in coarser sediments, and warm seasons comes with higher sedimentary flux as the glacier is melting. This suggests that the layering of alternating strong and weak signals in P6 can represent change in meltwater flux, thus varying sediment supply through warm and cold periods.

When the glacier oscillates in the same area for some time, the glacier front can build up huge ice-front accumulations as moraine ridges (Andersen et al., 1995). A buildup of such a ridge on the top of a fjord sill will eventually lead to overload of deposits, causing some of the deposits from the ridge to slide down the cliff and into the fjord as gravity flows. This may represent the connection between P9 (moraine ridge) and P6.

Sequence P5 has similar internal reflection configurations as P6, but smaller volume. The package is present in all radargrams, including Grid 2. Top surface of the package is found at 20-23m depth (98-95m a.s.l), with package thickness between 2-6m. The radar signals show less stratification and more chaotic, weak reflections. The chaotic signals, including hyperbolic diffractions, are prominent at the end of the slope towards South-East, and can represent a mixture of boulders and finer sediments together. The environmental setting, and the 3D external shape of P5 (Table 4-3), may suggest that this succession is a slump/slide of sediments overlaying P5, and belongs to number 5 of the key processes for glaciomarine sedimentation. P5 can be the start of a subaqueous grounding-line fan-buildup.

Continuous oscillation of the ice front at grounding line leads to an unstable ice-front environment, thus a lot of sediments slumping/sliding in to the fjord forming diamict deposits with chaotic fabric and deformed internal bedding (Eilertsen et al., 2006). Such gravity flows, in association with a subaqueous fan, are also commonly referred to as *debrisflow* (Hansen et al., 2009; Lønne & Nemeč, 2011b). Blikra and Nemeč (1998) define debrisflow as a type of sediment gravity flow, where the deposits from it are pebbly to bouldery with gravel beds ranging from matrix- to clast-supported. The composition of the debrisflow deposit depends on the composition of the source deposit of the avalanche, which in this case is a diamict moraine ridge (P9). Figure 5-8 gives an indication of what a low-viscosity/watery debrisflow deposit may look like, with lenticular beds with imbrication or stacking.

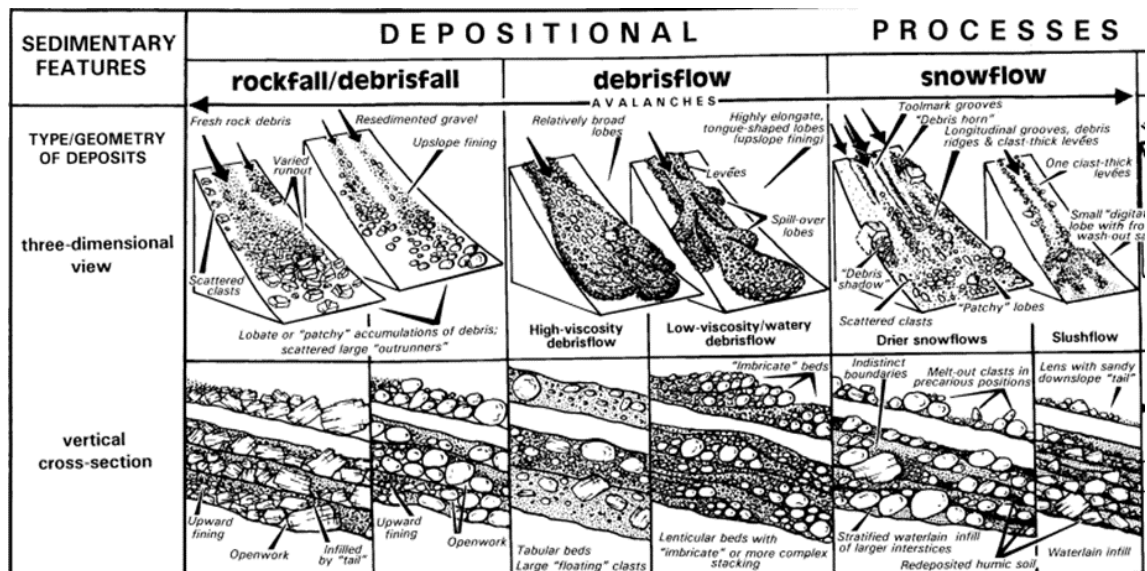


Figure 5-8 - Summary of main depositional processes and facies of colluvial fans/aprons, including debrisflow avalanches which represent the depositional process of radar package P5. [Illustration from "Postglacial colluvium in western Norway: depositional processes, facies and palaeoclimatic record" by Blikra and Nemeč (1998, p. 6), presented with permission from publisher John Wiley and Sons. Permission license number: 4582541490423]

P5 and P6 may be of the same origin and composition, but deposited in two different depositional events. The boundary between them is not prominent truncational, but rather a flat horizon with a strong reflector. This can indicate an energy shift of the meltwater flux into the fjord basin. The thickness of P5 and P6 together is between 11-20m. Comparing the results from this survey to nearby drilling logs in the *geodatabase*, one can find at least 5m of registered diamict deposits from 99m a.s.l and down in well 5S (Figure 5-4). Well 4S has observations of sandy moraine/diamict from 98m a.s.l and downwards. Other nearby drillings stops at approximately 20m depth (98m a.s.l), which is above many of the radar packages. This fits with Bennett and Glasser (2010, p. 318) suggesting that marine-based glaciers typically deposit tills between 5m and 20m, compared to terrestrial glaciers which only deposit 1-2m thick tills.

P4 – BOTTOM SET IN SUBAQUATIC FAN

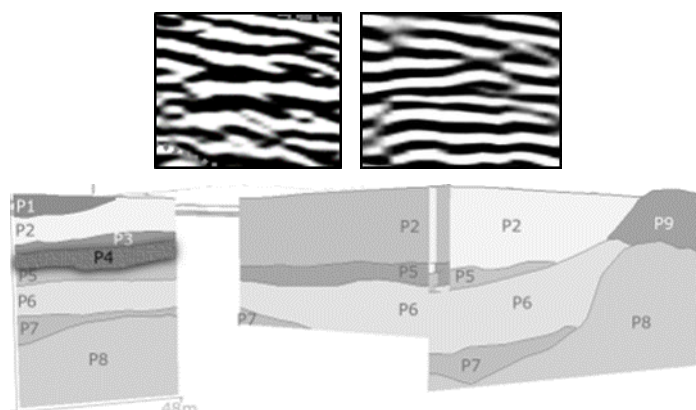


Figure 5-9 - Top: Sections of dominating radar facies' in radar package P4. Bottom: Highlighting of package P4 (on the left) among the other identified radar packages from this survey.

Package P4 has only been identified in Grid 2 and Line 3 (50 MHz profiles). The sequence is dominated by strong signals of undulating and, to some degree, discontinuous reflectors (top in Figure 5-9), slightly sloping towards South-East. Orientation of inclination for the upper bounding surface of P4 was analyzed with *ArcScene*. The result is presented in Ch. 4.2.2 (p.62), and show an average sloping towards East and South-East, the same direction as Bø Valley. This may also be the main meltwater flow direction, of which has been transporting and dumping sediments at the grounding line.

The majority of successions above P4 is a part of a prograding subaqueous fan succession; hence, P4 is interpreted to be a part of the bottom sets for these fan successions. The upper surface boundary for P4 is located between 14-18.5m depth (104-99.5m a.s.l), and ranges in thickness from 3.5m to 5.5m. Drilling logs with grain sizes from O6, O5 and O4 (Figure 5-4) in the *geodatabase* show coarse sand to fine gravel in a coarsening upwards sequence between 109-99m a.s.l.

As the bottom set (P4) is a part of the prograding subaqueous fan successions above, the depositional process is identified as number 3 of the eleven key processes of glaciomarine sedimentation, suggesting deposition from meltwater flow. Key process number 4 is also a part of the depositional process for P4, which includes settling from suspended material introduced to the sea. The formation of bottom sets by settling from suspension is supported by Bennett and Glasser (2010, p. 340).

P3 – GRAVITY FLOW/DEBRISFLOW DEPOSIT

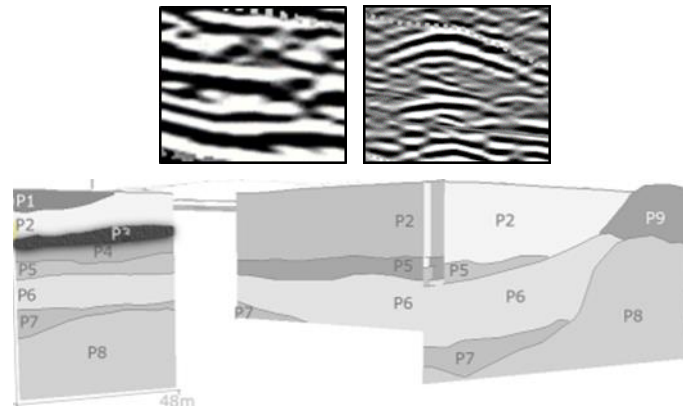


Figure 5-10 - Top: Sections of dominating radar facies' in radar package P3. Bottom: Highlighting of package P3 (on the left) among the other identified radar packages from this survey.

The 3D external form of package P3 is a mounding shape with apex in the middle (Figure 5-3), and decreasing thickness in both South-East and North-West direction. The package comprises hyperbolic and chaotic signals among strong and continuous reflectors (top left Figure 5-10), and has a top surface between 12.5m and 15.5m depth (105.5-102.5m a.s.l.). The thickness of the package is <4m and is sloping in South-East direction. The hyperbolic signal characteristics at the end of the slope in P3 are interpreted to represent boulders (top right Figure 5-10). The package is identified as a deposition from a slumping/gravitational process, number 5 of the eleven key processes for glaciomarine sedimentation, where the weaker and chaotic signals in between the stratified reflectors may indicate finer sediments as silt and fine sand. P3 could be the first sequence of the prograding fan succession, hence may be included in the larger fan succession of P2.

The boulders indicated by hyperbolas, at the end of the package, are also present at the end (downslope) of package P2. It can be discussed whether these hyperbolic signals are part of a push moraine from an earlier position of the ice front, and that the subaqueous grounding-line fan is terminating into this moraine ridge. This theory is a part of the illustration in Figure 5-18 from Bennett and Glasser (2010). Another suggestion is that the hyperbolic signals represents boulders transported to this position by gravity falls or avalanches from the valley side, which is number 6 of the key processes for glaciomarine sedimentation. There are no drillings in the *geodatabase* close enough to Line 3 to be able to say what the package may consist of.

P2 – SUBAQUATIC GROUNDING-LINE FAN (DELTA)

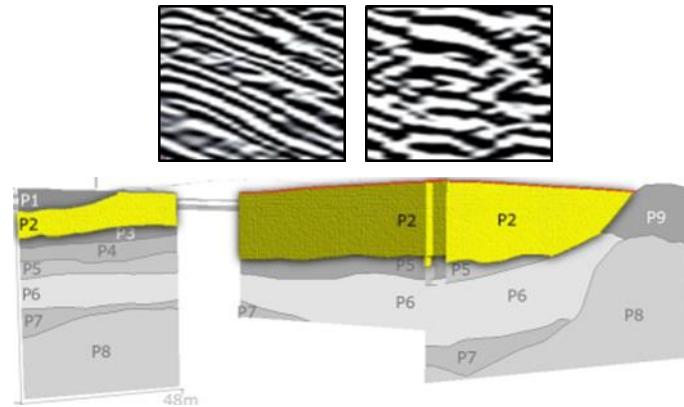


Figure 5-11 - Top: Sections of dominating radar facies' in radar package P2. Bottom: Highlighting of package P2 (yellow) among the other identified radar packages from this survey.

P2 is set to start at the groundwater table at approximately 3m depth (115m a.s.l), except for the locations where P1 truncates P2 (bottom left line in Figure 5-11). The package is confined by the moraine ridge (P9) in North-West (bottom right in Figure 5-11), and has a ranging thickness between 6.5m and 20m. P2 is dominated by continuous, conform and strong radar signals with parallel, high angle inclining layers (top left in Figure 5-11). These inclining, parallel layers are typical for delta foreset beds, and the package is thus interpreted to be a subaquatic grounding-line fan. Subaqueous grounding-line fans have a steep gradient of alternating progradational sequences, caused by rapid sedimentation close to the meltwater outlet (Bennett & Glasser, 2010, p. 337). Such fans develop close to the point where meltwater emerges from a glacier, confirming a former position of meltwater outlet at the bedrock threshold (at P9 in Figure 5-11). This grounding-line fan includes number 3 of the key processes for glaciomarine sedimentation, stating deposition from meltwater flows into the sea. Also key process number 5 of subaqueous resedimentation by gravity flows is a part of package P2.

Because the survey is conducted this close to the previous meltwater outlet, the subaqueous fan deposits contain little or no fine sediments as clay/silt. This is probably why the radargrams have very good penetration ability, providing strong signals with little attenuation.

Figure 5-12 show distribution of grain sizes with depth from drilling points around the gravel pit. Data for the illustration are gathered from the *geodatabase*, with legend for grain sizes on the right hand side of the figure. Position for all drilling points is found in Figure 5-4. The trend of grain sizes worth to notice for P2, is the alternating beddings of

sand and gravel. These alternations are consistent from the top (118m a.s.l) and 20m down, providing good information about what grain sizes P2 may consist of. The lack of finer sediments as silts and fine sand is prominent through the drilling logs, which verifies the theory of these deposits being dumped close to the meltwater outlet. The fact that the grain size change almost every meter can be a result of variation in amount of meltwater supply into the fjord, caused by an advancing (cold period) or retreating (warm period) glacier front. Eilertsen et al. (2011) conducted a study in Holocene valley-fill sediments in Målselv Valley in Northern Norway, aiming to characterize different facies' and architectures related to ancient fjord-delta sediments. They describe the foreset beds as steeply inclined, tangential, laterally continuous, mainly sand to gravelly sand beds, with a thickness between 3- 27m. These identifications fit very well with the observations done in the subaquatic grounding-line fan (delta) of package P2.

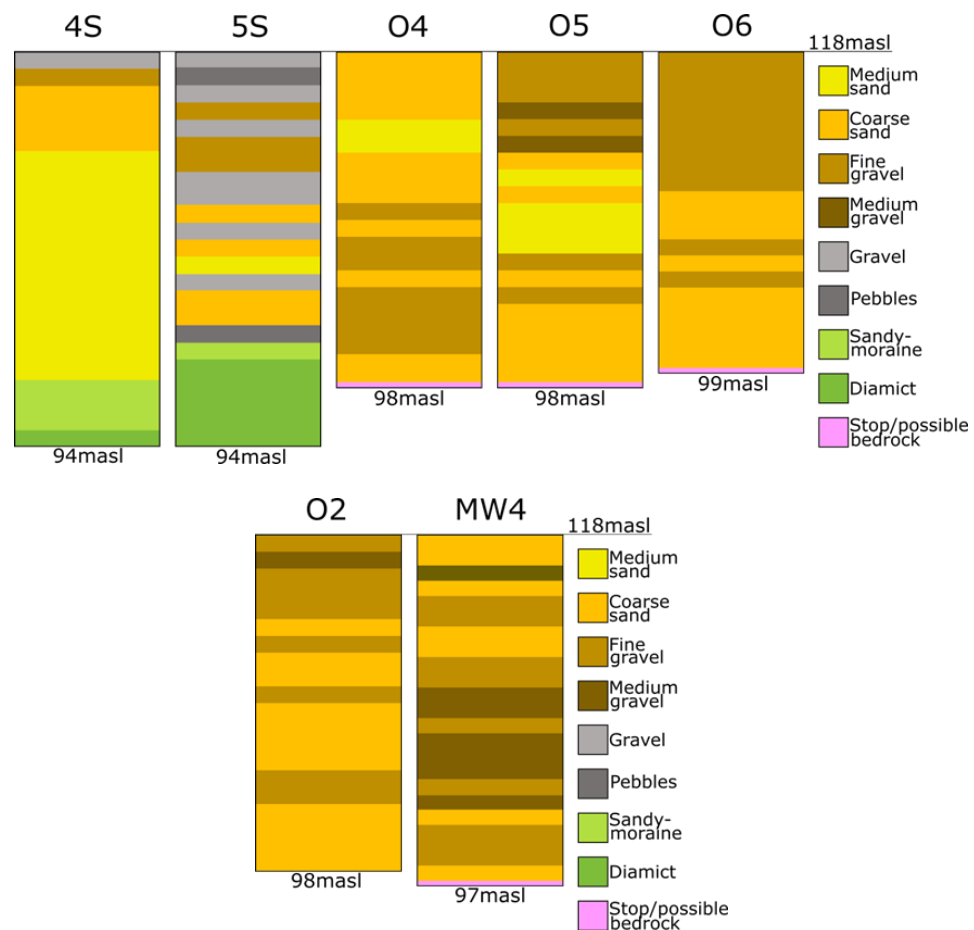


Figure 5-12 - Drilling logs with grain sizes from drilling points 4S, 5S, O4, O5, O6, O2, and MW4. Legend for colors on different grain sizes is put on the right hand side, and all logs start at approximately 118m a.s.l. The logs are illustrated from data registered in the geodatabase. Position for each drilling point can be found in Figure 5-4.

P1 – SCOUR POOL- OR KETTLE HOLE INFILL

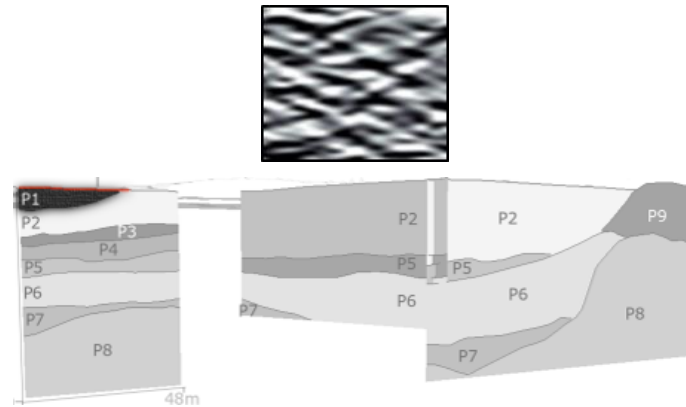


Figure 5-13 - Top: Section of dominating radar facies in radar package P1. Bottom: Highlighting of package P1 (black) among the other identified radar packages from this survey.

P1 is confined to the upper South-Eastern part in Line 3 of the 50 MHz profiles (bottom left in Figure 5-13), and in Grid 2. The lower sequence boundary of the package has a concave shape, truncating into the underlying deposits of P2. Thickness of P1 is <6m, and the upper boundary is undefined, as the gravel pit probably has been dug through the package. Dominating reflection patterns for the package is wavy and to some degree chaotic/poor (top in Figure 5-13). According to Huggenberger (1993), poor configuration can indicate massive, homogeneous gravel deposits, and hummocky/wavy reflection configurations can represent bedded gravel deposits. Because of the shape of P1, its truncation into underlying deposits and the internal structure standing out from adjacent packages, P1 is interpreted to be scour pool infills. The shape can also indicate a kettle hole. Drilling point 7S in the *geodatabase* is penetrating P1. The drill log is only 4m deep, and show gravel and pebbles all the way down.

Before the gravel pit was dug out to the extent of today, Jansen (1980) did a surface mapping of the quaternary deposits, including kettle holes. The outlines for these kettle holes were digitalized by Harald Klempe in 2010 for usage in ArcMap. A 3D map was put together, including interpreted subsurface packages from this survey and the digitalized kettle holes from Jansen's surface mapping. Figure 5-14 presents the result, where correlation between the outline of P1 and the kettle hole mapped on the surface is evident. Because the results from Grid 2 did not manage to capture the whole scour pool fill of P1, no conclusions can be made saying there is an absolute correlation between the mapped kettle hole and the interpreted package P1.

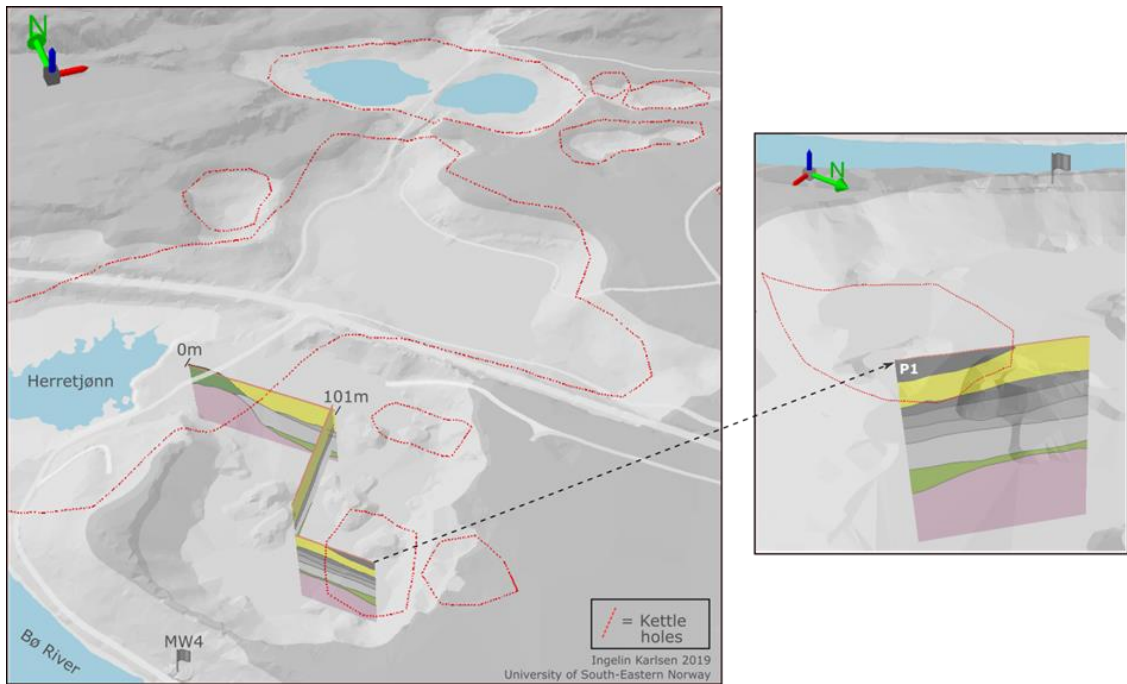


Figure 5-14 - Topographic map of Verpe gravel pit with 3D subsurface model of 50 MHz interpretations and Jansen's (1980) mapped kettle holes (red lines) draped on the DTM. The small map to the right is a close up of Line 3, turned 360 degrees relative to the left map.

P9 – ICE-CONTACT RIDGE (MORaine RIDGE)

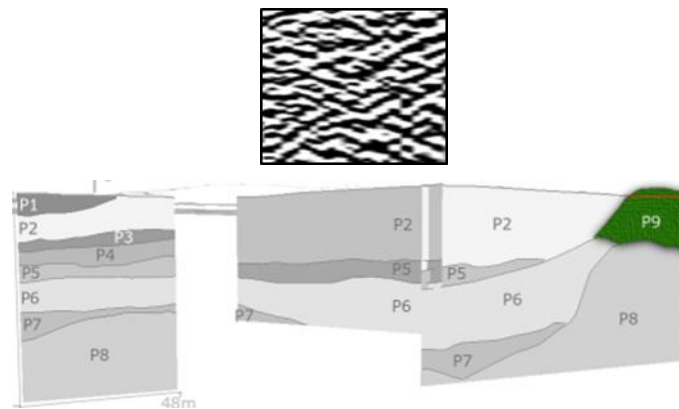


Figure 5-15 - Top: Section of dominating radar facies in radar package P9. Bottom: Highlighting of package P9 (dark green) among the other identified radar packages from this survey.

P9 is a prominent ridge in the start of Line 1 of the 50 MHz profiles, with highly chaotic/wavy, discontinuous, and strong internal radar signals (top of Figure 5-15). As the sequence is located on the top of the anticipated bedrock sill of P8, P9 is interpreted to represent the ice-contact ridge (moraine ridge) formed directly at the front of the fjord-valley glacier during periods of glacial oscillation and/or still stand. The ridge is up to 16.5m high, and has a connection with the gravity flow deposits of P6 (bottom right in

Figure 5-15), and the subaquatic grounding-line fan of P2. This is supported by Bennett and Glasser (2010, p. 319), suggesting that grounding-line fans may be associated with subaqueous push-moraines. The chaotic signals with hyperbolic diffractions can indicate a diamict composition with boulders and coarse sediments. There are no drilling points that can be directly used as indicator for grain size composition in P9.

5.3 Depositional Development for the Identified Subsurface Deposits

Line 1 of the 50 MHz profiles gives the most details regarding previous depositional environment (right side in Figure 5-2). The interpreted profile consist of a sill of bedrock (P8) in the previous glacial fjord, which also represent the grounding line for the glacier front. As the glacier stagnated at this grounding line, parallel with Hagadragnuten and Kupaþjónn, a massive ice-front accumulation built up in the former fjord. This ice-front accumulation of redistributed erosional material from glacial transport consists of an ice-contact ridge (moraine right of P9) proceeding out into the former fjord as a subaqueous grounding-line fan with gravity flows. Work from several researchers addresses a glaciomarine setting where an ice-contact ridge of diamict material evolves into a subaqueous fan/ice-contact delta (e.g. Aarseth et al., 1997; Bennett & Glasser, 2010; Eilertsen et al., 2006; Lønne et al., 2001).

There seem to be proof of several bedrock highs, or grounding-line zones, dividing the Bø Valley basin into separate accommodation spaces for sediment accumulation. One of these are Herrefoss waterfall threshold (lower red area in Figure 5-16), which sets a quite high erosional base level for Bø River. Another one is the bedrock sill detected in Line 1 of the 50 MHz profiles, most likely spreading out under the largest red area in Figure 5-16. In addition, a last bedrock high could probably be damming Lake Seljord, a theory discussed with Professor Harald Klempe. A study done by Eilertsen et al. (2006) about valley-fill stratigraphy and evolution of Målselv Valley is carried out in a very similar setting as Bø Valley. The study show that also in Målselv Valley, a sill with a waterfall is present. Eilertsen et al. (2006) characterized the sill as a local confining level for an upper basin in the fjord valley, which also seem plausible to apply to Herrefoss-sill with a sedimentary basin both above and below Herrefoss waterfall.

In short, the following twelve steps could represent the younger geological history for Bø Valley, with a focus on the deposits in the middle basin between Hagadragnuten and Herrefoss waterfall:

1. Excavation of U-shaped Bø Valley from numerous of glaciations. As the land was pressed down by a massive ice cap, the ocean entered the valley.
2. A layer of lodgment till deposited over the bedrock as the glacier was covering the valley, before retreating inwards.
3. The ice front stagnated in a narrowing part of the valley (Hagadragnuten), making direct contact between fjord- and proximal glacial environment (glaciomarine).
4. A variation between colder and warmer periods lead to oscillation of the fjord-glacier-front, building up a large ice-contact moraine ridge.
5. Meltwater outlet and pushing by the ice front at grounding line lead to glacial outwash deposits and gravity flow deposits, such as stratified tills and debris flow diamicts. Coarser sediments was dumped near the meltwater outlet, and finer sediments would be suspended and settled further out in the fjord.
6. During deglaciation, a high flux of redistributed material was flushed out from the subglacial tunnel by the grounding line and into the fjord as a subaquatic fan (delta).
7. A possible colder period may have caused readvance of glacier-front in the fjord, bulldozing and eroding into the preexisting sedimentary successions.
8. A hard packed layer of lodgment till was established on top of the preexisting underlying successions, now representing the floor of Verpe gravel pit.
9. A final deglaciation took place, and the glacier-front retreated inwards Bø Valley, followed by the ocean. The deglaciation lead to a new high flux of redistributed materials dumped into the fjord, building a delta up to the ocean surface (Herremo delta, 134m a.s.l and local marine limit).
10. A braided river system developed on top of the delta, with river courses that today can be identified as abandoned river channels on LiDAR maps (Figure 5-16).
11. Isostatic uplift after the ice-cap melted lead to a drastic lowering of base level. The fjord of Bø Valley became dry, and the river eroded into underlying successions, making fluvial terraces.
12. The most modern depositional processes is the erosion and depositions by Bø River, of which is still ongoing.

5.3.1 Conceptual Models for Glaciomarine Sedimentation

There are several conceptual models for glaciomarine deposits corresponding with the depositional history of the grounding-line environment examined in this thesis. Nevertheless, I have chosen to include three conceptual models for exemplification, with permission from each publisher. The model in Figure 5-17 is from Bennett and Glasser (2010), and presents a general model for assumed conditions in Bø Valley-fjord during formation of the deposits reviewed in this thesis. The conceptual model shows a fjord sill (Herrefoss) delineating the depositional fjord basin. All the eleven key processes for glaciomarine sedimentation, presented earlier, are present in the figure. In the illustration, the study area for this thesis comprises the *glacial dumping*, some of the *settling from suspension*, *outwash zone*, and *sediment flows*. The model does a good illustration on how grain sizes get coarser closer to the subglacial meltwater outlet, and finer in the distal parts of the fjord.

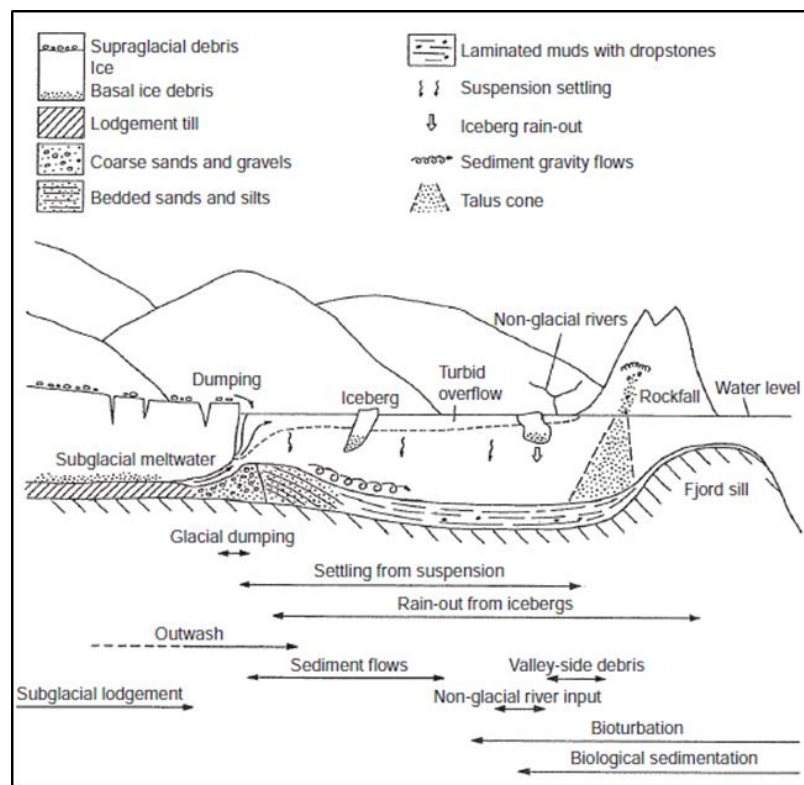


Figure 5-17 - Conceptual model diagram for sediment sources and processes within a glacially influenced fjord. The study area for this thesis is located within the zone for glacial dumping and sediment flows. [Model obtained from "Glacial Geology – Ice Sheets and Landforms, 2nd Edition" by Bennett and Glasser (2010, p. 318), with permission from John Wiley and Sons. Permission license number: 4577750498895]

Bennett and Glasser (2010) also present a more detailed approach to a conceptual model fitting this environment (Figure 5-18). The model does not take sea level change into account as this would give a very complicated model. The model shows how subaquatic push-moraines can originate, and how they interact with the buildout of glacial/marine muds, sands and diamicts in a glaciomarine environment. The accumulation of boulders observed as hyperbola diffractions at the end of the subaquatic fan in Line 3 and Grid 2, can be a part of such a push moraine, with sediment flow building up against it. The model also illustrates how the glacier can move on the top of preexisting sediments during a readvance, leaving a layer of diamict lodgment till. This layer is identified as the floor of Verpe gravel pit. Yet, the presence of a grounding-line threshold is missing in this model, which leads us to the last conceptual model used as an exemplification for evolution of identified successions in this thesis.

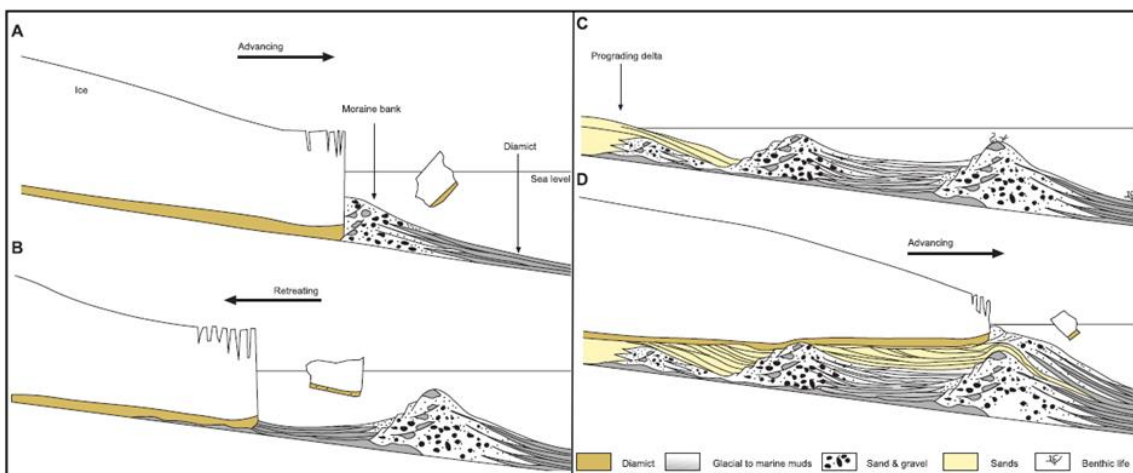


Figure 5-18 - Conceptual model for hypothetical facies architecture associated with retreat and advance of ice front in a marine fjord. The model can present a good example for evolution of the reviewed deposits in this thesis. [Illustration from “Glacial Geology – Ice Sheets and Landforms, 2nd Edition” by Bennett and Glasser (2010, p. 318), with permission from John Wiley and Sons. Permission license number: 4577750498895].

Figure 5-19 is made by Lønne and Nemeč (2011a) as an illustration of depositional processes in front of a tidewater glacier in a Spitsbergen fjord in Norway. The ice-contact submarine deposits in Bø Valley may have been formed under similar conditions. Section b) shows the processes during ice front advance, comprising sediment delivery into the fjord from subglacial beds, sediment outwash deposition by meltwater flow and formation and erosion of the ice-contact ridge above the grounding line. Section c) presents the final deposits after glacial advance and stillstand of glacier front. The deposits are very similar to all the interpreted successions in this thesis, including the

older deposits at the bottom of possible older moraine, which can be compared to package P7 with stratified tills. The only package of which is not present in any of the conceptual models is P1 with scour pool infill, assumed to be infill of a former kettle hole.

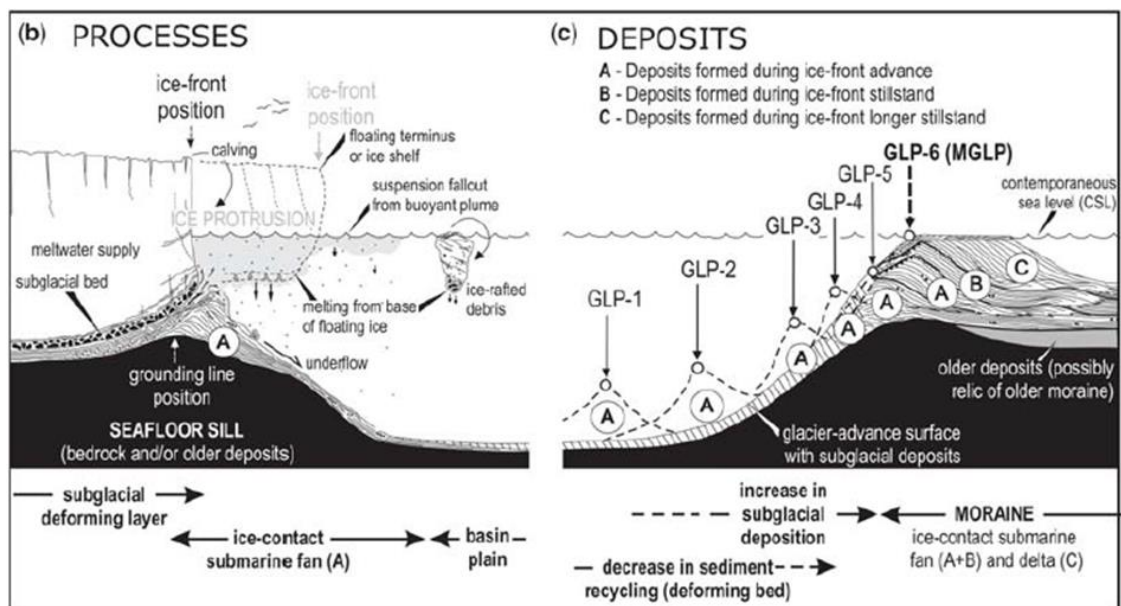


Figure 5-19 . Conceptual model for formation of ice-contact submarine deposits with the presence of a seafloor sill. The model includes processes taking place when the glacier front is situated right above the grounding line, and what deposits are formed during advance and stillstand. [Illustration from Open Access Article “The kinematics of ancient tidewater ice margins: Criteria for recognition from grounding-line moraines” by Lønne and Nemeč (2011a)].

5.3.2 Comparison to Maps of Superficial Deposits

In this master thesis, the results represent a three-dimensional geological model of the subsurface in the relevant area. This is in contrast with general mapping of superficial deposits, e.g. in Figure 2-3 where the mapped superficial deposits around the study area are presented. This map is put together by data gathered from NGU’s online national database for superficial deposits. NGU describe these data as representative for the main prevalence of deposits covering the bedrock, showing what soil type dominates the uppermost meters of the terrain surface (NGU, 2017). Taking a closer look at the map in Figure 2-3, the map show glaciofluvial deposits (orange) covering the whole study area, fluvial deposits and some marine/fjord deposits. Having the results from this thesis in mind, we know that the subsurface conceals a more complex depositional system. With the help of radargrams from the GPR survey and the use of an excavated gravel pit as study area, the survey was able to reveal the deeper geological conditions more detailed than the glaciofluvial delta described by Jansen (1983) in the same area. Beneath the

orange area of glaciofluvial deposits in the map of Figure 2-3, the subsurface conceals mainly glaciomarine deposits and diamicts/tills including a moraine ridge. This is important information, especially for creation of new water wells. The resulting 3D models from this thesis reflects the sedimentary heterogeneities in the subsurface and their three-dimensional formation. Hence, the model can be used as a model for hydrogeological prospecting, which maps of superficial deposits cannot.

5.4 Hydrogeological Properties for the Identified Subsurface Deposits

As concluded by Åberg et al. (2017), knowledge about 3D structure of sediments in the subsurface helps to better understand the hydrogeological setting and can be directly applied in 3D groundwater modeling, as well as for planning of possible new water wells in the relevant area. With this in mind, more surveys should be carried out to be able to say something about the hydrogeological properties for each identified subsurface package. When dimensioning water well 4 for Bø municipality, Klempe (2009) did a hydrogeological classification of the subsurface units and their abilities as an aquifer or aquitard. He defined the upper 3m, above the groundwater table, to be hard packed lodgment till with very low permeability (aquitard). This is also the floor of Verpe gravel pit. Next, he defined a 7-10m thick subaquatic fan with very good permeability and yield (aquifer). Below the subaquatic fan, he registered a deposit of meltout-moraine with unsorted material of hard packing ranging from 10m to 20m thickness. These unsorted materials was identified as a part of the aquifer with medium good permeability and yield, and can most likely be related to the stratified tills/glacial outwash in P7, P6 and P5 from the results of this thesis. The moraine ridge found at the start of Line 3 was specified as an aquitard, and possibly a watershed for the aquifer.

A more detailed hydrogeological mapping and modeling could be implemented to Hagadrag aquifer by combining Professor Harald Klempe's classifications, the hydraulic properties from the drillings in the *geodatabase* and the subsurface model established in this thesis. This could be useful if Bø municipality, in the future, want to establish a new drinking water well in this area.

6 Conclusion

A 3D subsurface geological model has been generated from a GPR survey, with aid from a *geodatabase* containing information on grain sizes from drilling points. The survey reveals a complex, heterogeneous subsurface composition beneath Verpe gravel pit in Bø Valley, concealing a grounding-line zone on a bedrock threshold, an ice-contact ridge (moraine ridge), stratified tills, gravity flow deposits, a subaquatic grounding-line fan and scour pool infill.

These identified subsurface features are important observations, and are probably more common than one may have thought for other areas in Norway where superficial maps and drilling points show glaciofluvial delta deposits. The identified subsurface features yield information about hydrogeology therein, and suggest that similar deposits may be good resources for groundwater supply.

A 3D conceptual model for the subsurface in an interesting area for Hagadrag aquifer is now generated. Such models are important for establishment of new water wells for Bø municipality, and can be used in groundwater- and transport modeling. The model also yields valuable information about unconsolidated aquifers in glaciomarine deposits in general, and can be used as guidance in similar subsurface investigations elsewhere.

7 Bibliography

- Aarnes, T. A. (2015). *Development of flow pattern and hydrochemistry during test pumping of a new production well : case of the Hagadrag aquifer*. (Masterthesis), Høgskolen i Telemark - Institutt for natur, helse-og miljøvern, Bø i Telemark, Norge.
- Aarseth, I., Austbø, P. K., & Risnes, H. (1997). Seismic stratigraphy of Younger Dryas ice-marginal deposits in western Norwegian fjords. *Norsk Geologisk Tidsskrift*, 77(2), 65-85.
- Anderson, M. P. (1989). Hydrogeologic facies models to delineate large-scale spatial trends in glacial and glaciofluvial sediments. *GSA Bulletin*, 101(4), 501-511. doi:[https://doi.org/10.1130/0016-7606\(1989\)101<0501:HFMTDL>2.3.CO;2](https://doi.org/10.1130/0016-7606(1989)101<0501:HFMTDL>2.3.CO;2)
- Annan, A. P. (2003). *Ground Penetrating Radar: Principles, Procedures & Applications*. Mississauga, Canada: Sensors & Software Incorporated.
- Asprion, U., & Aigner, T. (1999). Towards realistic aquifer models: three-dimensional georadar surveys of Quaternary gravel deltas (Singen Basin, SW Germany). *Sedimentary Geology*, 129(3), 281-297. doi:[https://doi.org/10.1016/S0037-0738\(99\)00068-8](https://doi.org/10.1016/S0037-0738(99)00068-8)
- Bayer, P., Huggenberger, P., Renard, P., & Comunian, A. (2011). Three-dimensional high resolution fluvio-glacial aquifer analog: Part 1: Field study. *Journal of Hydrology*, 405(1), 1-9. doi:<https://doi.org/10.1016/j.jhydrol.2011.03.038>
- Bennett, M., & Glasser, N. (2010). *Glacial Geology: Ice Sheets and Landforms, Second Edition*. Chichester: Wiley-Blackwell (Permission licenses: 4578780941124 and 4577750498895).
- Bergstrøm, B. (1999). Glacial geology, deglaciation chronology and sea-level changes in the southern Telemark and Vestfold counties, southeastern Norway. *Norges geologiske undersøkelse Bulletin 435*, 23-42.
- Bersezio, R., Bini, A., & Giudici, M. (1999). Effects of sedimentary heterogeneity on groundwater flow in a Quaternary pro-glacial delta environment: joining facies analysis and numerical modelling. *Sedimentary Geology*, 129(3), 327-344. doi:[https://doi.org/10.1016/S0037-0738\(98\)00145-6](https://doi.org/10.1016/S0037-0738(98)00145-6)
- Blikra, & Nemeč. (1998). Postglacial colluvium in western Norway: depositional processes, facies and palaeoclimatic record. *Sedimentology*, 45(5), 909-959. doi:<https://doi.org/10.1046/j.1365-3091.1998.00200.x>
- Boggs, S. (2011). *Principles of sedimentology and stratigraphy* (5th ed.). Boston: Prentice Hall.
- Bristow, C. S., & Jol, H. M. (2003). An introduction to ground penetrating radar (GPR) in sediments. In *Ground Penetrating Radar in Sediments* (Vol. 211, pp. 1-7). London: Geological Society of London.
- Bø-Kommune. (2014). *Internkontrollsystem for Bø Vassverk - Driftshandbok og beredskapsplan*. Teknisk eining (Bø Kommune) og Driftsassistansen i Telemark Retrieved from <https://www.bo.kommune.no/Handlers/fh.ashx?MIId=1371&FilId=2758>

- Carstens, H. (2015). Grunnvann – ressurs og problemmaker. Retrieved from <https://www.geo365.no/geoforskning/grunnvann-ressurs-og-problemmaker/>
- Cassidy, N. J. (2009). Ground Penetrating Radar Data Processing, Modelling and Analysis. In H. M. Jol (Ed.), *Ground Penetrating Radar: Theory and Applications* (pp. 141-176). Amsterdam: Elsevier.
- Connor, R. (2015). *The United Nations World Water Development Report 2015: Water for a Sustainable World*. Paris, France: UNESCO Retrieved from <https://unesdoc.unesco.org/ark:/48223/pf0000231823>
- Dahlgren, S. (1993). Litt om geologien i det sentrale Telemark. In *Stein* (Vol. 20, pp. 73-79).
- Dimick, D. (2014). If You Think the Water Crisis Can't Get Worse, Wait Until the Aquifers Are Drained. Retrieved from https://www.google.com/search?q=groundwater+emptied&rlz=1C1GGRV_enN0809NO809&oq=groundwater+emptied&aqs=chrome..69i57.7335j0j9&sourceid=chrome&ie=UTF-8
- Eilertsen, R., Corner, G., Aasheim, O. D. D., Andreassen, K., Kristofferson, Y., & Ystborg, H. (2006). Valley-Fill Stratigraphy and Evolution of the Målselv Fjord Valley, Northern Norway. In R. W. Dalrymple, D. A. Leckie, & R. W. Tillman (Eds.), *Incised Valleys in Time and Space* (Vol. 85, pp. 179-195). California: Society for Sedimentary Geology.
- Eilertsen, R., Corner, G., Aasheim, O. D. D., & Hansen, L. (2011). Facies characteristics and architecture related to palaeodepth of Holocene fjord–delta sediments. *Sedimentology*, 58(7), 1784-1809. doi:<https://doi.org/10.1111/j.1365-3091.2011.01239.x>
- Gaut, S. (2017). *Grunnvannskilden som hygienisk barriere - Styrker og svakheter i et klima i endring*. Paper presented at the Norsk Vannforening. <https://vannforeningen.no/wp-content/uploads/2017/10/Gaut.pdf>
- GoldenSoftware. (2018). What are the required fields for importing a collars table into Voxler 4? Retrieved from <https://support.goldensoftware.com/hc/en-us/articles/226805568-What-are-the-required-fields-for-importing-a-collars-table-into-Voxler-4->
- Green, A., Pugin, A., Beres, M., Lanz, E., Büker, F., Huggenberger, P., . . . Maurer, H. (1995). 3-D High-Resolution Seismic and Georadar Reflection Mapping of Glacial, Glaciolacustrine and Glaciofluvial Sediments in Switzerland. In *Symposium on the Application of Geophysics to Engineering and Environmental Problems 1995* (pp. 419-434). Switzerland: Society of Exploration Geophysicists.
- Halvorsen, M., & Strømme, K. (1989). *Vassforsyning Bø kommune*. (Masterthesis), Telemark distriktshøgskole, Bø.
- Hansen, L., Beylich, A., Burki, V., Eilertsen, R., Fredin, O., Larsen, E., . . . Tønnesen, J. F. (2009). Stratigraphic architecture and infill history of a deglaciated bedrock valley based on georadar, seismic profiling and drilling. *56*(6), 1751-1773. doi:<https://doi.org/10.1111/j.1365-3091.2009.01056.x>

- Herweijer, J. C. (1997). *Sedimentary Heterogeneity and Flow Towards a Well. Assessment of flow through heterogeneous formations*. (PhD), Vrije Universiteit Amsterdam, Amsterdam.
- Huggenberger, P. (1993). Radar facies: Recognition of facies patterns and heterogeneities within Pleistocene Rhine gravels, NE Switzerland. 75(1), 163-176. doi:<https://doi.org/10.1144/GSL.SP.1993.075.01.10>
- Huggenberger, P., & Aigner, T. (1999). Introduction to the special issue on aquifer-sedimentology: problems, perspectives and modern approaches. *Sedimentary Geology*, 129(3-4), 179-186. doi:[https://doi.org/10.1016/S0037-0738\(99\)00101-3](https://doi.org/10.1016/S0037-0738(99)00101-3)
- Jansen (Cartographer). (1980). Detaljkartlegging av sand og grusressurser i Bø kommune, Telemark
- Jansen, I. J. (1983). *Detaljkartlegging av sand og grusressurser i Bø kommune, Telemark* (Vol. 11). Bø: Prosjekt Temakart.
- Jansen, I. J. (1986). *Kvartærgeologi : jord og landskap i Telemark gjennom 11000 år : beskrivelse til kvartærgeologisk kart i målestokk 1:250000*. Skien: Fylkeskontoret i Telemark.
- Jol, H. M. (2009). *Ground penetrating radar : theory and applications*. Amsterdam: Elsevier Science.
- Kartverket. (2018). Høydedata. Retrieved from <https://hoydedata.no/LaserInnsyn/>
- Kjensli, B. (2010). - Vi bruker for mye grunnvann. Retrieved from <https://forskning.no/havforskning-landbruk/vi-bruker-for-mye-grunnvann/823681>
- Klempe, H. (1979). *Grunnundersøkelser på Hagadrag i forbindelse med grunnvannsforsyning til Bø kommune* (Vol. 1/79). Bø: Telemark distriktshøgskole.
- Klempe, H. (1988). *Eika grunnvannsmagasin : sedimentologi, hydrogeologi og praktisk anvendelse*. (PhD), Norges landbrukshøgskole,
- Klempe, H. (2004). Identification of Quaternary subsurface glacial deposits using 3D databases and GIS. *Norsk Geografisk Tidsskrift - Norwegian Journal of Geography*, 58(2), 90-95. doi:<https://doi.org/10.1080/00291950410006823>
- Klempe, H. (2009). *Undersøkelser for en ny brønn til Bø vassverk*. Institutt for naturhelse og miljøvern fag. Høgskolen i Telemark.
- Klempe, H. (2010). *Ressursgeologisk utgreiing for Bø vassverk og Herremo, Bø kommune, Telemark*. Høgskolen i Telemark, Institutt for natur-, helse- og miljøvern fag Retrieved from http://webhotel3.gisline.no/GisLinePlanarkiv/0821/02_32_2009/Dokumenter/Hele%20rapporten.pdf
- Klempe, H. (2015). The hydrogeological and cultural background for two sacred springs, Bø, Telemark County, Norway. *Quaternary International*, 368(C), 31-42. doi:<https://doi.org/10.1016/j.quaint.2014.10.048>
- Kraft, P. (2011). *Planomtale med konsekvensutgreiing - Områdereguleringsplan Bø vassverk Herremo*. (522947). Retrieved from

http://webhotel3.gisline.no/GisLinePlanarkiv/0821/02_32_2009/Dokumenter/Planomtale%20med%20konsekvensutgreiing%201.6.12.pdf

- Lamminen, J. (2011). Provenance and correlation of sediments in Telemark, South Norway: status of the Lifjell Group and implications for early Sveconorwegian fault tectonics. *Norwegian Journal of Geology*, 91(1), 57-75.
- Lang, J., Sievers, J., Loewer, M., Igel, J., & Winsemann, J. (2017). 3D architecture of cyclic-step and antidune deposits in glacial subaqueous fan and delta settings: Integrating outcrop and ground-penetrating radar data. *Sedimentary Geology*, 362, 83-100. doi:<https://doi.org/10.1016/j.sedgeo.2017.10.011>
- Langeland, K., & Moe, J. O. (2003). *Ny brønn ved Bø vassverk : matematisk modell av akviferen og oversikt over akviferegenskapar og vasskvalitet*. (Cand. Scient Miljø- og helsevern, hydrogeologi), Høgskolen i Telemark, Bø i Telemark, Norge.
- Lavik, V. (2017). *Subsurface mapping of Øverbømoen and locating optimal aquifers for drinking water supply : a hydrogeological survey using geophysical methods*. (Master's thesis), Høgskolen i Sørøst-Norge, Bø.
- Li, J., & Heap, A. D. (2008). *A Review of Spatial Interpolation Methods for Environmental Scientists*. Australia: Geoscience Australia.
- Lønne, I., & Nemeč, W. (2011a). The kinematics of ancient tidewater ice margins: Criteria for recognition from grounding-line moraines. *Geological Society London Special Publications*, 354, 57-75. doi:<https://doi.org/10.1144/SP354.4>
- Lønne, I., & Nemeč, W. (2011b). Modes of sediment delivery to the grounding line of a fast-flowing tidewater glacier: Implications for ice-margin conditions and glacier dynamics. *Geological Society, London, Special Publications*, 354, 33-56. doi:<https://doi.org/10.1144/SP354.3>
- Lønne, I., Nemeč, W., Blikra, L., & Lauritsen, T. (2001). *Sedimentary Architecture and Dynamic Stratigraphy of a Marine Ice-Contact System* (Vol. 71).
- Margat, J., & van der Gun, J. (2013). *Groundwater around the World: A Geographic Synopsis*. Leiden: CRC Press.
- Mele, M., Bersezio, R., & Giudici, M. (2012). Hydrogeophysical imaging of alluvial aquifers: electrostratigraphic units in the quaternary Po alluvial plain (Italy). *International Journal of Earth Sciences*, 101(7), 2005-2025. doi:<https://doi.org/10.1007/s00531-012-0754-7>
- Neal, A. (2004). Ground-penetrating radar and its use in sedimentology: principles, problems and progress. *Earth-Science Reviews*, 66(3), 261-330. doi:<https://doi.org/10.1016/j.earscirev.2004.01.004>
- NGU. (2017). Produktark: Løsmasser N50/N250. Retrieved from https://www.ngu.no/upload/Aktuelt/Produktark_LosmasseN50N250_NGU.pdf
- Olsen, L., Fredin, O., & Olesen, O. (Eds.). (2013). *Quaternary geology of Norway*. Norway: Geological Survey of Norway (NGU)
- Powell, R. D. (1990). Glacimarine processes at grounding-line fans and their growth to ice-contact deltas. *Geological Society, London, Special Publications*, 53(1), 53. doi:<https://doi.org/10.1144/GSL.SP.1990.053.01.03>

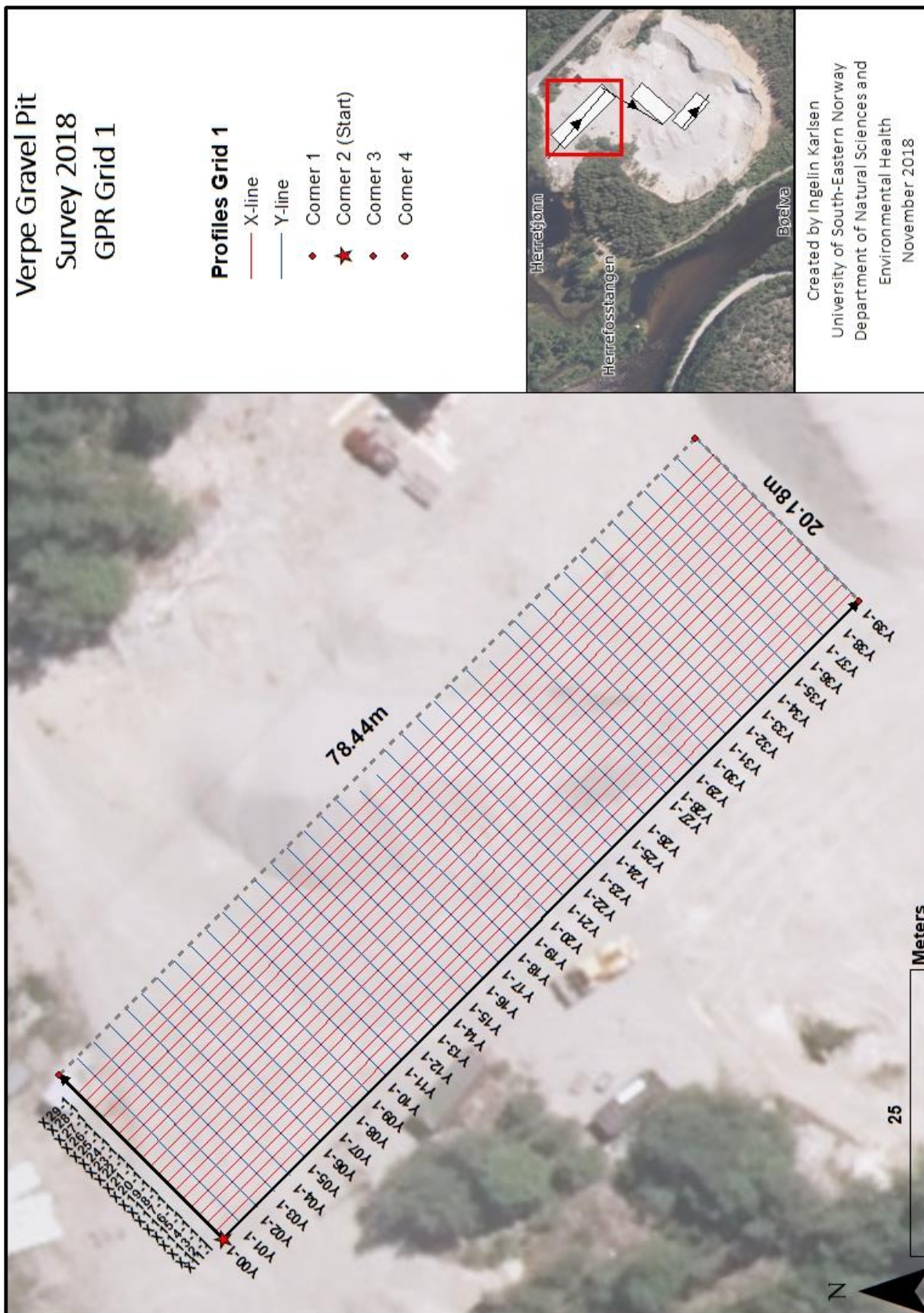
- Ramberg, I. B., Bryhni, I., Nøttvedt, A., & Rangnes, K. (Eds.). (2013). *Landet blir til : Norges geologi* (2 ed.). Trondheim: Norsk geologisk forening (NGF).
- Robinson, M., Bristow, C., McKinley, J., & Ruffell, A. (2013). Ground Penetrating Radar. In S. J. Cook, L. E. Clarke, & J. M. Nield (Eds.), *Geomorphological Techniques* (pp. 1-26). London, UK: British Society for Geomorphology.
- SDGS. (2015). *2030 Agenda on Sustainable Development*. New York: The United Nations Retrieved from https://www.un.org/sustainabledevelopment/wp-content/uploads/2019/01/SDG_Guidelines_January_2019.pdf
- Sensors & Software Inc. (2012). pulseEKKO PRO User's Guide. In (pp. 90). Mississauga, Canada: Subsurface Imaging Solutions.
- Sensors&Software. (2009-2018). EKKO_Project (Version V5).
- Sensors&Software. (2018). EKKO_Project - Processing Module. In *User's Guide*. Mississauga, Canada.
- Sigmond, E. M. O., Bryhni, I., & Jorde, K. (2013). *Norsk geologisk ordbok : med engelsk-norsk ordliste*. Trondheim: Akademika forlag.
- Solli, A., & Nordgulen, Ø. (Cartographer). (2013). Berggrunnskart over Norge - og kaledonidene i Sverige og Finland
- Sumner, T. (2015). Many of Earth's groundwater basins are drying out. Retrieved from <https://www.sciencenewsforstudents.org/article/many-earth%E2%80%99s-groundwater-basins-are-drying-out>
- Takahashi, K., Preetz, H., Igel, J., & Kuroda, S. (2012). Basics and Application of Ground-Penetrating Radar as a Tool for Monitoring Irrigation Process. In M. Kumar (Ed.), *Problems, Perspectives and Challenges of Agricultural Water Management* (pp. 156-180). Croatia: Intech.
- Vannressursloven – vrl. (2001). *Lov om vassdrag og grunnvann (vannressursloven)*. (LOV-2000-11-24-82). Retrieved from <https://lovdata.no/dokument/NL/lov/2000-11-24-82>
- Weight, W. D. (2008). *Hydrogeology field manual* (2 ed.). New York: McGraw-Hill.
- Weissmann, G. S., Pickel, A., McNamara, K. C., Frechette, J. D., Kalinovich, I., Allen-King, R. M., & Jankovic, I. (2015). Characterization and quantification of aquifer heterogeneity using outcrop analogs at the Canadian Forces Base Borden, Ontario, Canada. *GSA Bulletin*, 127(7-8), 1021-1035. doi:<https://doi.org/10.1130/B31193.1>
- Zuk, T. (2011). *Acquisition, 3-D Display and Interpretation of GPR data in Fluvial Sedimentology*. (Master's Thesis Geography, Earth and Environmental Sciences), University of Birmingham, United Kingdom. Retrieved from <https://etheses.bham.ac.uk/id/eprint/2913/1/Zuk11MPhil.pdf>
- Østmo, S. R. (1974). *Hydrogeologisk undersøkelse for Bø kommune*. Oslo: NGU
- Åberg, A. K., Salonen, V.-P., Korkka-Niemi, K., Rautio, A., Koivisto, E., & Åberg, S. C. (2017). GIS-based 3D sedimentary model for visualizing complex glacial deposition in Kersilo, Finnish Lapland. *Boreal environment research*, 22, 277-298.

8 Appendix

Content for appendix

Appendix 1: Detailed map of Grid 1 (GPR)	94
Appendix 2: Detailed map of Grid 3 (GPR)	95
Appendix 3: System Setup Parameters – Grid 1	96
Appendix 4: System Setup Parameters – Grid 2.....	97
Appendix 5: System Setup Parameters – Grid 3.....	98
Appendix 6: System Setup Parameters – 50 MHz profiles	99
Appendix 7: <i>Geodatabase</i> maps 1	100
Appendix 8: <i>Geodatabase</i> maps 2	101
Appendix 9: Xline10 from Grid 2 with interpreted radar packages	102

Appendix 1: Detailed map of Grid 1 (GPR)



Appendix 3: System Setup Parameters – Grid 1

Coordinates Grid 1 (ETRS89 / UTM zone 32N)		
Corner 1	X: 493047.455	Y: 6588261.776
Corner 2	X: 493033.189	Y:6588247.506
Corner 3	X: 493088.662	Y: 6588192.049
Corner 4	X:493102.928	Y: 6588206.319
GPR Parameters		
Antenna Frequency	100 MHz	
Antenna Separation	1 m	
Assumed Velocity	0.06 m/ns	
Time Window	760 ns 20.51 m	
Number of points	950	
Sampling Interval	0.8 ns	
Step Size	0.250 m	
System Stacking	8	
Pulsar Setting	PE100 400V	
Trigger method	Odometer	
Odometer calibration	1104 forward	
Trace delay	0.5	
Start delay	None	
Start Position	0 m	
Antenna step size	0.250 m	
Data directory	20	
Grid survey type	x-y	
X line spacing	1 m	
Y line spacing	2 m	

Appendix 4: System Setup Parameters – Grid 2

Coordinates Grid 2 (ETRS89 / UTM zone 32N)		
Corner 1	X: 493052.383	Y: 6588116.850
Corner 2	X: 493063.443	Y: 6588129.801
Corner 3	X: 493094.429	Y: 6588102.957
Corner 4	X: 493083.770	Y: 6588089.781
GPR Parameters		
Antenna Frequency	100 MHz	
Antenna Separation	1 m	
Assumed Velocity	0.06 m/ns	
Time Window	760 ns 20.51 m	
Number of points	950	
Sampling Interval	0.8 ns	
Step Size	0.250 m	
System Stacking	8	
Pulsar Setting	PE100 400V	
Trigger method	Odometer	
Odometer calibration	1106.75 forward	
Trace delay	0.5	
Start delay	0	
Start Position	0 m	
Antenna step size	0.250 m	
Data directory	20	
Grid survey type	x-y	
X line spacing	1 m	
Y line spacing	1 m	

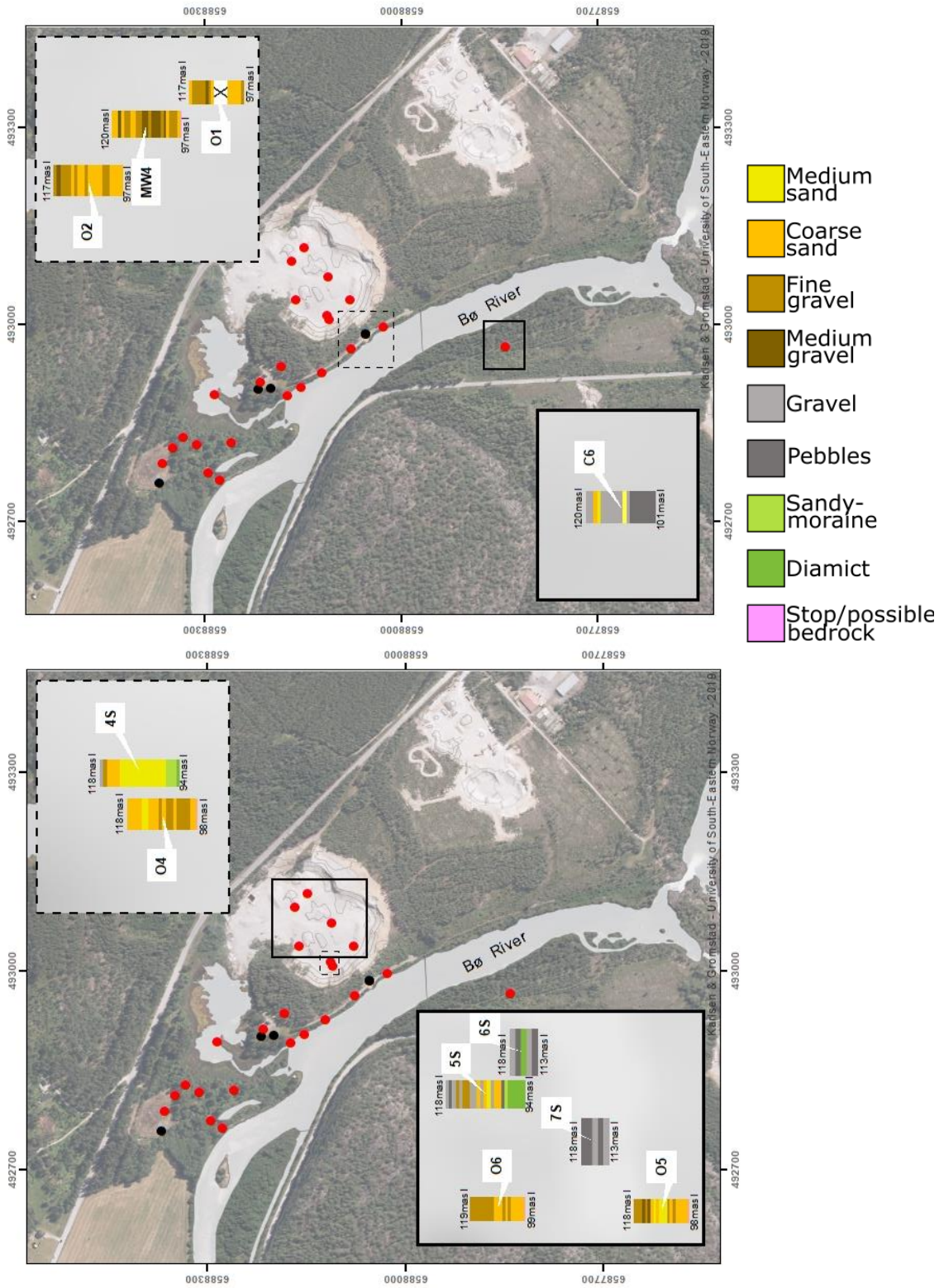
Appendix 5: System Setup Parameters – Grid 3

Coordinates Grid 3 (ETRS89 / UTM zone 32N)				
Corner 1	X: 493059.704		Y: 6588140.736	
Corner 2	X: 493090.067		Y: 6588175.300	
Corner 3	X: 493103.863		Y: 6588162.977	
Corner 4	X: 493073.130		Y: 6588127.992	
Extra profile X50-3	Start	X:493062.744 - Y:6588147.496	End	X:493089.276 Y:6588122.156
Extra profile X51-3	Start	X:493081.767 - Y:6588182.821	End	X:493113.910 Y:6588154.111
GPR Parameters				
Antenna Frequency	100 MHz			
Antenna Separation	1 m			
Assumed Velocity	0.06 m/ns			
Time Window	760 ns - 20.51 m			
Number of points	950			
Sampling Interval	0.8 ns			
Step Size	0.250 m			
System Stacking	8			
Pulsar Setting	PE100 400V			
Trigger method	Odometer			
Odometer calibration	1106.75 forward			
Trace delay	0.5			
Start delay	0			
Start Position	0 m			
Antenna step size	0.250 m			
Data directory	20			
Grid survey type	x-y			
X line spacing	1 m			
Y line spacing	1 m			

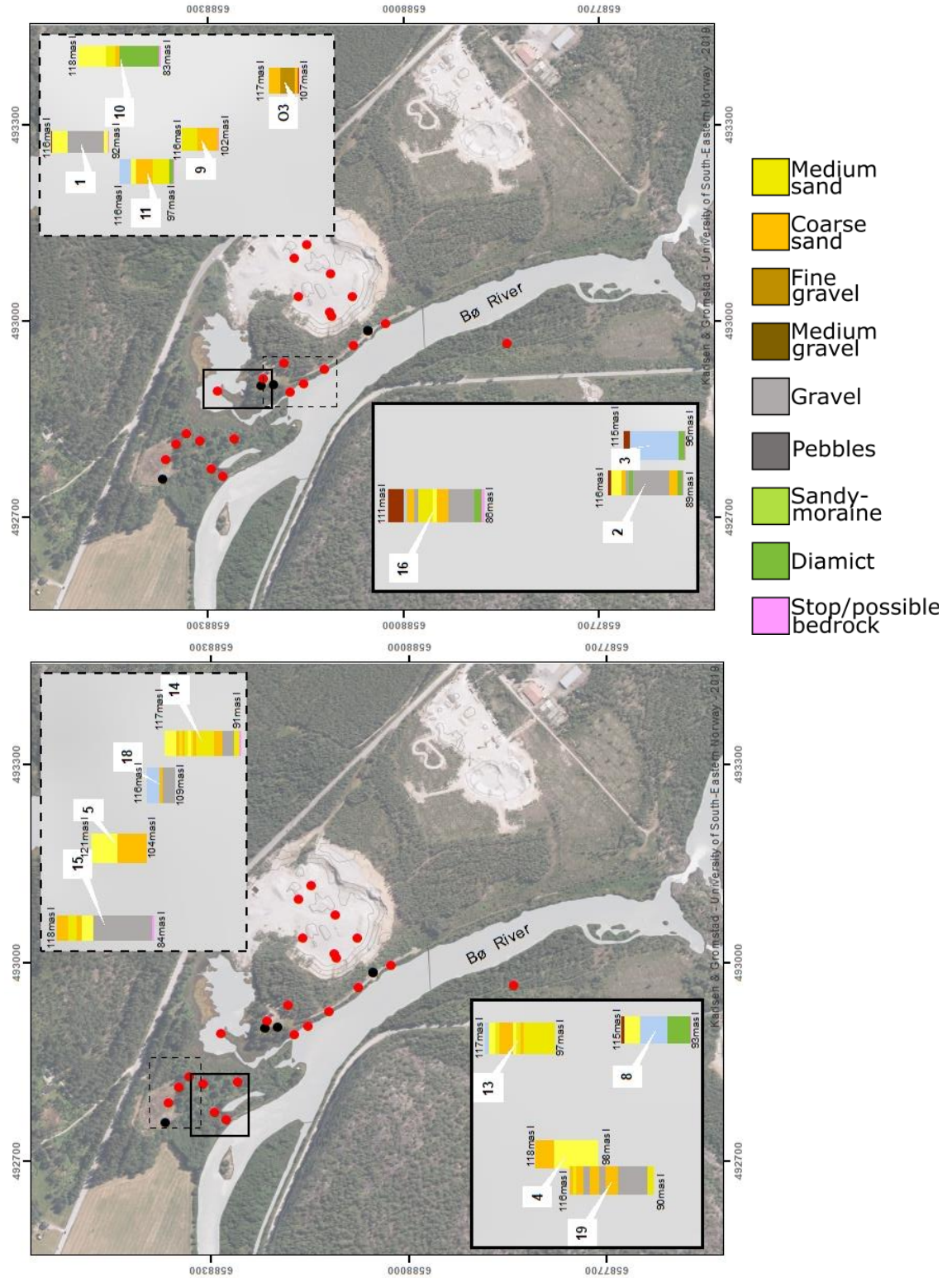
Appendix 6: System Setup Parameters – 50 MHz profiles

Coordinates 50 MHz Profiles (ETRS89 / UTM zone 32N)				
Line 1	Start of line	X: 493022.276 Y: 6588264.657 Z: 118.597 masl	End of line	X: 493099.587 Y: 6588200.613 Z: 118.959 masl
Line 2	Start of line	X: 493099.470 Y: 6588206.378 Z: 118.780 masl	End of line	X: 493058.727 Y: 6588139.443 Z: 118.863 masl
Line 3	Start of line	X: 493055.099 Y: 6588119.862 Z: 118.233 masl	End of line	X: 493091.836 Y: 6588089.119 Z: 118.161 masl
GPR Parameters				
Antenna Frequency	50 MHz			
Antenna Separation	1.8 m			
Assumed Velocity	0.1 m/ns			
Time Window	Line 1	Line01 = 1480ns (66m depth) Line02 = 1480ns (66m depth) Line03 = 880ns (39.59m depth)		
	Line 2	Line04 = 880ns (39.59m depth) Line05 = 1120ns (50.39m depth)		
	Line 3	Line06 = 1120ns (50.39m depth) Line07 = 1320ns (59.39m depth)		
Number of points	575			
Sampling Interval	0.8 ns			
Step Size	0.5 m			
System Stacking	Line 1	Line01 = Stacking 8 Line02 = Stacking 16 Line03 = Stacking 16		
	Line 2	Line04 = Stacking 16 Line05 = Stacking 16		
	Line 3	Line06 = Stacking 16 Line07 = Stacking 16		
Pulsar Setting	PE100 400V			
Trigger method	Free run			
Trace delay	0.5			
Start delay	None			
Start Position	0 m			
Antenna step size	0.5 m			

Appendix 7: Geodatabase maps 1



Appendix 8: Geodatabase maps 2



Appendix 9: Xline10 from Grid 2 with interpreted radar packages

